Estimation of Soil Damping Contribution on Offshore Monopiles Using Plaxis 3D Approach

TUDelft

MSc Thesis

Luka David Đilas

September - 2018

- *This page intentionally left blank* -

Estimation of Soil Damping Contribution on Offshore Monopiles Using Plaxis 3D Approach

by

Luka David Đilas

in partial fulfilment of the requirements for the degree of

Master of Science

in Civil Engineering

(Geo-Engineering Track)

at the Delft University of Technology

to be defended publicly on Tuesday September 25, 2018 at 11:30 AM.

Graduation Committee:

Prof. Dr. K.G. Gavin	TU Delft – Chairman
Dr. F. Pisanò	TU Delft
Dr. A. Askarinejad	TU Delft
Dr. L.J. Prendergast	TU Delft / University of Nottingham – Daily Supervisor

---

Cover Page: Windmills D1-D4 (Thornton Bank Windfarm - Belgium) © Hans Hillewaert

An electronic version of this thesis is available at: http://repository.tudelft.nl/

- *This page intentionally left blank* -

Abstract

Offshore wind has achieved many milestones considering this relatively new and emerging industry. Its huge advancement is mostly driven by lowering the overall project cost and renewable energy targets which are set by the EU. One of the potential cost savers can be found in the foundation structure design in which the monopiles are the most used choice. The area from which the design of these structures can be improved is quite complex and it can be related to the field of Dynamic Soil-Structure Interaction (DSSI). Offshore Wind Turbine (OWT) has several damping sources but in the last few years soil damping phenomena has attracted a lot of interest within the offshore wind research community because it is believed that potential benefits can be achieved if the contribution of this damping source can be estimated with reliability. Offshore wind design codes do not provide a methodology for the estimation of this damping type and therefore there is a need for the research. For the purpose of soil damping estimation, a geotechnical Finite Element (FE) software – Plaxis 3D was utilized. Firstly, the chosen soil model was verified through the three-step verification process which involved a comparison between experimental field data and numerical data from Plaxis. Once successfully verified, the soil model is utilized further in the design of the simplified OWT structure which is exposed to the dynamic wave and wind loads based on the serviceability and ultimate limit conditions. What is of the particular interest leads to the free vibration phase and monopile positioning (position of structure at the start of free vibration) from which the necessary information regarding the decay of displacement amplitudes is obtained and further analysed with the logarithmic decrement method for damping estimation. Adding on soil damping, as part of research additional topics were also considered and they relate to soil behaviour and natural frequency. The final results are compared to the other research papers and they are found to be well within the proposed literature damping range which highly depends on a certain combination of monopile geometry, soil type and loading conditions. From the research it was concluded that soil damping value increases as the wave and wind loads increase. Also, it was proven that a damping potential in offshore wind exists and that eventually soil damping should be implemented in the future offshore wind design codes.

Keywords: Damping, Soil Dynamics, Monopile, Offshore Wind, Natural Frequency, Soil-Structure Interaction, Sand

Acknowledgements

This 9-month long journey started in January, 2018 with the thesis topic being proposed from the Gavin and Doherty Geosolutions (GDG) where I have concluded my internship. I want to thank Julie and Soroosh for giving me an opportunity to work on this challenging and also quite interesting topic.

The real work started in February with the formation of my thesis committee and it lasted about 8 months. I have to mention few people who gave their contribution and helped me to carry on the research and finish this process successfully. Firstly, I want to thank Luke for being my daily supervisor at TU Delft and helping by putting me on the right direction when I was in doubt. Without him, the thesis could have been much different experience and it would probably have gone in some different research direction. He “equipped” me with the essential and meaningful research papers which served as good guidance and reference. We have concluded many short meetings which answered my questions and helped me to stay on the right path. Luke, thanks a lot!

Also, I want to the rest of my committee: Ken, Federico and Amin. They have proposed many things during our kick-off and progress meetings. Their expertise and purposeful tips have helped me to raise the thesis on a higher level but also to implement ideas and concepts into the research.

Finally, I want to thank my friends from Delft, more specifically my flatmates (Telis and Uroš) for being there when the things did not go smooth and as planned, and Marko for helping me with the Matlab issues.

List of Abbreviations

1P – 3P	OWT Frequency Range (Rotor - Blades)
API	American Petroleum Institute
DNV	Det Norske Veritas
DSSI	Dynamic Soil Structure Interaction
FEM	Finite Element Method
FFT	Fast Fourier Transform
GL	Germanischer Lloyd
HP	High Pass Filter
HS	Hardening Soil Model
HSS	Hardening Small-Strain Model
IFFT	Inverse Fast Fourier Transform
LCOE	Levelized Cost of Electricity
L/D	Length over Diameter Ratio
LP	Low Pass Filter
MP	Monopile
MSL	Mean Sea Level
OWT	Offshore Wind Turbine
PSD	Power Spectral Density
PWP	Pore Water Pressure
SLS	Serviceability Limit State
SSI	Soil-Structure Interaction
ULS	Ultimate Limit State
U-P	Pore Pressure over Mean Stress Formulation

Table of Contents

Chapter 1 - Introduction

Currently the offshore wind industry is booming on a high rate and future trends will definitely keep growing in the upcoming years as more and more countries are turning towards sustainable energy sources such as the offshore wind, wave and tidal energy. The focus of this MSc Thesis research will be on the effect of soil damping on offshore monopiles which are used as foundation structures for offshore wind turbines. The effect of soil damping is still questionable among the research community, for example in the current design codes (e.g. DNV-GL or API), there is no exact methodology on how to determine the effect of soil damping.

This MSc thesis research aims to shed some light on the current issues regarding this phenomenon and it provides an overview of the theory necessary to tackle problem like the one discussed in the thesis. Further in the document, the proposal and methodology (research plan) are explained along with the previous studies that were done on the similar or same topic. Finally, the methodology is employed by means of numerical simulations and for this purpose the geotechnical finite element software – Plaxis 3D is utilized. When looking to the previous studies which were considered during the research process, this is the first time that Plaxis 3D is used specifically for this offshore damping topic.

1.1 Offshore Wind Industry

In the last decade the Europe has seen a tremendous number of new project developments in the field of renewable energy and particularly in the offshore wind. The growth in the mentioned industry is highly related to the global Initiatives and policies such as the Paris Agreement or European Union energy targets. Nowadays, the Europe can be considered as a global market leader in the Offshore Wind Industry and countries such as United Kingdom, Denmark and Germany are on the top of the list by the number of installed megawatts (MW). Also, the European Union and different involved companies have invested a lot of funds in the various research projects which eventually have led to the lowering of the Levelized Cost of Electricity (LCOE) which is now almost competitive with other traditional energy sources. It can be said for sure that the Europe is the pioneer of the industry and as the part of the learning curve the mentioned countries and other offshore developer companies (e.g. Siemens, Vestas, Ørsted, and many more) have spent a lot of funding and time into the new developments.

Over the years, many different energy targets were set as guidelines towards reducing CO_2 emissions, decreasing the usage of fossil fuels, etc. The most recent one was set by the European Union which has a goal of reaching at least 27% from the renewable energy sources as a part of total energy consumption and the goal to reach this target is set by the year of 2030 (European Wind Energy Association, 2015) Fortunately, the political consensus has been reached on the renewable energy targets and it is well accepted among the EU member countries. The desire to reach the goals can be seen through various stimulations to the renewable energy sector over the past years (research, funds, permits, etc.). The product of these mentioned initiatives led to a major increase in a renewable energy production which is strongly driven by the offshore wind developments with most projects being done in the area located in the North Sea by the United Kingdom, Denmark, Germany, Belgium and the Netherlands.

1.1.1 Offshore Wind Market Trends

The most recent data from the Wind Europe has shown that year of 2017 was the most successful one, and this is related in terms of installed capacity in megawatts. To be more exact, the 2017 was concluded with 3,148 MW of new installed capacity which established the new record line and a new goal to be broken for the upcoming years. This capacity corresponds to 560 new offshore wind turbines which are located over 17 different wind farms. Also, currently there are ambitious, but on the other hand realistic predictions that the total capacity is expected to grow up to 25 GW until 2020 (Wind Europe, 2018).

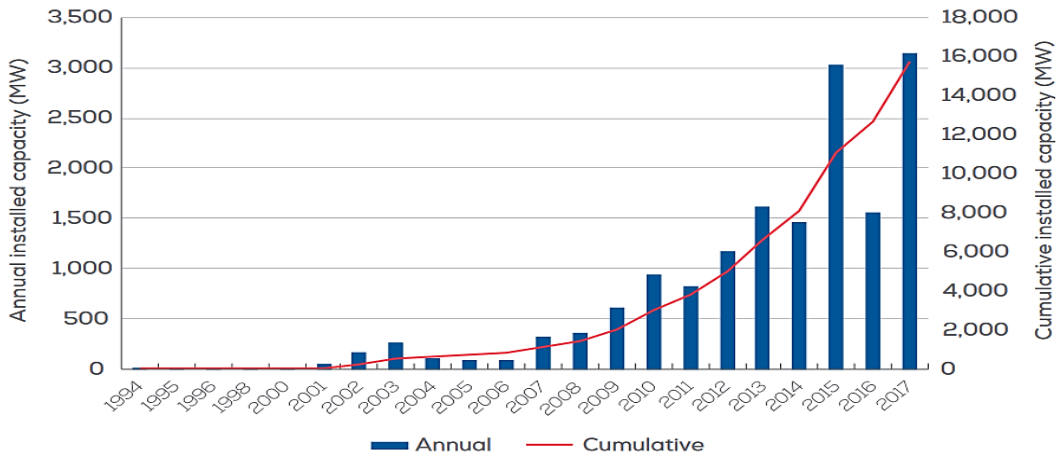

Figure 1: Installed Annual and Cumulative Capacity. Source: Wind Europe

Moreover, the current market trend is going towards some larger capacity turbines with a current average capacity of a single, newly installed wind turbine now being around 6 MW. This value also represents about 23% increase compared to the 2016 (Wind Europe, 2018). So far, the monopiles are still a dominant foundation structure option (81.7% in total market share), despite the current trend of installing the new turbines in deeper water depths, which was in average about 27 meters for the year of 2017 (Wind Europe, 2018). According to the Wind Europe, during the last year (2017), the monopiles had about 87% of the foundation market share, followed by jackets, gravity base foundation and a newly installed type – floating spar buoy foundation.

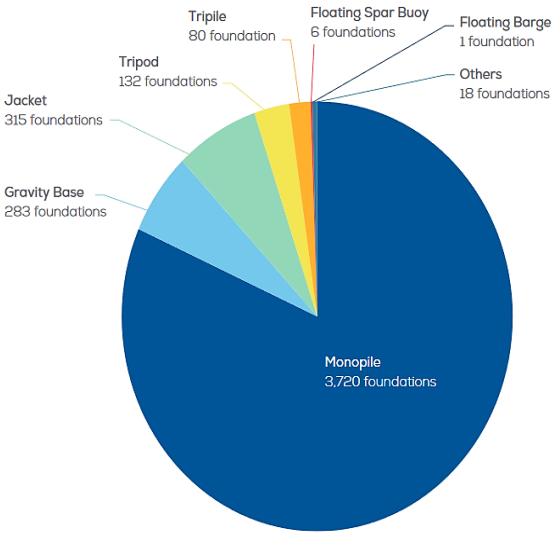

Figure 2: Share of substructure types (up to 2018). Source: (Wind Europe, 2018)

1.1.2 Why Monopiles?

Still the monopiles are the most popular design option for the offshore wind turbine foundations although there are multiple foundation types available such as: jackets, gravity base foundations, and the newest foundation solution - floating wind turbines which are anchored to the sea bottom and

therefore the installation depth increases dramatically compared to the monopile solution. The monopiles gained its popularity since they are relatively easy to design, construct, and to handle during the installation phase. Due to time constraints for the thesis project, only the monopiles will be in the focus of the thesis research. Naturally, the monopiles seem the most interesting topic to research since they make the most of the current offshore wind market share. Another reason can be found in the fact that in the following decade some of the first installed monopiles will be reaching the end of their operational phase (life-cycle) and they will be probably decommissioned and replaced with the newly designed monopile solutions which would be the result of the numerous research projects over the past years. Also, this opens more space for new opportunities such as the installation of a large diameter monopiles (e.g. XL monopiles with diameter range from 8 to 10 meters), therefore these mentioned facts and reasons definitely attract more potential for the future research in this field.

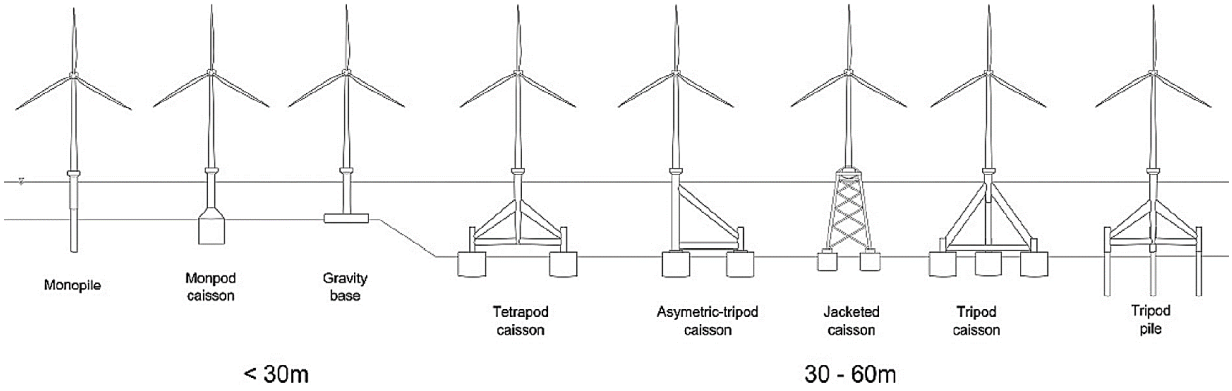

Figure 3: Available Foundation Structure Options for the Offshore Wind Turbines. Source: (Bhattacharya, 2014)

1.2 Research Motivation – Reducing Cost and Increasing Damping

The cost has been a major obstacle for the offshore wind projects due to enormous high cost for the developers, governments and investment companies. The cost is driven by many factors and if the offshore wind turbine is compared to the onshore wind turbine, the offshore counterpart has a much higher total cost due to robust design, harsh environment conditions, heavy maintenance, remote locations from the coast, etc. This has led to various research initiatives which aimed to lower the cost of the offshore wind (lower LCOE), and in the recent years the offshore industry has achieved a lot in terms of lowering the total project cost. What attracts attention for the geotechnical engineers is the fact that the offshore foundations for wind turbines can take about 20 to 25% of the capital project cost (Navigant Consulting Inc., 2013) while in some projects such as the North Hoyle project in the United Kingdom the cost of foundation went up to 34% of the overall cost (Bhattacharya, 2014). The mentioned total cost of foundation structure represents a challenge to the engineering and research community since it is deemed that the total cost can be lowered overall. Various foundation designs have been improved a lot since the offshore industry started with its rapid expansion, but still there are some areas within foundation design part that could be improved which will eventually lead to more economic and efficient design. For this mentioned reason of lowering the foundation structure cost, the thesis research will focus on one particular mechanism which is still not understood well enough and it is known as soil damping contribution to the total offshore wind turbine damping. The following paragraph will additionally justify the research motivation which is apart from lowering the foundation cost based on the soil damping uncertainties and lack of topic understanding.

Soil damping can be simply described as dissipation of energy from the vibrating or cyclically loaded structure to the surrounding environment which in this case is soil medium. In this thesis research the structure is presented as an OWT (Offshore Wind Turbine) foundation substructure (monopile) and the surrounding environment is presented as sand soil which surrounds the monopile foundation over its embedment length. There are multiple sources of damping within the OWT structures such as: aerodynamic, hydrodynamic, sloshing damper, structural and soil damping. While the other sources can be determined and included in design calculations with fairly good approximations, the soil damping is not that well understood and its contribution cannot be calculated with certain desired accuracy like the other damping sources. The well-known companies which provide the whole offshore industry with various design codes and standards such as the Germanischer Lloyd (now DNV-GL) noted that the soil damping contribution to the total OWT damping is the most uncertain one (Germanischer Lloyd, 2005). Probably the most used standards and regulations come from the DNV-GL classification society company and in their design regulations they stated that a realistic assumption regarding soil damping in the OWT soil-structure interaction design shall be considered, but there is no exact recommendation or methodology to calculate the soil damping contribution (Det Norske Veritas AS, 2014). The various soil damping mechanisms will be explained in the upcoming theoretical chapter. Generally, it is known that an increase in soil damping values lead to the multiple positive effects which are related to foundation design and extension of the structure lifetime. The reasoning for this is explained below in the two following bullet points

- **Fatigue Life**

Fatigue life of the structure is one of the decisive design factors for the OWT since it decides how robust the design will be. For example, if the monopile is exposed to more damping, this will lead to lower stress amplitudes during cyclic loading and therefore the accumulation of fatigue damage will be smaller which in other hand can lead to increase in lifetime of the structure. Since the OWT's are typically designed for at least 20 years in the harsh offshore sea environment and exposed to millions of loading/unloading cycles it is an imperative to achieve a progress in having a better understanding about the contribution of soil damping which could eventually increase foundation structure lifetime and improve their safety.

- **Cost Reductions**

Potentially if the value of soil damping is increased, this could lead to more economic designs which is one of the current goals and imperative for the offshore wind industry in order to become even more competitive to other energy production technologies. Related to the above-mentioned fatigue life, after considering the soil damping increase, an improved design could yield smaller dimensions of the monopile structures which is again highly related to a potential cost-savings. This means that cost reduction can be found in less amount of steel within structure itself (e.g. reduced thickness or more shallow pile embedment depth). On the other side, smaller dimensions or decreased total weight of the components means that there could be more storage on the installation vessels or that a vessel with less capacity (e.g. crane capacity or installation vessel deck space) can be utilized which could lead towards more savings during the logistical/installation phase of the project. Moreover, a potential decrease in the monopile length leads to more time savings, since the installation with less monopile length naturally requires less time. This could be highly beneficial to increase the production rate since the time frame that can be spent in offshore sea environment is limited. Finally, a decrease

in installation time is more environment friendly due to fact that installation piling techniques can produce noise which could be harmful for sea animals.

From the above-mentioned reasons, it is clear that the soil damping mechanism requires more attention (in terms of research), the mechanism has to be understood well enough so it would be eventually implemented in the future offshore design codes and standards. A possible gain in knowledge which is related to the field of offshore geotechnics could be potentially utilized towards more reliable, durable and cost-effective design of offshore wind foundation structures.

1.3 Thesis Description

This subchapter will shed some light on the objectives which are expected to be answered upon conclusion of the thesis research. Continuing from the objectives, the formulation of the main research question can take place along with other sub questions which are interconnected to the main research question. Also, this subchapter will present the scope of the research along with its basic assumptions and limits. The approach is shortly explained by introducing the necessary steps which are related to the research methodology. Finally, the outline of the thesis report is presented where the chapters are briefly revealed to ensure that the reader knows what to expect.

1.3.1 Research Problem Statement and Objectives

Considering all OWT damping sources that are known, the soil damping source is still not understood well enough within the research community due its complexity and high uncertainty of soil medium. When talking about aims and expectations of this research, some objectives and problem question statements have to be formulated. From the thesis title, the main research question could be easily established. Going forward, the main research question can be supplemented and followed by multiple sub questions which are expected to be answered after the thesis is concluded.

What is the contribution of soil damping on offshore monopile under different loading scenarios?

Continuing on from the main question, a several sub questions can be formulated as they are directly related to the main one:

- What is the most suitable constitutive model to describe dynamic soil-structure behaviour under allowed research conditions and constraints?
- What are suitable loading scenarios or load tests necessary to estimate soil damping efficiently?
- What is the most appropriate method to estimate/measure soil damping from the Plaxis 3D output results?
- How boundary size, time step, and mesh quality are influencing the output Plaxis 3D results?

After concluding the main research questions and sub questions the focus can be redirected on the additional topics which are also closely related to soil damping and dynamic behaviour of offshore wind structures. Additional research sub questions can be seen below:

- What is the state of soil medium and its behaviour during cycling loading conditions?
- Is there an influence of loading rate on natural frequency degradation?

1.3.2 Research Scope and Methodology Approach

The main question is expected to be answered using the mentioned Plaxis 3D approach, where the software capabilities of this geotechnical FEM software will be used to model and simulate complex dynamic soil-structure behaviour. The results are expected to be presented in form of a percentage (percentage of energy dissipated from the foundation structure to soil medium which can be assigned to soil damping phenomena). The offshore soil damping topic can be considered as novel research, as only few studies are available; therefore, the results will be compared to other similar studies and research papers performed over the period of last few years.

Due to complexity and thesis time limitations, the research will be solely directed towards estimation of soil damping contribution on offshore monopiles, followed by couple sub topics which are highly linked to it. Other foundation structure options such as jackets or gravity base foundations will not be considered in this study. Modelling of the structure (monopile and tower) will be simplified and it will not include the transition piece which is used to attach and to connect two mentioned structures. Also, the model will be simulated in Plaxis as a half-space model since this modelling option allows for crucial time savings due to reduction in computational time.

The study can be undertaken on any soil medium but for this purpose only dense sand will analysed since the soil parameters were available as an input for the Plaxis HS small-strain soil model. For this reason, the estimated soil damping is specifically assigned to this type of soil. Regarding the flow conditions, the study will utilize drained approach since this is one of the model limitations which will be described in the HS Small Strain model subchapter (2.3.1 HS Small Strain Soil Model).

For the purpose of soil damping estimation there are different measuring techniques in both time and frequency domain. This study will consider only time domain technique since its application was more convenient way of estimation for the Plaxis output results.

Initially as a part of Plaxis constitutive soil model verification process, the thesis research will focus on the paper (Prendergast & Gavin, 2016) which deals with pile natural frequency and soil damping, therefore this is one of the reasons why the study also takes into consideration natural frequency which is also one of the crucial design factors in terms of Target Natural Frequency (TNF) and it also ensures the safety of the OWT structure during its lifecycle.

The research methodology will be consisted out of five main parts which were followed from the start of thesis research till its final conclusions. The central part of thesis work is placed in so-called steps 3 and 4 (see Figure 4), where the Plaxis HSS constitutive soil model is verified and compared with existing case study based on experimental data (Step 3), and later, once all verification conditions are met the simulations take place on the OWT foundation structure, where the soil damping contribution is estimated by means of simulating a dynamic soil-structure interaction between a monopile and dense sand soil (Step 4). Most of the research time will be spent on the Case I and II, since they require extensive and time-consuming numerical calculations in the Plaxis 3D software. In a nutshell, the methodology is briefly described in the following Thesis Outline (Subchapter 1.3.3), while the Figure 4 depicts a general process which was utilized in this study.

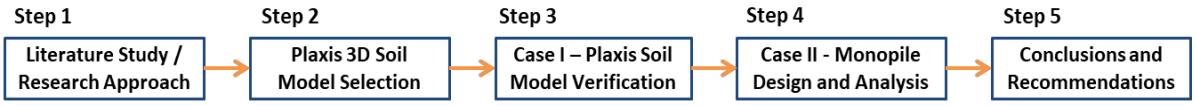

Figure 4: Thesis Research Methodology Divided into Five Essential Steps

1.3.3 Thesis Outline

The thesis report almost exactly follows the methodology steps which are revealed in the Figure 4. The only difference accounts for the Step 2 – "*Plaxis Soil Model Selection*", which is partially divided between theoretical part from the literature study and also implemented into Case I where the model characteristics are described further. The outline of the Thesis will be divided into five chapters which are as it follows below:

The current ***Chapter 1 – Introduction*** which provides some guidelines to the potential reader to get acquainted with the current trends, future plans and initiatives of the offshore wind industry. This chapter also elaborates on the research motivation, reveals the main and additional research questions and it justifies the reasons which are behind the choice of those questions. Furthermore, this chapter defines what will be the research scope covered by this study and also, what is equally essential what will not be studied.

In the ***Chapter 2 - Literature and Essential Theoretical Background*** the reader can find fundamental information which was studied and obtained in the literature phase but also during the course of the thesis project. This chapter is deemed crucial for performing the project which tends to tackle on the issues such as soil damping or natural frequency of monopile foundations. The chapter consists of the information which is related: to importance of estimation of OWT structure natural frequency, offshore damping sources and soil damping sources, constitutive soil modelling in Plaxis 3D, and damping estimation technique. It also deals with topics such as time and frequency domain techniques which are necessary for conversion of acceleration and displacement data. Finally, it describes the process of filtering which is crucial step when it comes to signal analysis.

Following from the theoretical part, the ***Chapter 3 - Case I – Blessington Piles Plaxis Model Verification*** deals with the first thesis "Case", where the capabilities of the Finite Element Plaxis 3D software are tested out on the presented case study. The Case I was a project milestone, since it served as a decision-making case where it was decided to advance forward to the Case II with utilization of the same soil model. Briefly describing, the Case I consisted of simulation which were employed to capture the pile response after the impact hammer force was applied on the pile head. The response was measured in terms of natural frequency and soil damping ratio, while on the other hand, the Plaxis 3D software was verified and confirmed as a handy tool for estimation of these mentioned responses.

The most important ***Chapter 4 - Case II – Monopile Design and Soil Damping Assessment*** deals with estimation of soil damping contribution on offshore monopiles. For this purpose, a simplified OWT structure was modelled in Plaxis 3D which was later utilized in numerical simulations by applying time-load scenarios coming from the wave and wind forcing's which are acting at the monopile-tower structure. The goal was to capture the dynamic response of the structure while the structure is in its free vibration phase. Some additional topics (stress-strain, natural frequency degradation) which are deemed beneficial were also covered by this chapter.

Finally, the last ***Chapter 5 – Conclusions*** wraps up the report and it also serves as connecting chapter which offers potential answers to the mentioned research questions established in the introductory part. In this chapter, the conclusions are drawn which were based on the conducted research project and its results. The chapter further elaborates and discusses the obtained soil damping values and it explains why it is not simple to establish a single value for soil damping. Lastly this chapter also provides some recommendations for future research but it also touches on the limitations of the conducted research.

Chapter 2 - Literature and Essential Theoretical Background

The second Chapter provides some necessary tools and information which are required to complete this thesis project. The relevant theory is briefly described and presented as needed. Most of the information focuses on concepts which are relevant to the OWT natural frequency and its various damping sources with focus on soil damping types. Furthermore, the relevant Plaxis constitutive soil models are described. Finally, the conversion techniques (frequency and time domain) are presented along with damping estimation techniques.

2.1 Importance of Natural Frequency

Offshore Wind Turbines are considered as lightly damped structures and its natural frequency plays an important role during the production life-cycle. OWT's are slender structures which are also dynamically sensitive; this happens due to fact that the external environmental forces (wind and wave) and mechanical loadings (rotor) are in close proximity to the overall structural natural frequency (Lombardi, Bhattacharya, & Muir Wood, 2013). If the structure as a whole system is not designed well and its natural frequency is not estimated accurately, then there is a high possibility of structural resonance with other dynamic (already mentioned) forces. The structural resonance leads to a dynamic amplification of response and it also develops larger stress amplitudes, therefore, the total fatigue is accumulated on a higher rate (Shirzadeh, Devriendt, Bidakhvidi, & Guillaume, 2013) and (Swagata & Sumanta, 2014).

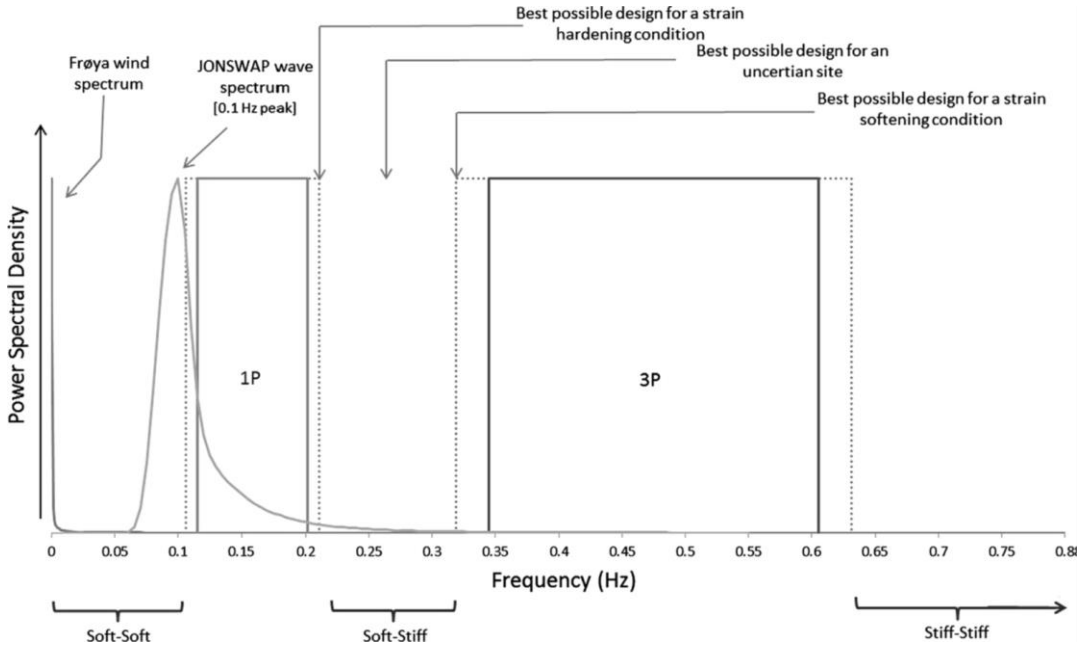

Figure 5: Forcing Frequency and OWT Positioning for Natural Frequency. Source: (Bhattacharya , et al., 2013)

From the Figure 5 it can be concluded that a potential designer has a variety of options available when it comes to deciding what should be an overall-global first natural frequency. In order to avoid resonance negative effects, the target natural frequency of the total structure should be apart from the 1P (rotor frequency) and 3P (blade passing frequency). Moreover, in the offshore wind design codes it is recommended to place the structure about 10% from the "undesired" forcing frequency regions (Det Norske Veritas AS, 2014). When considering natural frequency estimation, a potential designer shall take into consideration total structural system and therefore analyse soil – monopile –

tower interaction as a whole system, since this can have a major influence on a total response (Swagata & Sumanta, 2014). Considering serviceability and its loading conditions, the structure shall not pass 0.5° tilt or rotation, which is consisted of 0.25° for construction phase and other 0.25° for accumulation of permanent rotation (Det Norske Veritas AS, 2014). Soil stiffness plays an important role when it comes to natural frequency. The degradation of natural frequency (which includes accumulation of displacements, e.g. rotation 0.5° criteria) is highly related to change in the soil stiffness; this implies that the natural frequency is dependent on foundation (e.g. monopile) stiffness which is in turn also dependant on stiffness and strength of the surrounding soil (Lombardi, Bhattacharya, & Muir Wood, 2013). This frequency degradation happens due to numerous loading/unloading cycles which the soil medium is experiencing in interaction with the structure. Currently, the degradation of soil stiffness which happens in a certain time period is a consequence of series of cyclic loads (load/unload) and accumulated displacements or rotation; this issue is not considered in current design codes (Doherty & Gavin, 2011).

Usually, the designer has a choice which includes three different design approaches which can be seen in the Figure 5 (soft-soft, soft-stiff and stiff-stiff). So far, for the design purposes the most popular choice is the soft-stiff range which lies between 1P and 3P frequency. The stiff-stiff choice is the safest one, but it also requires a robust design which dramatically increases the price due to a large amount of steel in structural sections. The estimation of natural frequency ($f_{0\text{-}design}$) is often under-predicted and the study (see Figure 6) was conducted on natural frequency values for 400 OWT's founded on monopiles in different soil conditions which confirmed that a designed f_0 is in almost every case lower than the measured one (Kallehave, Byrne, LeBlanc Thilsted, & Mikkelsen, 2015). Some of the natural frequencies were more than 20% under-predicted in their design phase which implies that the industry needs more reliable techniques to tackle this issue.

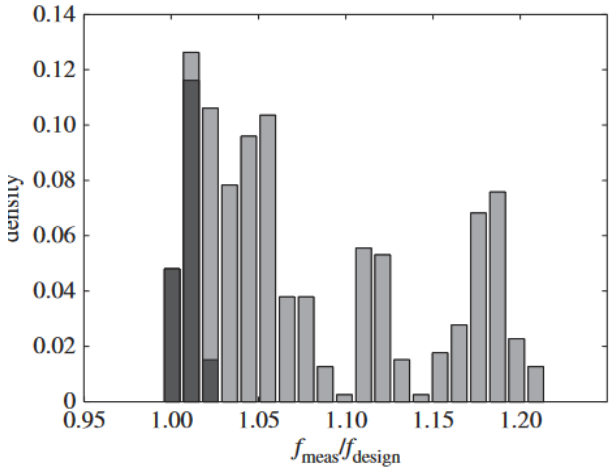

Figure 6: Measured and Designed f_0 Ratio. Source: (Kallehave, Byrne, LeBlanc Thilsted, & Mikkelsen, 2015)

To conclude, estimation or so to say, to be able to quantify both the natural frequency and damping values is crucial to improve the reliability and to increase the length of life-cycle of the OWT's (Shirzadeh, Devriendt, Bidakhvidi, & Guillaume, 2013).

2.2 OWT Damping Sources

Briefly explained, damping for the purposes of this thesis can be considered as a dissipation of the energy from the structure (in this case foundation – monopile) to the environment (in this case sand soil medium) which means that an analysis of Soil Structure Interaction is needed to assess this damping contribution. On the other hand, the offshore wind turbines can experience a combination of damping which originate from diverse damping sources. Moreover, the total system damping of OWT structure can be approximated as a linear combination of aerodynamic damping, hydrodynamic damping, structural damping, tower oscillation (sloshing) damper and finally soil damping (Damgaard M. , Ibsen, Andersen, & Andersen, 2013) and (Shirzadeh, Devriendt, Bidakhvidi, & Guillaume, 2013). The sum of these mentioned sources represents the total system damping which can be seen in the Eq. 1 and the total OWT damping can have a great range of values depending if the turbine is in the parked condition (1-3% damping) or in operational condition (7-10%) (Chen & Duffour, 2018).

$$\zeta_{total} = \zeta_{aero} + \zeta_{tower} + \zeta_{hydro} + \zeta_{struct} + \zeta_{soil} \qquad Eq.(1)$$

ζ_{aero} or aerodynamic damping source is a result of OWT foundation vibrations caused by interaction of wind turbine and forcing air acting on the structure. The vibrations of the OWT structural parts are very much related to the aerodynamic mechanisms of the total system (Shirzadeh, Devriendt, Bidakhvidi, & Guillaume, 2013). In production state, the OWT experiences a high portion of aerodynamic damping while during the parked condition (e.g. rotor stop test) the amount of damping is almost negligible which is convenient for assessment of other damping sources.

ζ_{tower} is the damping which comes from the tower oscillation damper. This is an additional part which is now standard piece of equipment integrated in the structure to reduce the vibrations. It is basically the mechanism which vibrates at similar natural frequency comparable to the system frequency. The spring in the damper absorbs the excitations and the damper takes the energy are basically it converts it into heat energy (Stewart, 2012). Usually, the damping in the tower sections has a high amount of damping and in some studies, it was estimated as high as 1.36% (Damgaard, Ibsen and Andersen, 2012).

ζ_{hydro} is the hydrodynamic damping which comes from two sources: one is product of wave radiation and the other one is viscous damping due to hydrodynamic drag. The drag force which is proportional to velocity is almost neglected due to low velocity of the foundation structure and the wave radiation has a larger influence since it is proportional to relative velocity. In some studies, the hydrodynamic damping was assessed in a range between 0.07% to 0.23% (Arany L. , Bhattacharya, Macdonald, & Hogan, 2016) and in similar studies such as (Damgaard, Ibsen and Andersen, 2012).

ζ_{struct} or structural damping is the dissipation of energy through structural steel sections in form of heat transfer. Usually, this value increases if the number of connections increases (welded joints and grouted connections). In this study it is adopted that the value of structural steel damping is equal to 0.19% which was reported in many previous studies such as (Damgaard, Ibsen and Andersen, 2012), (Swagata & Sumanta, 2014) and it is implemented in the Eurocode (EN 1991, 2005). Although, the values from 0.15% to 1.5% can be expected (Arany L. , Bhattacharya, Macdonald, & Hogan, 2016) in this study it is assumed that the structure is modelled in a simplified manner, which means without joints, connections or the transition piece which has a grouted connection. All those connections could be a potential source of additional damping, therefore with omitting them, it is possible to assume such a low damping value for structural steel sections.

This concludes all possible damping sources in the OWT structure however, the focus of the study is soil damping source, therefore the following subchapter is dedicated for further insight into this mechanism.

2.2.1 Soil Damping Sources

With usage of advanced numerical methods, the other damping sources can be estimated with a decent level of accuracy while soil damping is still the most uncertain damping source in the OWT case. Typically, soil damping is neglected and its "contribution" to other damping sources is often not included in the design calculations due to non-existing methodology in the current design guidelines such as DNV-GL (Carswell et al., 2015). To get a better understanding of soil damping contribution it can be further divided into three separate mechanisms: viscous damping, hysteretic damping and radiation damping.

In the case of offshore wind, ***viscous damping*** is considered to be a saturated problem since it is submerged by the sea water. In this soil-water interaction the water fills the voids between sand particles and this can cause viscous damping force on the foundation structure. These forces can happen due to a monopile movement which is forced by the external forces. Moreover, viscous damping is velocity and frequency dependant but it does not depend on strain level (Brinkgreve, Kappert, & Bonnier, 2007). It is a common thing to use viscous damping to capture damping at small strains and low load frequency which is using the first natural mode (Bayat, Andersen, & Ibsen, 2015). In the Plaxis 3D formulation, viscous damping (Eq. 2) can be obtained by means of Rayleigh damping which includes a damping matrix *C* and additional two matrices for mass (*M*) and stiffness (*K*).

$$C = \alpha \cdot M + \beta \cdot K \qquad Eq.(2)$$

Where parameters α and β are the Rayleigh coefficients for mass and stiffness. Usage of Rayleigh damping formulation provides an effective frequency dependent damping but the user has to carefully choose relevant frequency modes to capture ground motion response in desired period and frequency range (Hashash & Park, 2002). It was reported that viscous damping is negligible for frequencies below 1 Hz, which is the case in the offshore wind (Arany L. , Bhattacharya, Macdonald, & Hogan, 2016).Therefore, due to complexity of setting up Rayleigh target frequencies and potential small contribution of viscous damping, this type was not considered in the study.

The second type of soil damping relates to ***hysteretic damping*** or also called material damping where the energy dissipation is caused by the friction of the system with its surrounding environment. In the case of offshore environment, the energy dissipates by the friction in the granular structure of the soil which is a hysteretic loss (Versteijlen, 2011). Unlike viscous damping, the hysteretic damping is frequency independent but it depends on the strain level of the soil and it is also affected by the loading history (Aasen, Page, Skau, & Nygaard, 2017). Hysteretic damping can be captured through hysteretic loading-unloading cycles if a non-linear soil model is used (Hashash & Park, 2002) and these loading-unloading cycles are more known as hysteresis loops which can be seen in the Figure 7, where the stress-strain curves are used to represent loading-unloading cycles. The area enclosed within the

loop represents an amount of energy lost in a single loading cycle (ΔW). A damping ratio (D) which is typically calculated from these loops, it simply represents the amount of energy which is lost per loading cycle divided by the maximum stored energy in the system (W). In offshore environment it is considered that the largest (and almost only) contribution to soil damping comes from the hysteretic damping (Page, Skau, Jostad, & Eiksund, 2017). In the Plaxis 3D, the HS Small Strain constitutive model is capable of describing this soil behaviour.

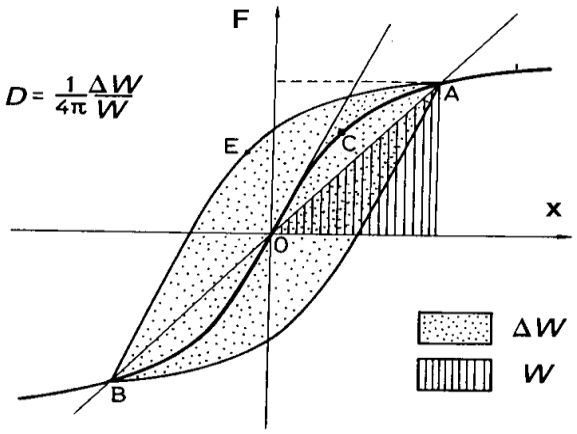

Figure 7: Hysteresis Loop and Energy Dissipation. Source: www.researchgate.net

The last soil damping source relates to ***radiation damping*** or also known as geometrical damping. In this case, the energy dissipation occurs due to elastic waves spreading across the soil volume surrounding the monopile. This type of damping is frequency dependant and it can be considered in problems where the loadings occur on a higher frequency level. In the case of offshore wind monopiles, this type of damping is typically not considered because its contribution to the total damping is of little significance and therefore negligible. More specifically, when the loading frequency of wind and wave loadings is below 1 Hz (which is the case in the offshore wind environment) then this type of damping can be neglected (Carswell et al., 2015), (Arany L. , Bhattacharya, Macdonald, & Hogan, 2016) and (Aasen, Page, Skau, & Nygaard, 2017).

2.3 Structural Dynamics and Plaxis Constitutive Soil Models

Before describing the potential constitutive soil models, it is essential to emphasize the dynamic behavior since these types of simulations will be undertaken as a part of the thesis project, therefore it is beneficial to briefly describe how dynamics equations are solved in the Plaxis software environment. In the Eq. 3 it can be seen that the structural systems which have dynamic behaviour in time dependent problem are described by the differential equation, which is here presented in form of matrices and vectors:

$$[M]\,\underline{\ddot{u}} + [C]\,\underline{\dot{u}} + [K]\,\underline{u} = \underline{F}(t) \qquad Eq.(3)$$

Where the M is the mass matrix (soil, water or any construction), C is the material damping matrix (described in the Eq. 2) and the K is the stiffness matrix while the F is the force vector. On the other side $\ddot{u}$, $\dot{u}$ and u are the acceleration, velocity and displacement vectors respectively, which can vary over time. The above-mentioned equation is solved in the dynamic Plaxis iterations for every time step. It has to be mentioned that damping matrix C depends on its input parameters - Rayleigh coefficients (α and β).

A structure experiences damping to some certain degree and the damping can have an influence on the undisturbed (Eigen) natural frequency of the structure. The Eq. 4 (Chopra, 1995) describes this relation where ω_0 is the Eigen frequency and the ω_d is the damped frequency, while the ζ is the

damping ratio. Typically, the offshore monopiles are considered to be underdamped structures, which means that the ζ is between zero and one.

$$\omega_d = \omega_0\sqrt{1-\zeta^2} \qquad Eq.(4)$$

In the last decade, FEM software simulations are used on the large scale, especially for the design and testing of offshore foundation structures such as monopiles which are exposed to an external environmental loading. The usage of FEM decreases the potential cost expenses which are attributed to the real physical/experimental testing. For this thesis project, Plaxis 3D is utilized as the FEM package, therefore various options are available which are associated with soil constitutive models. There are many soil models integrated in the Plaxis, but only the few are capable of describing cyclic soil-structure behavior realistically. Initially, few soil models were considered as potential candidates for the final analyses but only the one was chosen to proceed with. Mohr-Coulomb and Hardening Soil models were discarded since they do not take into account small-strain stiffness. As another option, the Hypoplastic soil model with intergranular strain was considered and this model is implemented in the Plaxis as user defined model, therefore it is not a standard one. The model is considered as one of the most advanced ones which are available, since it accounts for small strain stiffness, anisotropy, it describes the non-linear behavior well and it accounts for soil state dependency. The model considers two state variables which are the Cauchy stress (T) and the void ratio (e). In the Eq. 5, the term $\dot{T}$ is the stress rate tensor, F is the tensor function which highly depends on the variables (stress and void ratio), while D is the stretching rate.

$$\dot{T} = F(T, e, D) \qquad Eq.(5)$$

On the other side the Hypoplastic model has very complex input parameters which are not easily obtained. Some of the model parameters are three pressure dependent void ratios, various material constants or the granular hardness parameter. Considering the complexity of the model, the expertise of the geotechnical professionals was considered in order to get an advice regarding suitable soil model. The limitations of the Hypoplastic model had to be discussed, and this is mostly related to the complexity of the model and its difficulty to be applied with proper parameter calibration; on the other side, the undrained behavior is not well described (Brinkgreve R. , 2018). The limitations were discussed in the personal communication with Dr. Ronald Brinkgreve and after weighing the positive and negative sides it was decided to proceed with the Hardening Soil model with small-strain stiffness which will be described in the upcoming subchapter 2.3.1.

Prior continuing onto HS Small Strain model, the study was made which considered both the Hypoplastic and HS Small Strain model combined with the simulations on the monopiles (Sheil & McCabe, 2016). The mentioned study concluded that the HS Small Strain is not describing well the monopile behavior when the loading is applied from multiple directions and in this thesis project only the co-directional loading (application of wave and wind load from same direction) is applied. In the Figure 8, it can be seen that both models gave a reasonable output results in terms of their hysteresis loops, which means that the cyclic loading is well captured.

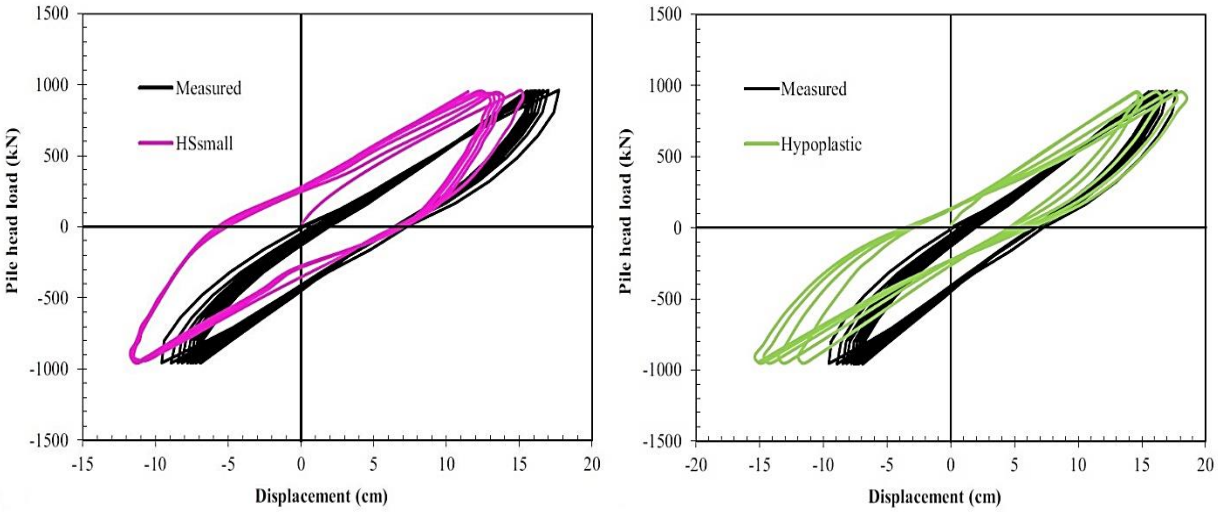

Figure 8: Comparison between measured and predicted load-displacement responses for both models: (Sheil & McCabe, 2016)

2.3.1 HS Small Strain Soil Model

When considering the behaviour of the large-diameter monopiles some crucial factors should be considered when the appropriate model is being chosen. Nowadays, the monopiles are getting larger in terms of their diameter which means they are capable of mobilizing more lateral resistance from the soil, moreover it is essential to describe well this non-linear response which happens in multiple loading cycles. In this case, the accumulation of plastic deformations in the soil can trigger plastic displacements and rotations which result in a non-linear load - displacement structural response (Aasen, Page, Skau, & Nygaard, 2017). Another factor that should be considered is the different stiffness value for loading, unloading and reloading cases since the soil shows different stiffness behaviour in each of those mentioned cases. Last factor that should be considered is damping and in the case of offshore monopiles only hysteretic damping can be considered. All of those mentioned factors are well described by the HS Small Strain model and therefore this model was chosen as the suitable one for the thesis simulations. The HSS model was also utilized in the other papers such as the one from (Aasen, Page, Skau, & Nygaard, 2017) where it was concluded that the HSS model was the most suitable approach for lateral and cyclic loading of monopiles since it accounted for different stiffness (depending on loading conditions) and non-linear hysteretic behaviour. On the other side, a perfect model which can satisfy all the conditions necessary to describe soil-structure behaviour to the finest detail does not yet exist. The drawbacks of the HSS model can be found in the fact that the model is not capable of accumulating the irreversible volumetric strains and also the pore water pressures (PWP) cannot be accumulated. Although the model itself does not allow for accumulations of the PWP, in the boundary value problem (such as monopile simulation) it will accumulate PWP's and plastic strains to some extent (Brinkgreve R. , 2018).

The HS Small Strain is basically a continuation of the Hardening Soil model. The HSS was a necessary extension of the Hardening model in order to deal with high stiffness values that soils show when exposed to small strains (Brinkgreve, Kappert, & Bonnier, 2007). The model was proposed by the PhD thesis research (Benz, 2006) and it was extensively verified before it was implemented in the Plaxis software environment.

The Hardening soil basically assumes that soil behavior in unloading and reloading cycles is elastic but actually the strain range where the soils are considered completely elastic is very small. An increase

of strains leads to nonlinear soil stiffness decay and this can be seen in the Figure 9 which represents a stiffness reduction curve (Plaxis BV, 2017).

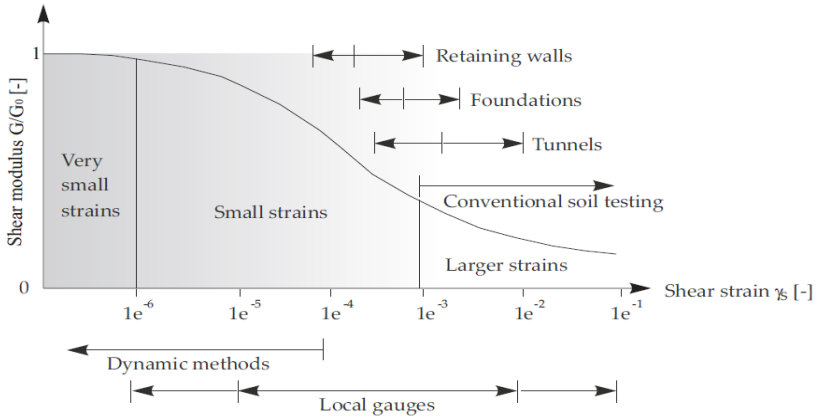

Figure 9: S –Shaped stiffness and strain behaviour of soils. Source: (Plaxis BV, 2017)

The HSS model is an overlay of the Hardening model and they share almost the same soil parameters; the only difference is in two additional small-strain parameters, namely: initial small strain shear modulus (G_0) and the shear strain level ($\gamma_{0.7}$) at which the secant shear modulus (G_s) is reduced to the value of 70% of G_0. In the case of small strains, the stress-strain curve can be sufficiently characterized by the simple hyperbolic law which was proposed by (Hardin & Drnevich, 1972) and in Plaxis, the decay of the secant shear modulus (G_s) depends on the value of shear strain which can be seen in the Eq. 6, where the combination of $\frac{\gamma}{\gamma_{0.7}}$ and factor 0.385 gives the ratio of $\frac{G_s}{G_0}$ of 72.2% (reduction of G_s) (Plaxis BV, 2017).

$$G_s = \frac{G_0}{1 + 0.385\left(\frac{\gamma}{\gamma_{0.7}}\right)} \qquad Eq.(6)$$

The decay in small-strain stiffness is related to the loss of intermolecular and surface forces in the soil skeleton. From the Figure 5 it can be seen that the stiffness can be reduced by the shear strains reaching far into plastic domain (large strains). In the case of the HSS model, the stiffness reduction, which is a product of plastic strains follows the strain hardening procedure. The small strain stiffness reduction curve has a certain lower limit which limits further degradation of stiffness, therefore this cut-off limit is determined by tangent shear modulus (G_t) which is a derivative of G_s with respect to the shear strain (γ). The lower stiffness cut-off value of the G_t is introduced at the unloading-reloading stiffness G_{ur} (Plaxis BV, 2017).

$$G_t = \frac{G_0}{\left(1 + 0.385\,\frac{\gamma}{\gamma_{0.7}}\right)^2} \qquad Eq.(7)$$

The cut-off shear strain value $\gamma_{cut\text{-}off}$ can be also calculated with the Eq. 8 and the whole lower cut-off stiffness concept is depicted in the Figure 10.

$$\gamma_{cut-off} = \frac{1}{0.385}\left(\sqrt{\frac{G_0}{G_{ur}}} - 1\right)\gamma_{0.7} \qquad Eq.(8)$$

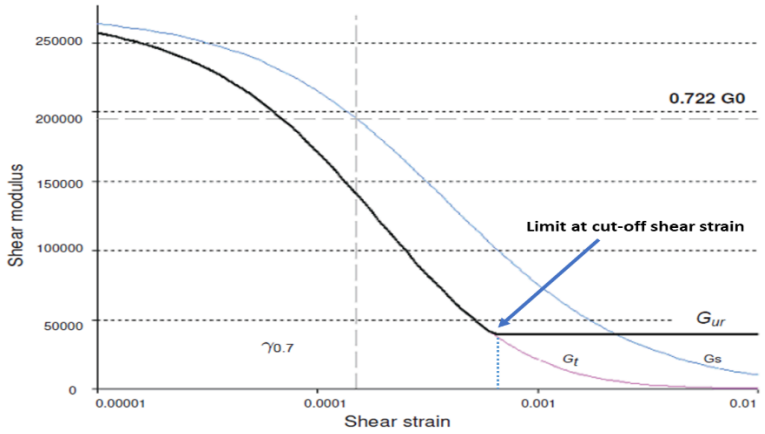

Figure 10: Secant and Tangent modulus reduction curve and cut-off. Source: (Plaxis BV, 2017)

From the Figure 10 it can be concluded that for shear strains larger than cut-off shear strain ($\gamma_{cut\text{-}off}$) the unloading-reloading stiffness is used further, and if the strains are low, then the tangent stiffness is utilized.

The crucial part for the thesis research lies in the hysteretic damping capabilities of the HSS model which happens when the soil experiences cyclic shear loading. When the soil is exposed to first loading cycle, the soil small-strain stiffness (G_0) will reduce with increase in shear strain and upon load reversal this stiffness will be taken back to the initial G_0 and then again further reduce until the new load reversal. The hysteretic damping was already depicted in the Figure 7 which represents typical hysteresis loop and explains the energy concept and dissipation of energy from the loop. In the HSS model, the damping value is applied only when the material behavior remains elastic and the shear modulus is decreased by the small strain formulation; if the G_{ur} is reached the damping value will not increase (Brinkgreve, Kappert, & Bonnier, 2007). Another thing to note is related to the loading frequency, which does not have an effect on the damping value since the model is based on the stress-strain relation, which are in this case purely time independent (Brinkgreve, Kappert, & Bonnier, 2007). Further in the following Chapter 3 the soil model parameters will be mentioned and the derivation of additional small strain parameters is elaborated.

2.4 Output Signal Processing

Short but quite relevant chapter of the thesis is related to processing the output signals (either from experimental data or Plaxis 3D output). In the real-world applications, the most used device to capture the dynamic response of structures is an accelerometer transducer which is in the case of a pile usually placed on the pile head. The structural dynamic motions of a system produce a complex signal patterns and these output signals are usually a sum of different harmonics, periods, amplitudes and wavelengths (Versteijlen, 2011). In the structural vibrations, the main purpose of the signal analysis is to obtain relevant information on amplitudes, natural frequencies, etc. (Han, 2010). In the case of this thesis project, the purpose of the signal processing leads to recovering pile displacements from experimental acceleration data sets and also to analyse the signals in frequency domain and then reduce the impact of the other non-dominant frequencies by means of filtering. The goal of this displacement signal recovery is to produce a decent displacement signal so the numerical data from the Plaxis 3D can be compared and verified with experimental data sets.

Two most common techniques which are used to recover displacements from acceleration data are direct double integration of acceleration which relates to *time domain* and the other one is applying a Fast Fourier Transform (FFT) to acceleration data and this one relates to *frequency domain* technique. According to (Han, 2010), there is a guideline which can be followed in order to choose a proper technique for signal processing and recovery of displacements. The guideline says that the time domain should be used when the Nyquist frequency of the signal is much higher than the highest frequency of the signal analysed, otherwise the frequency domain (FFT) technique is preferred. Moreover, according to (Han, 2010) these conditions are rarely satisfied in the real-world situations due to signal leakage, high-frequency and low-frequency component in the signal. These mentioned issues occur almost in every vibration measurement and the choice of the appropriate technique should be analysed well. The Nyguist frequency can be calculated from the following Eq. 9, where Δt represents time step length between two measured data points; briefly explained, the Nyquist frequency equals one half of the sampling frequency.

$$f_{ny} = \frac{1}{2 \cdot \Delta t} \qquad Eq.(9)$$

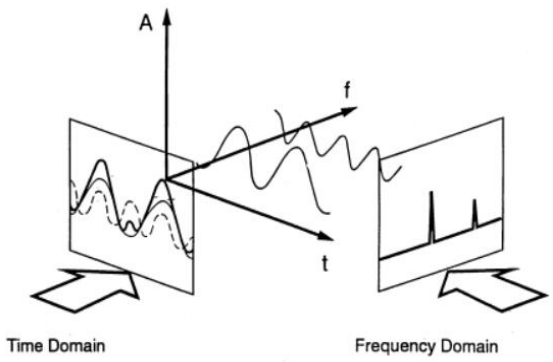

Figure 11:Time and Frequency domain. Source: masters.donntu.org

2.4.1 Time Domain Approach (Numerical Integration)

A time domain technique can be utilized for signal processing and recovery of displacements. This can be done by twofold numerical integration due to inherent integration relation which involves acceleration, velocity and displacement (Yang, Li, & Lin, 2006). Basically, the acceleration signal undergoes first set of integration which converts the signal into velocity and the second integration yields displacement. The procedure is described with the following Eq. 10 and 11 where *a*, *v* and *u* represent acceleration, velocity and displacement respectively.

$$a(t) = \int_0^t v(t) \cdot dt \qquad Eq.(10)$$

$$u(t) = \int_0^t v(t) \cdot dt \qquad Eq.(11)$$

Generally, the time domain technique yields unrealistic drifts in derived displacements (Yang, Li, & Lin, 2006). The Trapezoidal Method of integration was utilized in this thesis and it did not provide the desired results and this could be due to numerous issues such as that the constant value cannot be recovered while integrating (approximation error accumulating). Also, according to (Yang, Li, & Lin,

2006) time domain procedure may bring potential problems of numerical instability because the technique involves a double integration along with application of low-pass filter on the acceleration data and then again the application of high-pass filter on the recovered displacements; the combination of these factors could lead to potential unsatisfactory results which was the case in this thesis research.

2.4.2 Frequency Domain Approach (FFT)

The second technique utilizes a frequency domain approach which involves an application of Fast Fourier Transform. This highly beneficial operation takes the information about frequency (from a time domain signal) and then it transforms this information to the frequency domain. The end result can be seen in terms of a Power Spectral Density (PSD) graphs which represent all the frequencies from the time signal (with dominant frequencies having amplitude peaks), based on this information a potential user can see if the signal has high or low frequency components and therefore it can proceed forward with filtering techniques in order to remove unwanted frequencies which are usually source of noise in the signal. The approach which was utilized in this thesis was so-called Omega Arithmetic (Mercer , 2006) and (Kupfer, 2018). Since we are dealing with frequency, a Greek (omega) character is used which represents radians and of course in order to convert this to Hertz we utilize a relation $\omega = 2\pi f$. The Omega Arithmetic involves operations and manipulation with omega (ω) and therefore comes the name of this technique. In order to understand the approach first we represent displacement *u(t)* and acceleration *a(t)* in terms of Fourier Transforms which are U(ω) and A(ω) (Kupfer, 2018).

$$u(t) = \int U(\omega) \cdot \exp(i\ \omega\ t)\, d\omega \qquad Eq.(12)$$

$$a(t) = \int A(\omega) \cdot \exp(i\ \omega\ t)\, d\omega \qquad Eq.(13)$$

Due to fact that the acceleration and displacement are related (*a(t)* is the second derivative of the *u(t)* or $a(t) = \frac{d^2}{dt^2}u(t)$) it is possible to get the following Eq. 15 which was achieved by combining Eq. 13 with Eq. 14.

$$a(t) = \int -\omega^2 U(\omega) \cdot \exp(i\ \omega\ t) d\omega \qquad Eq.(14)$$

$$U(\omega) = -\frac{A(\omega)}{\omega^2} \qquad Eq.(15)$$

This means that the Eq. 15 can be used in order to recover displacements from the acceleration data by just taking an FFT of acceleration data and dividing the acceleration *A (ω)* by the omega factor *(-ω ^{2})*. Following this procedure, an inverse Fourier transform (IFFT) can be utilized in order to return the obtained displacement signal back to the domain of interest which in this case is the time domain. Another thing to emphasise relates to fact that the displacement signal components scale inversely with the square of their frequency (Mercer , 2006). Because of this relation it can be concluded that the displacement signal is dominated by the low frequency components and this becomes an issue because the low frequency components distort the converted displacement signal, therefore an application of a high-pass filter is inevitable to get a true displacement signal. The whole procedure of conversion from the time domain to frequency domain which is utilized for converting the

acceleration to displacements is depicted in the following Figure 12 which follows all the necessary steps.

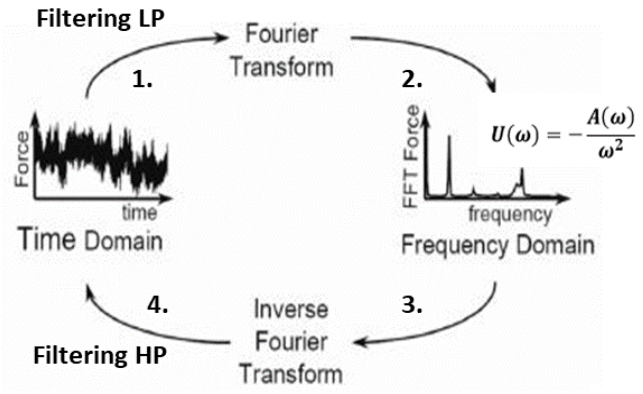

Figure 12: Utilization of FFT and IFFT to convert acceleration to displacements.

2.4.3 Signal Filtering Basics

Signal processing has an important role in the thesis project due to multiple attempts to recover displacements from experimental acceleration data; moreover, there are other signal outputs which require filtering in order to get smooth signal amplitudes. Usually, the measurements obtained with accelerometer device produce some noise components and this can be due to internal structural resonance (this is a high frequency noise) in a transducer. Another reason can be found in the impulse force, which is applied to the pile (during impact pile testing) which induces localised deformation in the close vicinity to the impact point (Prendergast & Gavin, 2016) and therefore produces high-frequency noise.

In order to take care of the abovementioned issues, there is a need to introduce filtering techniques and most common one includes Infinite Impulse Response (IIR) which are most efficient because they meet the specifications with much lower order compared to the Finite Impulse Response filter (FIR) (MathWorks, Inc, 2018). There are multiple types of filters and the popular ones are Butterworth, Chebyshev (T1 and T2) and Bessel. Butterworth seems to be most common one and it is used in this thesis as well; it has a flat band response which has no ripple in the signal, therefore it produces a smooth response in both passband and stopband. The typical increase in order can be seen in the Figure 13a which shows how the Butterworth filter behaves after the chosen cut-off frequency point. Increase in order also requires more computational time. A simplified explanation for dealing with low and high frequency components in the signal can be seen in the Figure 13b where the low pass filtering means getting rid of high-frequency noise and vice versa for high pass filter. The MATLAB programming environment is used for the application of filtering and some appropriate filtering examples can be seen in both Case I and II where the importance of filtering is confirmed.

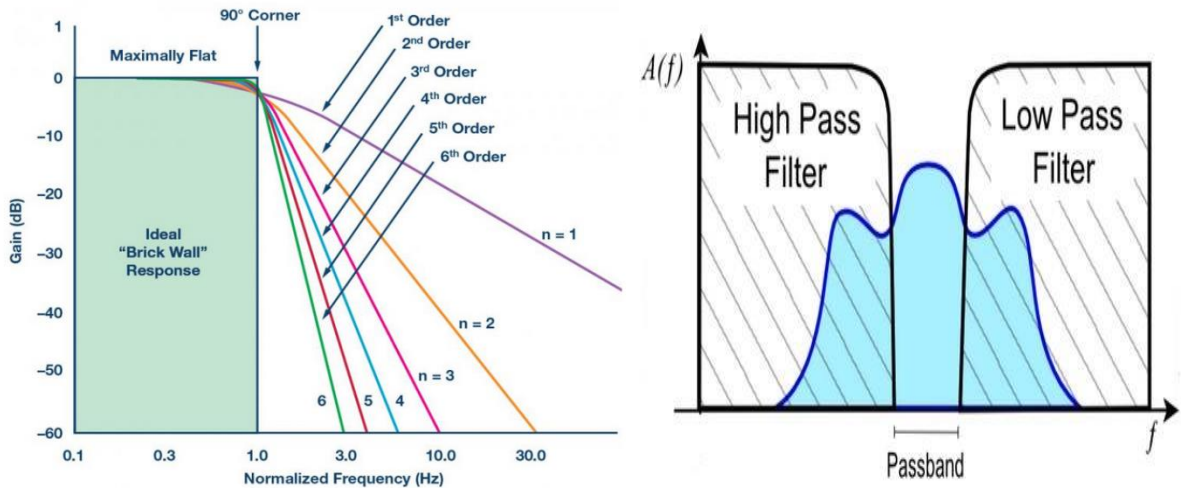

Figure 13: a) Increase in the Filter Order. Source: www.ecnmag.com b) Application of LP and HP filters. Source: en.wikipedia.org

2.4 Damping Estimation Technique – Logarithmic Decrement Method

The damping value can be estimated in both frequency domain and time domain. In the real experimental tests, the vibrations are usually recorded with accelerometers or some strain gauges which are capable of recording acceleration or displacement response. According to (Versteijlen, 2011) the identification and estimation of damping is not always a straight forward and it can be ambiguous process. Every technique has its negative sides and sometimes the estimation could lead to subjective results. The typical technique related to the frequency domain estimation is called half-power bandwidth method, which can be used to estimate damping on multiple frequencies which can be shown in the obtained FFT signal. The potential error can be found in the fact if the wrong frequency peak is chosen which could be the case if there is noise in the signal and other frequencies are showing up.

For this thesis research it was chosen to proceed with time domain technique which leads to the utilization of logarithmic decrement method. This technique is limited to assessment of only one frequency which in this case is the dominant natural frequency of the monopile foundation structure. If the other frequencies show up (e.g. 2nd bending frequency), they can be properly filtered out with usage of low pass filter. The method is quite straight-forward and its application is simple. The logarithmic decrement method was already used in the previous studies such as (Carswell et al., 2015) and (Versteijlen, 2011).

Underdamped systems such as the ones in the Case I – Blessington Piles and later in the Case II – Monopile Design which are described by some pile response (e.g. acceleration, velocity or displacements recorded at the pile head level) in a time domain can utilize the logarithmic decrement method for estimation of damping ratio. The method works well for the values of damping ratio up to 50%, therefore it is suitable for damping estimations of both Blessington Piles and true size monopile. The logarithmic decrement (δ) is described by the Eq. 16 where A_0 is the initial amplitude of interest and A_n is the final amplitude of interest which is n time periods apart from the initial amplitude.

$$\delta = \frac{1}{n} \cdot \ln\left(\frac{A_0}{A_n}\right) \qquad Eq.(16)$$

Since the soil damping ratio is a function of logarithmic decrement, the value of δ from the Eq. 16 can be utilized further to estimate soil damping ratio (ζ) which can be calculated from the following Eq. 17:

$$\zeta = \frac{1}{\sqrt{1 + \left(\frac{2 \cdot \pi}{\delta}\right)^2}} \qquad Eq.(17)$$

As a way of checking the damping ratio found from the logarithmic decrement method it is possible to use an exponential decay curve which should (in most cases) fit on the amplitude peaks in the desired time range if the damping ratio is correctly calculated. The decay curve can be seen in the Figure 14 (dotted line) and it is described by the function which can be seen in the Eq. 18 where the parameter *A* represents initial amplitude and ω_n which is a natural frequency of a pile in radians per second.

$$u(t) = A \cdot exp^{\ -\zeta \cdot \omega_n \cdot t} \qquad Eq.(18)$$

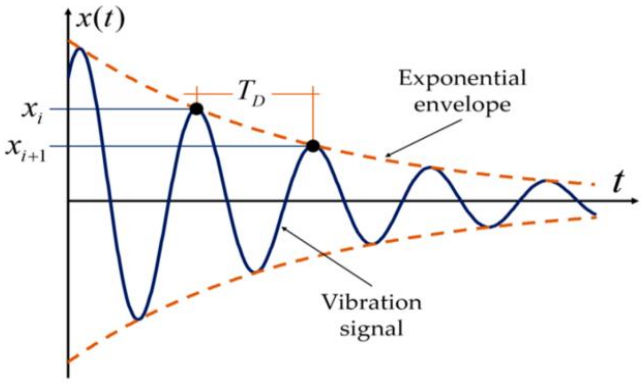

Figure 14: Logarithmic Decrement and Decay Curve. Source: www.mdpi.com

For the soil damping calculation purposes, the Plaxis 3D output in terms of displacements and accelerations in time domain was post-processed using a simple Matlab code for graphing and equation-setting purposes. An automated code in Matlab was developed which allows the user to pick a certain points of interest (amplitudes A_0 and A_n - depending how many amplitudes are chosen) and then to export that amplitude information to workspace (called "cursor-info") where the logarithmic decrement equations utilize that information for calculation of soil damping ratio by means of calculating the value of logarithmic decrement, establishing the decay curve u(t) and finally providing the estimate of soil damping ratio. For this technique the mean value of logarithmic decrement is used, which means that the logarithmic decrement is calculated for every two neighbouring amplitude peaks and then in the end, the final value of logarithmic decrement is averaged out and used for the final soil damping value estimation. The Matlab code, which was utilized for the logarithmic decrement damping estimation can be found in the Appendix B – Logarithmic Decrement Code.

Chapter 3 - Case I Blessington Piles and Plaxis Model Verification

The main purpose of the Case I is to test and verify the HS Small Strain model which will eventually lead to meaningful damping related simulations further in the Case II. For this verification process, a suitable case study was chosen in order to compare the Plaxis 3D simulation output results with real experimental data related to the two main research objectives of this thesis research, namely: natural frequency and soil damping. The following Figure 15 represents the general workflow which was followed in order to reach the desired outcome of this verification process. The workflow consists of three main steps which are briefly explained here and then they will be justified more further in this chapter. The first one is related to general calibration of the HSS soil parameters and remaking the model (Blessington Case model) in the Plaxis 3D. The second step relates to the 3D simulations which were done with Plaxis 3D, where the optimal mesh and time step was chosen. In the last step the output results were analysed and compared to the experimental data.

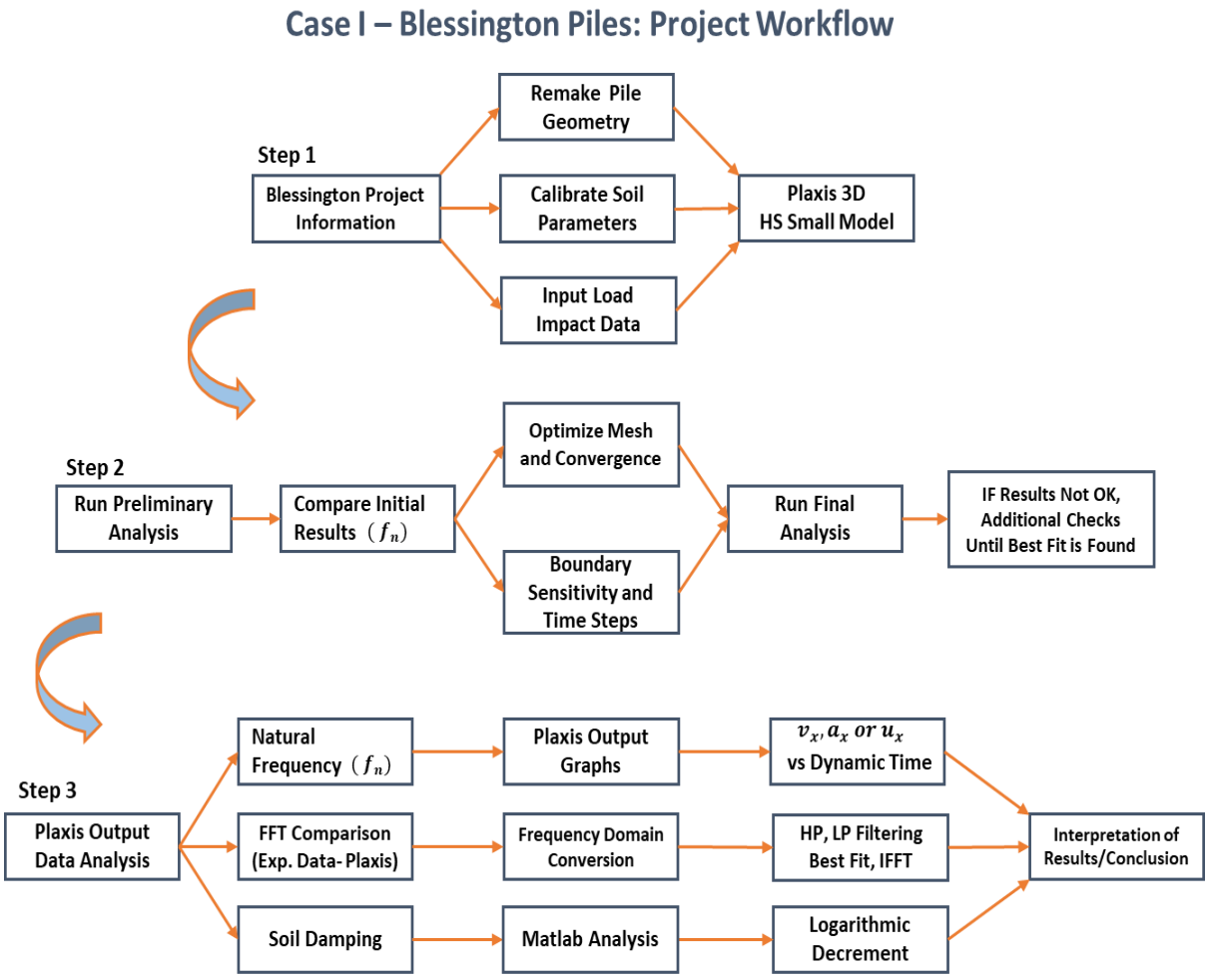

Figure 15: General workflow followed for the Case I - Blessington Piles

3.1 Purpose and Verification Goal

After a suitable constitutive soil model was finally decided to be used for the Plaxis 3D analyses, the research continues onto first case which will serve as a verification of the Plaxis 3D HS Small Strain model. The main purpose is to verify that the HSS soil model is capable of describing the cyclic loading and the behaviour of the monopiles with a decent accuracy. With a monopile behaviour, it is meant to describe the free vibration phase, when all the environmental loads are cut off and the monopile interacts with the soil. This free vibration is manifested with the decay of the displacement amplitudes over some certain time period and this shows an important information which is of particular interest (soil damping and natural frequency). Due to these research goals, it is necessary to verify the Plaxis HSS soil model before it is further tested on the true size monopile. Moreover, without the verification, the research would not have any concrete proof that this kind of simulations are relevant and credible. Although the Plaxis is quite user-friendly software it has to be used with care and certain knowledge, otherwise it is like a black box and the incorrect results could be a direct consequence of the potential user's mistakes.

3.2 Blessington Project Background

The Case I – Blessington Piles is based on the research project from (Prendergast & Gavin, 2016) and the main focus of this paper was to describe and simulate the dynamic soil-structure interaction, which is currently the area of many research projects worldwide. The paper serves as the perfect verification tool, since a meaningful comparison between experimental data and Plaxis simulation output can be achieved. The experimental research was conducted on two installed piles with different length over diameter (L/D) ratios to examine the effect of pile slenderness on the measured and predicted response of piles. The mentioned piles were exposed to the pile impact (loading) and then the free vibration was recorded in order to capture the natural frequency and damping response. Following the experimental field tests, the piles were also analysed with different theoretical approaches (implemented into a numerical Matlab code) in order to estimate pile's natural frequency.

Additionally, one of the authors had another research on the same test site which is called "Blessington Sand" and in his research Hardening Soil parameters were utilized in the Plaxis simulations, which meant that the soil parameters can be used for this research as well (Tolooiyan & Gavin, 2011). The only thing which had to be added leads to additional two small-strain soil parameters which were obtained using references and soil parameter relations (explained later in the chapter).

3.2.1 Pile Specifications and Experimental Information

In order to develop a representable model in the Plaxis 3D, the Blessington piles had to be modelled according to the paper from (Prendergast & Gavin, 2016). In this field test, two steel piles were tested at the Blessington Sand site with each of the piles having different L/D ratio. Both piles had a diameter of 340 mm and were driven to an embedment depth of 7 m. Following the installation, the sand around the Pile 1 and Pile 2 was excavated in order to get on desired L/D ratios, and the final slenderness ratios were equal to 13 and 9 respectively. The field test layout and geometry for both piles can be seen in the following Figure 16 where all the lengths, experimental equipment locations and sections with diameter and thickness sizes are shown in detail.

For the field test, three accelerometers were fitted near the pile head (Campbell Scientific CR9000x Datalogger was the accelerometer type) which were programmed to record and take samples at 1000 Hz sampling frequency. In the field test they have concluded both ambient and impact vibration testing, but for purposes of this paper only the impact test is considered for the estimation of natural pile frequency and soil damping at small strains since they are much more relevant to the research due to impact force being applied.

The impact test was performed by applying an impulse force to each pile using a calibrated modal hammer and measuring the dynamic structural output in terms of pile acceleration response. The hammer used for this experiment was the 086D50 model manufactured by the PCBPiezontronics. The hammer was calibrated to excite low frequency resonances by fitting its soft impact tip to the heavy impact head. Multiple experimental impulse tests were conducted in order to ensure repeatability of the results. For the calculation purposes, values from the impulse impact test were obtained and the force applied from a modal hammer was recorded. On the Pile 1 the applied force was in order of 14.48 kN and for the Pile 2 the force was 13.75 kN. The hammer impact was quite short and it lasted for approximately 0.01 seconds which was meant to produce a short impulse on the tested piles

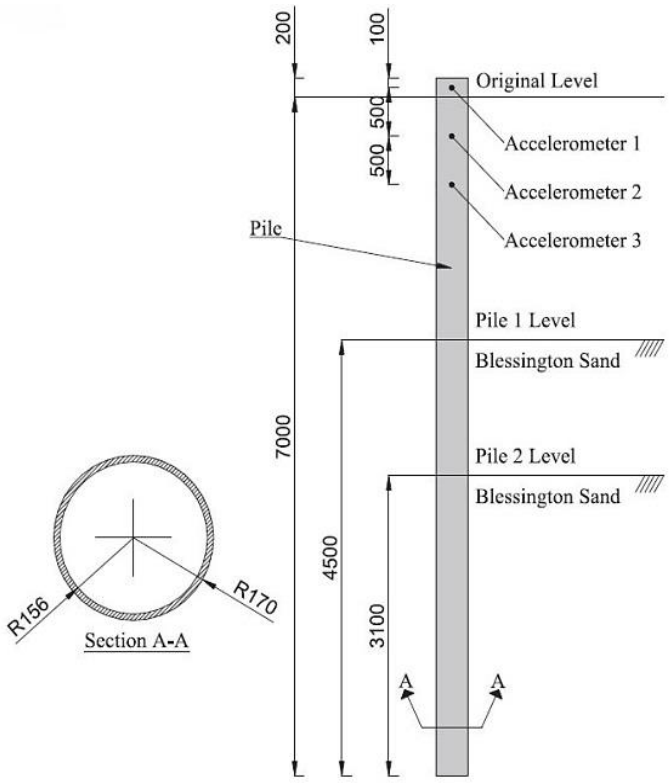

Figure 16: Blessington Piles Geometry and Accelerometer Equipment Positions. Source: (Prendergast & Gavin, 2016)

3.2.2 Soil Description and Parameters for Plaxis

The soil information is obtained from the Tolooiyan and Gavin research (Tolooiyan & Gavin, 2011) where the sand parameters from the Blessington Sand site were calibrated for the Hardening Soil model. This meant that only two additional parameters were needed to be calibrated for the HSS model and they were obtained using correlations from the literature. The soil used in this research was a dense sand soil, located near Blessington, which is about 25 km south-west of Dublin and it has been used in multiple occasions for the model, prototype and full-scale foundation experiments

(Prendergast & Gavin, 2016). The Blessington site sand is very dense, fine sand with a high relative density between 90% and 100%. The peak friction angle varies from 40° to 54° in the range of test depth interest and the constant volume friction angle is around 37°. The Blessington sand is partially saturated, with the degree of saturation between 63% and 75% and the water level is located approximately 13 m below ground level which meant that the drained approach can be utilized for the Plaxis 3D simulations.

As already mentioned above, the same test site was already used in the Plaxis simulations in 2011 (Tolooiyan & Gavin, 2011) where the Blessington Sand soil parameters had to be calibrated for Hardening Soil Model (HS). The calibration was done through testing the sand in oedometer and triaxial compression tests to obtain soil parameters which are related to the constitutive model used in simulation also the parameters were calibrated in the Plaxis virtual testing facility until the best fit between experimental and Plaxis results is obtained. The calibration of the soil parameters for oedometer and triaxial testing can be seen in the Figure 17 and more detail information for the parameter calibration can be found in the mentioned paper where the calibration procedure is explained. The soil parameters used for the Hardening soil model from the mentioned paper can be seen in the Table 1 below.

Table 1: HS model soil parameters for Blessington Sand. Source: (Tolooiyan & Gavin, 2011)

Hardening Soil Parameters – Blessington Sand	
Parameter	**Value [unit]**
P_{ref}	100 [kPa]
Unit Weight	20 [k/m^3]
E_{50}	44,000 [kPa]
E_{ur}	155,000 [kPa]
E_{oed}	25,000 [kPa]
Ultimate Friction Angle	42.4 [°]
Ultimate Dilatancy Angle	6.6 [°]
Poisson's Ratio	0.2 [-]
Power m	0.4 [-]
R_f	0.8 [-]
e_{init}	0.373 [-]
e_{max}	0.733 [-]
D_r	100 [%]

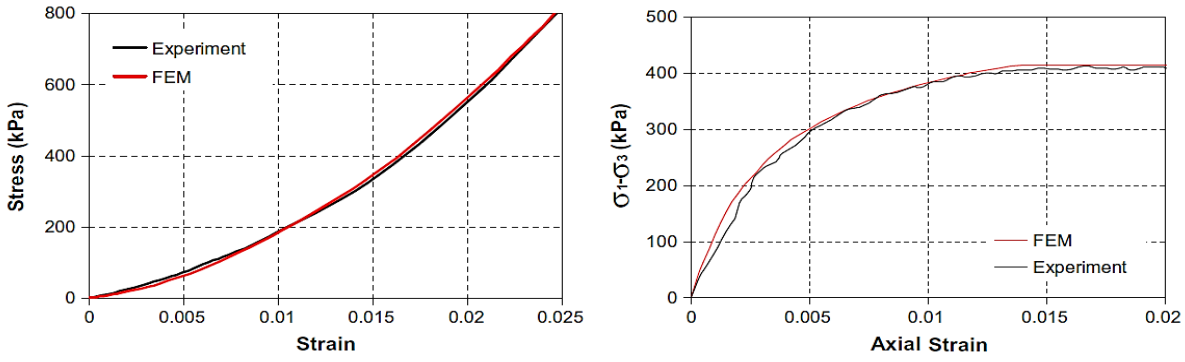

Figure 17: Parameter Calibration for Oedometer (left) and Triaxial Compression (right). Source: (Tolooiyan & Gavin, 2011)

Going towards the HS Small Strain soil model meant that additional two parameters had to be calibrated and obtained and these are G_0 and $\gamma_{0.7}$ which are already described in the subchapter 2.3.1. where the HSS model is described. According to the paper (Brinkgreve, Kappert, & Bonnier, 2007) when comparing curves of several different soil types it has been demonstrated that the particular shape of the curve (reduction of secant shear modulus with shear strain) does not change much and that $\gamma_{0.7}$ is generally between 1 and 2 times 10^{-4}. Therefore, the parameter $\gamma_{0.7}$ in this study was chosen and adopted in the model which is in the middle of this mentioned range ($\gamma_{0.7} = 1.5 \times 10^{-4}$).

On the other side, initially the small-strain parameter (G_0) was obtained using two different approaches and both resulted in a similar approximation of this small strain parameter. Since the initial void ratio (e_0) was provided in the paper it was very convenient to use it in the first approach where the initial void ratio was applied in the calculations for obtaining the small-strain (G_0) parameter. The first approach utilizes the equation which was obtained from the Plaxis soil model manual (Plaxis BV, 2017) and it can be seen in the Eq. 19 which describes this approximation below:

$$G_0 = 33 \cdot \frac{(2.97 - e)^2}{1 + e} \qquad Eq.(19)$$

The second approach utilizes an equation from (Brinkgreve, Kappert, & Bonnier, 2007) and this approach requires a two-step calculation with the first calculation of G_{ur} (shear modulus in unload/reload cycles – Eq. 20 where E_{ur} is the unload/reload stiffness and v_{ur} is the Poisons ratio) and then the second calculation (Eq. 21) where the G_0 is approximated using correlation for harder soil types (dense sand).

$$G_{ur} = \frac{E_{ur}}{2 \cdot (1 + v_{ur})} \qquad Eq.(20)$$

$$G_0 = 2.5 \cdot G_{ur} \ \ (for\ hard\ soils) \qquad Eq.(21)$$

Finally, both approaches produced very similar estimates of the G_0 parameter, which was equal to about 162,000 kPa. Although producing very similar estimates for the G_0 parameter, this approach did not yield desired results and therefore an alternative and more accurate approach had to be used. This was done by utilizing the shear wave velocity (V_s) profile from the Blessington sand (Prendergast & Gavin, 2016) and converting it back to G_0 parameter. This approach utilized the Eq. 22 which was used to estimate the small strain stiffness (G_0) using the V_s correlations, where the ρ is the soil density (kg m^{-3}) and V_s is the shear wave velocity (m s^{-1}).

$$G_0 = \rho\, V_s^2 \qquad Eq.(22)$$

Since the Pile 1 starts at depth of -2.5m, it utilizes layers 2, 3 and 4; while on the other hand the Pile 2 starts at of -3.9m and it utilizes layers 3 and 4. Based on this layering, the G_0 values were implemented and they can be seen in the following Table 2. The calculated values are considerably lower compared to the first two approaches where the e (void ratio) and E_{ur} (unload/reload stiffness) correlations were used. In the previous calculations the G_0 was about 162,000 KPa and it was used utilized for the whole soil profile, resulting in very stiff sand. In the new calculation case, the highest value is equal to about 148,500 KPa. Concluding the small strain parameters, the second approach lead to more accurate results which confirms that the V_s profile is a good way for estimation of small strain stiffness. The layering and V_s profile can be seen in the following Figure 18.

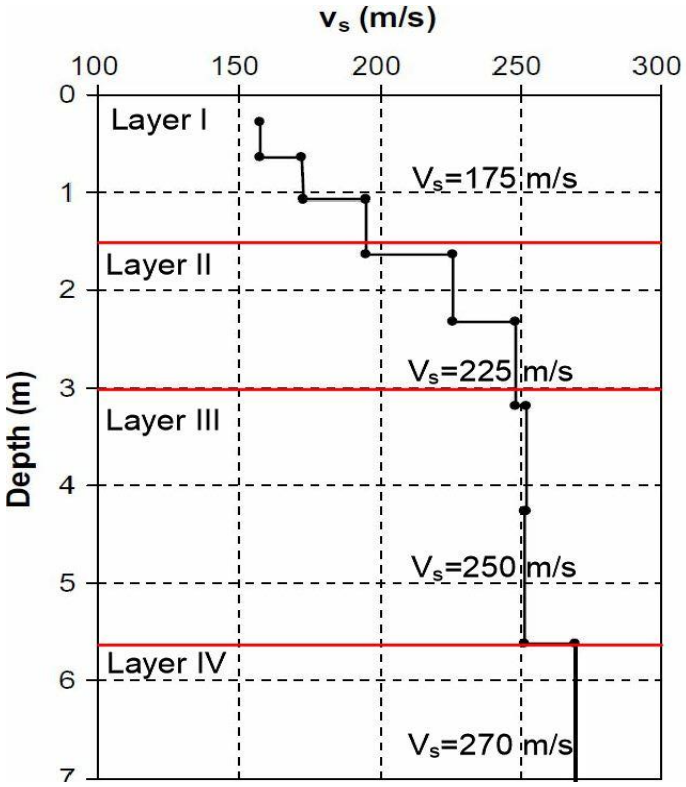

Figure 18: Shear Wave Velocity Profile – Blessington Sand. Source: (Prendergast & Gavin, 2016)

Table 2: V_s values and derived G_0 values from the V_s profile

Small Strain Stiffness - G_0		
Layer	**V_s [m/s]**	**G_0 [kN/m^2]**
1	175	62,436
2	225	103,211
3	250	127,421
4	270	148,624

3.3 Plaxis 3D Blessington Model Implementation

Multiple simulations were performed using the Plaxis 3D software and utilizing the calibrated Blessington soil parameters as an input for the HSS constitutive soil model. The simulation was divided into three phases consisting of: initial phase, phase one and phase two. The initial phase serves as a calculation of the initial stress field for the initial geometry boundaries. In the second phase the positive and negative interfaces are activated (in order to simulate a realistic soil-structure interaction) and the pile is activated which is also modelled as a plate element in the Plaxis 3D. The pile was assigned with steel material properties (Young's Modulus = 210 GPa) and its thickness and length were implemented according to the model from the Figure 16. The Second phase is chosen as dynamic calculation where the impact load (14.48 kN or 13.75 kN) is applied to the chosen pile (P1 or P2) and then free vibration response is recorded.

Dynamic environment in the phase two was assigned with a dynamic calculation time of 3 seconds which was used to compare the results to the Blessington Piles experimental case. A dynamic load was applied 0.1 m below the pile head and the dynamic load signal had to be implemented to achieve

almost identical impact as in the experimental tests. For this purpose, a dynamic multiplier option had to be applied in order to achieve a desired input signal for the pile impact. According to the Plaxis Reference Manual (Plaxis BV, 2017) the way this works in Plaxis, follows the Eq. 23 which can be seen below where F is the actual applied load in dynamic calculation, $\widehat{M}$ is the dynamic multiplier which is assigned to the multiplier table in dynamic mode and the $\hat{F}$ is the value of the load in the non-dynamic case (F_x).

$$Active\ Load = Dynamic\ Multiplier \cdot Input\ Value$$

$$F = \widehat{M} \cdot \hat{F} \qquad Eq.(23)$$

The product from the above Eq. 23 represents the amplitude of the dynamic load which can be suddenly applied in a single time step. The signal from the Blessington Piles had to be implemented through signal table in Plaxis where the only input parameters are dynamic multiplier and time. For this purpose, the regular input value (F_x) was fixed to the value of 1 kN which means that the amplitude of the applied load will depend on the value change of the dynamic multiplier (M) in time from the signal table.

Prior proceeding to the final simulation, the sensitivity analysis was undertaken to check the pile response when the model is exposed to different combinations of boundary size, time step and mesh coarseness. A typical response for the Pile 2 can be seen in the Figure 19 where the effect of time step increase was considered; from the Figure 19 it can be concluded that there is a slight variation in response, while the increase of the time step just provides a better approximation of the amplitude peaks. The same trend was observed with checking the boundary size influence. In the case of mesh coarseness, the very coarse mesh did not satisfy the accuracy criteria and the fine mesh did not improve the response but the calculation time was increased tremendously. The final model parameters can be seen in the following Table 3. Those parameters represent an optimal combination between providing enough accuracy but still achieving the desired results in a decent amount of computational time which is crucial for the available research time.

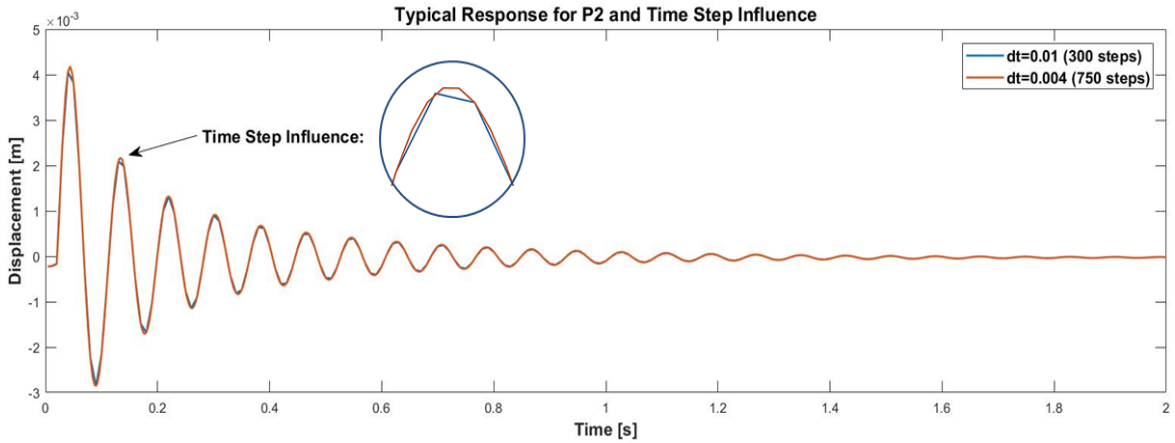

Figure 19: Time Step Influence on Model Response

Table 3: Blessington Piles Model Characteristics for Final Simulation

Blessington Piles - Model Characteristics	
Parameter	**Value**
Mesh Type	Medium
Number of Elements [-]	11,107
Number of Nodes [-]	17,607
Time Step dt [-]	0.006
Width [m]	12
Length [m]	6
Depth [m]	7

A typical model which was utilized for the final simulations can be seen in the Figure 20. It can be concluded that even the medium mesh coarseness provides a very dense packing of the elements in the close proximity to the pile which is an important factor considering small-strain calculations.

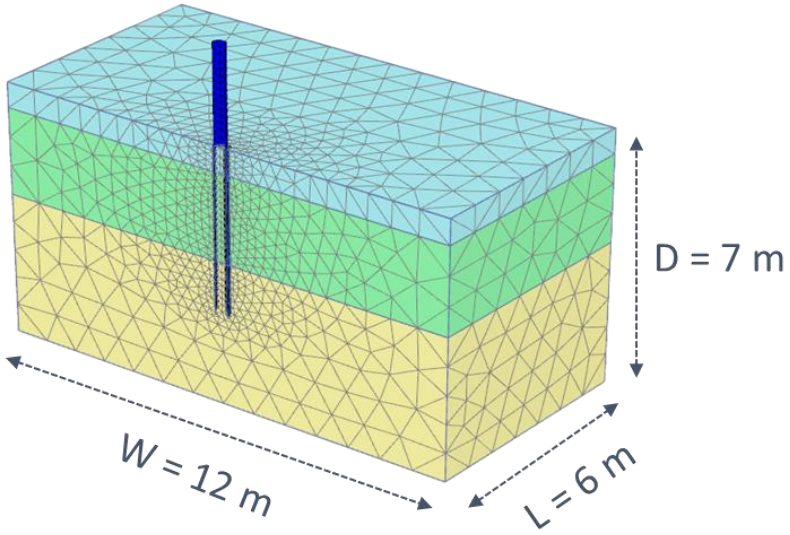

Figure 20: Medium Mesh Blessington Pile Model

3.4 Simulation Results and Comparison

Following the implementation of the Blessington Piles geometry and the input load-impact signals in the Plaxis 3D software, the dynamic analyses were undertaken in order to estimate pile's natural frequency and its damping ratio while the pile is vibrating freely at small-strain levels. Before proceeding to the final simulations, the sensitivity study was conducted through multiple simulations which were performed in order to check if there is an influence on the pile response. This was checked and incorporated in Plaxis by changing the boundary size or changing the coarseness of finite element mesh by increasing the number of elements. The results are presented on three levels: first set relates to estimation of natural frequency; the second set aims to estimate soil damping ratio and the last (third) set goes through procedures which were undertaken in order to get a final comparison and to concluded the verification process where the pile structural response between experimental and numerical displacement curves is compared.

3.4.1 Natural Frequency Estimation

The first thing which can be compared to the experimental data from the Blessington Piles is the natural frequency at which the piles are oscillating after the load impact has been applied to the pile head. In this case both Pile 1 and Pile 2 were used for an estimation of natural frequency by utilizing Plaxis 3D and its HS Small Strain constitutive soil model.

The natural frequencies of the piles from an experimental data were obtained using acceleration data, while in this study it must be said that the velocity (Pile 1), and displacement (Pile 2) output responses were used from the Plaxis 3D analyses. Generally, the velocity and displacement outputs were showing more accurate results and the pile response was more realistic (in terms of amplitude decay in time) and they were showing only one dominant natural frequency of the structure. Moreover, the displacement and velocity graphs were more suitable compared to the acceleration graphs which have shown more than one dominant natural frequency (usually higher bending modes and noise). Also, it seems that the acceleration data is quite sensitive in its response, especially if the number of time steps is increased where the acceleration data becomes very difficult to interpret.

Natural frequency which was estimated for each pile can be seen in the following Figure 21 and Figure 22 in which the outputs (velocity and displacement) were converted to the PSD curves by means of applying the Fast Fourier Transform (FFT). This meant that the output signal had to be converted from time domain to frequency domain.

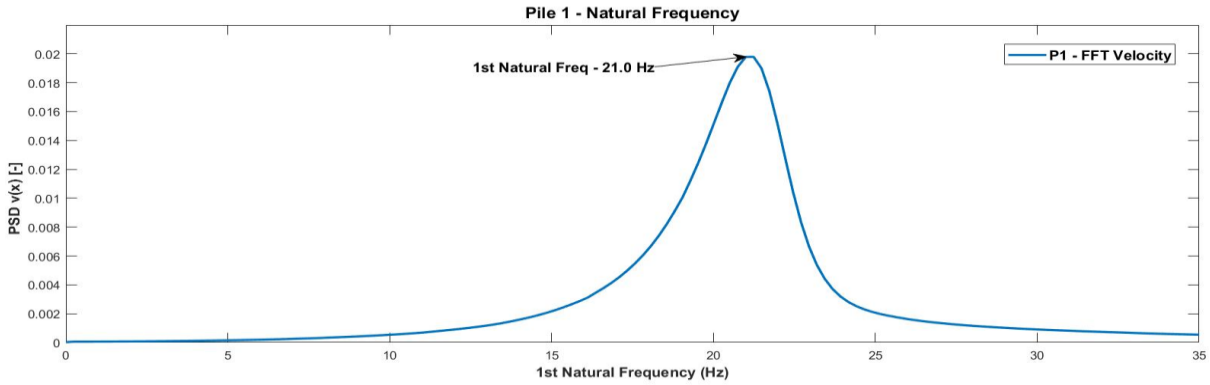

Figure 21: Pile 1 Natural Frequency Estimation (from Velocity)

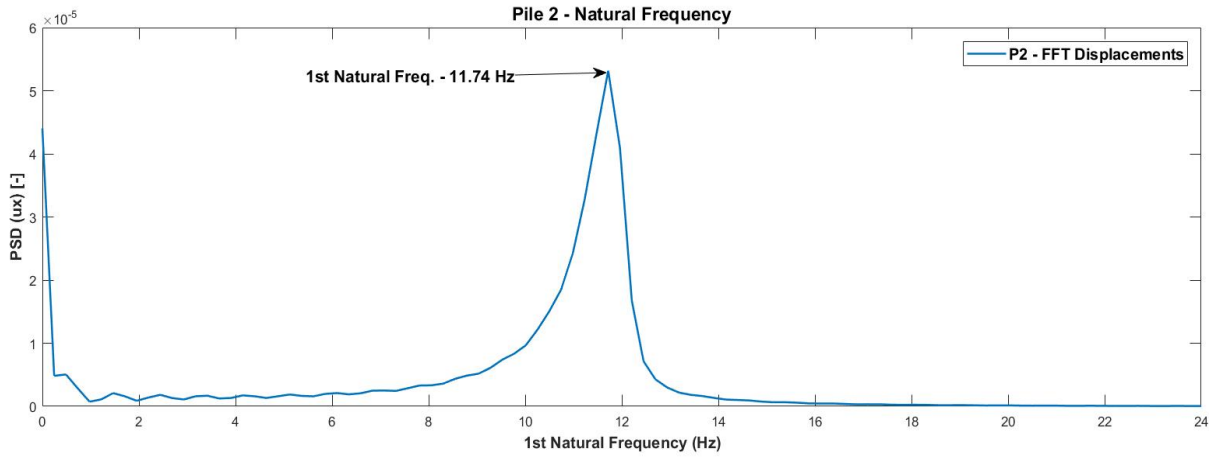

Figure 22: Pile 2 Natural Frequency Estimation (from Displacement)

The values which were estimated for natural frequencies obtained from the Plaxis 3D simulations are presented in the following Table 4, where they are compared to the other theoretical approaches which were utilized in the Blessington Piles paper and also, they are compared to the experimental data which is a true comparison point of interest (Prendergast & Gavin, 2016)

Table 4: Blessington Piles Natural Frequency: Comparison in Different Estimation Techniques. Source: (Prendergast & Gavin, 2016)

Blessington Piles - Natural Frequency			
Method	**Numerical Frequency (Hz)**	**Impact Experimental (Hz)**	**% Difference**
Pile 1 (L/D = 13)			
Biot	24.90	20.26	20.5
Vesic	23.93	20.26	16.6
M&B	26.12	20.26	25.3
K&G	27.83	20.26	31.5
Selvadurai	24.66	20.26	19.6
This Study - Plaxis	**21.0**	20.26	**3.6**
Pile 2 (L/D = 9)			
Biot	13.18	12.21	7.6
Vesic	12.70	12.21	3.9
M&B	13.43	12.21	9.5
K&G	14.16	12.21	14.8
Selvadurai	12.94	12.21	5.8
This Study - Plaxis	**11.74**	12.21	**3.9**

3.4.2 Soil Damping Estimation

The second step in this numerical to experimental comparison was done on estimation of soil damping ratio. From the Blessington Piles paper, the soil damping was estimated for both pile cases and this gives another level to which the numerical simulations from the Plaxis can be compared. In the case of soil damping, only the Pile 2 was suitable for the damping estimation, since the Pile 1 response was not showing enough amplitude peaks which were needed to employ the logarithmic decrement method. The reasoning behind this behaviour can be find in the fact that Pile 1 had a slenderer ratio (L/D =13) which means that it was surrounded by more soil medium compared to the Pile 2. More soil surrounding the Pile 1 means that the vibrations can be absorbed on a larger rate compared to the Pile 2 and considering that all of the vibrations were almost below 1 mm range then this seems like a realistic response, since it is really difficult to reproduce and capture these very small vibrations by numerical simulation.

Only the Pile 2 was suitable for the damping calculations since it has a sufficient number of amplitude peaks which are utilized for the calculation of the logarithmic decrement and hence for calculation of the soil damping. For the purpose of the logarithmic decrement calculation, in total 35 amplitude peaks were employed which yielded the value of $\delta = 8.37\%$. In the Matlab environment, an automated code that was developed enables the user to manually pick the desired amplitude peaks; following this the information is extracted to the work space. In Matlab, this information is so-called “cursor info” which has coordinates of each amplitude peak in the x and y direction; afterwards the cursor info information is utilized for the calculation of the mean logarithmic decrement value, which takes

average from all decrement values. Later, a single mean logarithmic decrement value is used in the damping equation as an input along with the natural frequency.

In the following Figure 23 an example of picking the amplitude peaks during Matlab processing is shown. Following the procedure from the mentioned paper, the first peak is omitted from the calculation because it is deemed that it shows unrealistic high value, which is of course a consequence from the impact hammer hitting the pile head at the beginning of the experimental test (this also produced a lot of noise in the acceleration data). In this analysis, the total of 35 peaks were used (since they were available) compared to the paper where exactly 30 peaks were used.

When the obtained information of the mean value of the logarithmic decrement was further utilized for the final damping estimation it resulted in soil damping value of 1.33% which is highly in agreement when compared to the experimental values from the (Prendergast & Gavin, 2016). It has to be mentioned that the experimental value of 1.26% which also had a possible deviation of ±0.1% which places the numerically calculated soil damping right in the desired range of values and it further gives confidence to this method. The Table 5 sums up all the values and information from the conducted analyses.

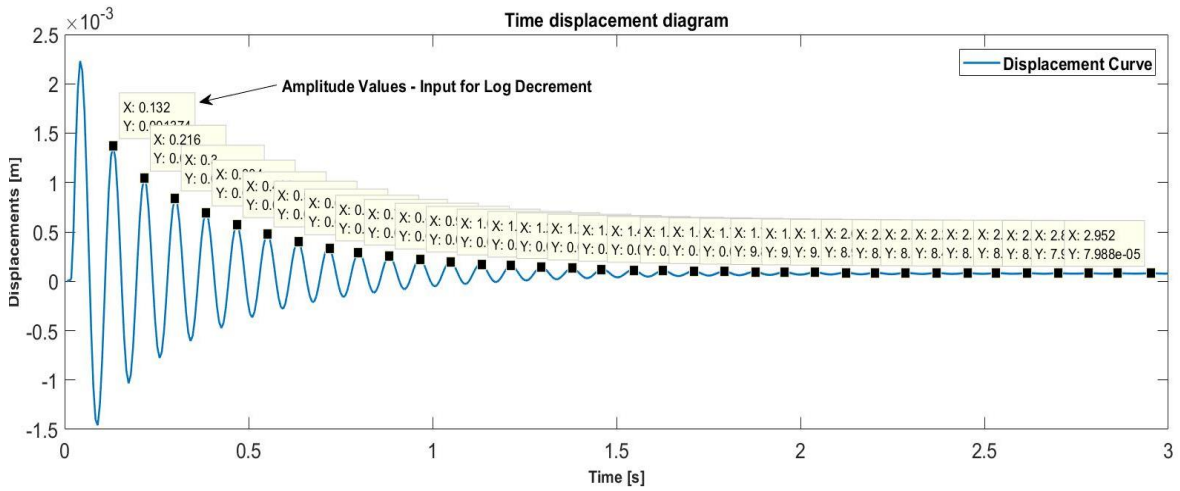

Figure 23: Input Amplitude Peaks for the Logarithmic Decrement – Pile 2 (First Peak Excluded)

Table 5: Pile 2 - Soil Damping Estimation

Soil Damping - Displacement Data (Pile 2)	
Parameter / Data	**Value**
Number of Peaks Utilized	35
Mean Logarithmic Decrement (δ)	8.37%
Soil Damping - Plaxis 3D (ζ)	**1.33%**
Damping – Experimental Data (ζ)	1.26% (±0.1)
Difference	**2.70%**

3.4.3 Retrieved Displacements Comparison

Apart from comparing the natural frequency and damping values a crucial step in the verification process of the Plaxis 3D capabilities lies in comparing the displacements which would serve as the final step in model verification. For this purpose, the experimental acceleration data had to be converted

to displacements in order to be compared with the numerical displacements from Plaxis 3D (since the acceleration data from the Plaxis seemed to be sensitive due to very short impact time on the pile). In order to convert experimental acceleration data to displacements two options were considered and they are already described in the theoretical part of the thesis (subchapters 2.4.1 and 2.4.2). The first option included time-domain analysis which did not yield a correct conversion, since the displacements were highly distorted, especially in the first part of the signal. A desired level of conversion accuracy could not be reached even with the help of low and high pass filtering. The reason for this could lie in the fact that double integration does not recover a whole signal while integrating since there is a missing signal information and this issue can be tracked from the integration constant (C) which is not translated into final converted signal. The second option included a frequency domain approach which means that the original data had to be transformed to frequency domain by means of applying the Fast Fourier Transform (FFT) and then utilizing the relationships between acceleration and displacements the calculated signal is transformed back to time domain by means of applying the inverse FFT (IFFT). The conversion of the signal is done in Matlab programming environment, which utilizes equations mentioned in the theory part (e.g. Omega Arithmetic – Eq. 15). In order to achieve the best fit, filtering techniques have been applied and the application of the filters will be described later in this subchapter.

The first step is related to applying the low pass Butterworth filter on the experimental acceleration signal since it has a portion of high-frequency noise which was made by the impact hammer force application at the pile tip; therefore, the application of low-pass filter is necessary to get a realistic response and smooth response. The following Figure 24 shows the effect of LP filtering where the high-frequency noise is removed with the LP Butterworth filter set at cut-off frequency of 18 Hz. The blue amplitudes at the start of the signal represent the high-frequency noise and red amplitudes show the filtered response. The filter order was set up at 8 and the sampling frequency utilized was set at 1000 Hz (3000 data points in 3 seconds time frame).

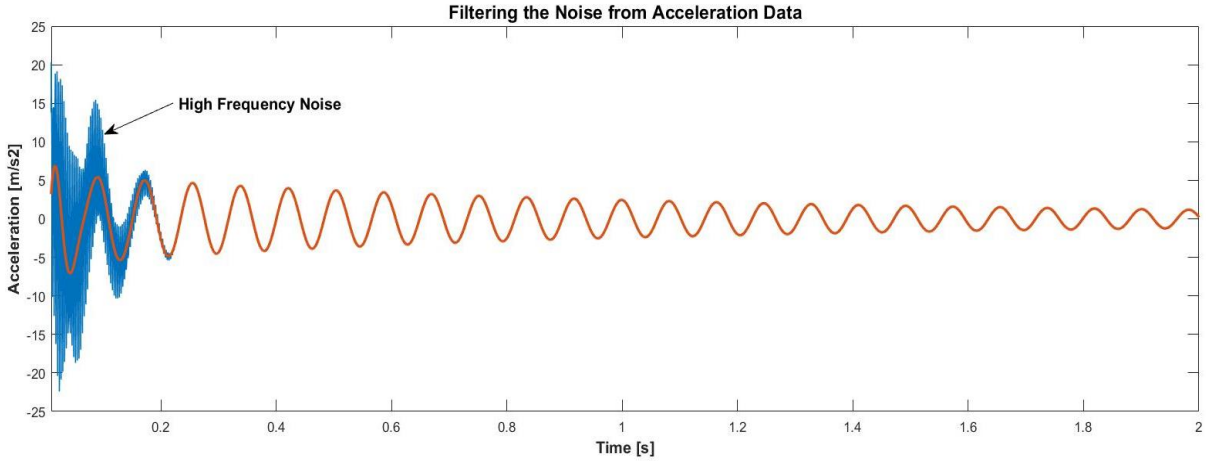

Figure 24: LP Filtering Application on the Experimental Acceleration

Second step involves the application of the FFT and IFFT and after the transformation (time-frequency-time domain) takes place, it is evident that conversion of the acceleration to displacements produces a low-frequency component which this happens due to fact that the acceleration FFT values are divided by the squared radial frequency - omega ($\omega^2 = (2\ \pi\ f)^2$) which produces this low-frequency noise component. The product of this division has an influence on the converted signal which gets a

distorted shape and this leads towards next step which includes filtering of this low-frequency component. Typical application of the high-pass filtering can be seen in the Figure 25.

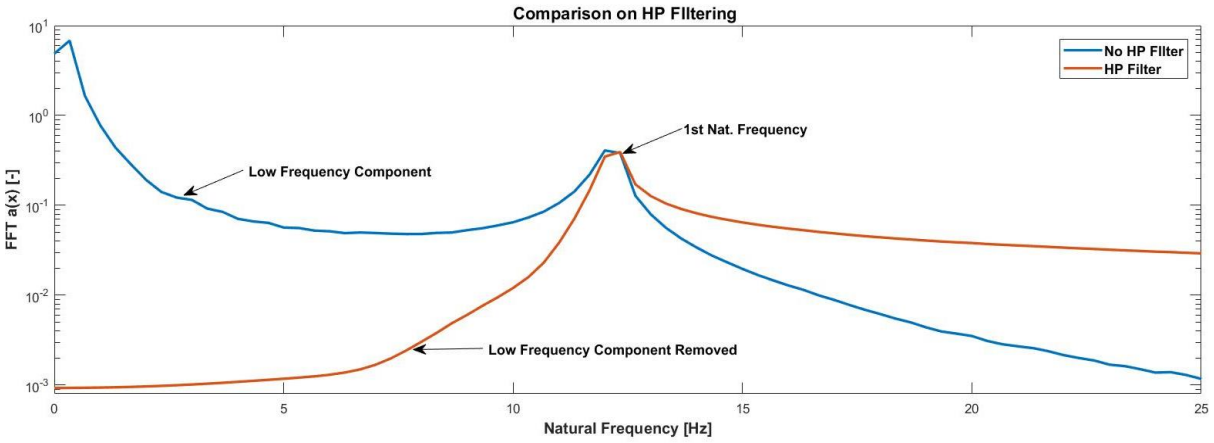

Figure 25: HP Filtering Comparison – Frequency Domain on a Logarithmic Scale for Pile 2

The converted signal was filtereted out with 10th order Butterworth Highpass (HP) filter and the cut-off frequency was set around 11 Hz (all the freqeuncies below that limit are discarded and hence not included in the PSD spectrum). The conseqeunce of the HP filter application yields a normal response in time domain which can be seen in the Figure 26, where the red line represents the final converted displacement response.

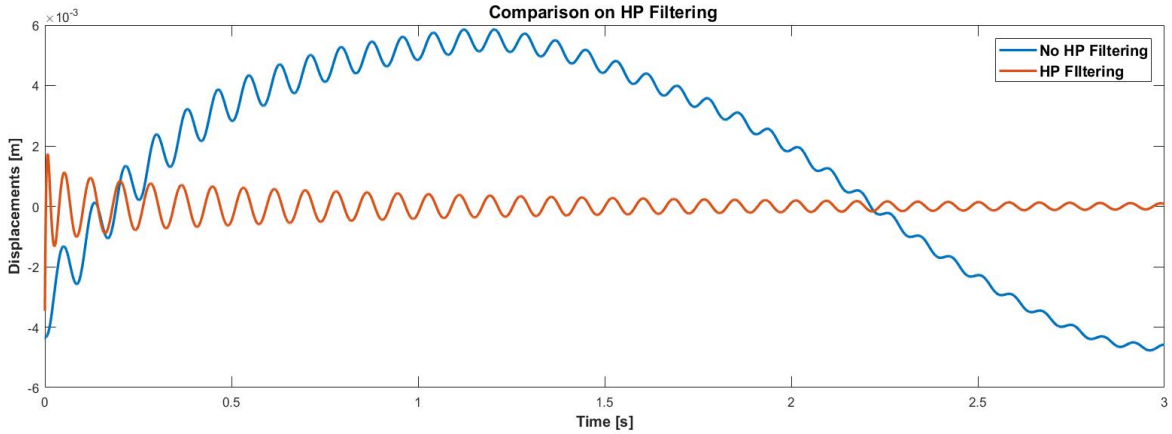

Figure 26: HP Filtering Comparison – Time Domain

Finally, after both LP and HP filter were applied (along with usage of FFT and IFFT transformation in the frequency domain) the comparison between experimental (converted) displacements and the numerical Plaxis displacements can be made. In the following Figure 27, a comparison between converted experimental data and numerical data can be seen. The Plaxis 3D displacements and converted displacements resulted in a desirable and acceptable curve fit which confirms that the conversion process was successful but also that the Plaxis 3D simulation yielded some satisfactory results in terms of estimating first natural frequency and pile behaviour during the free vibration phase.

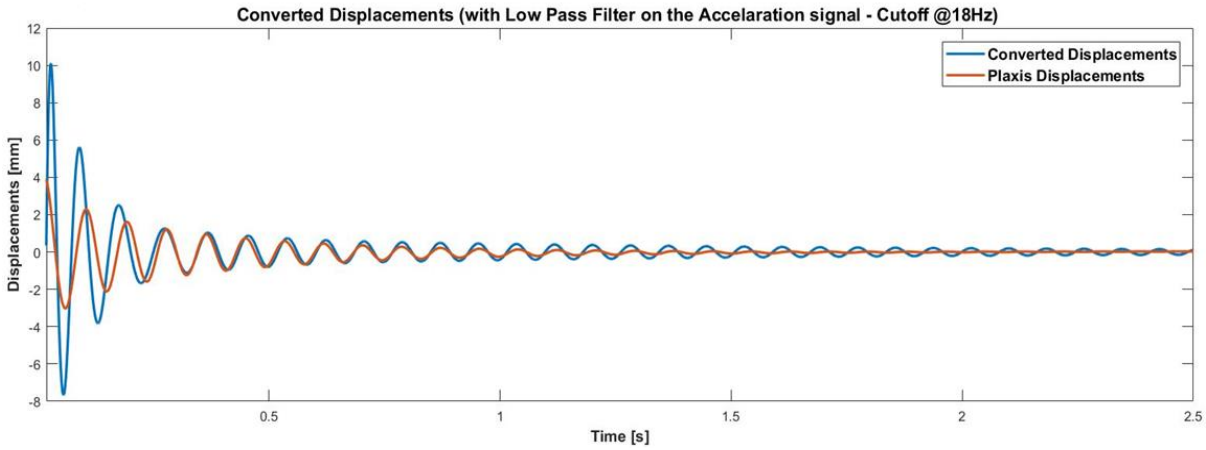

Figure 27: Comparison of Experimental-Converted and Numerical Displacements

A slight phase drift can be seen between two signals but this is a normal behaviour since the signals do not have the same natural frequency and therefore this small shift is expected. Another observation can be seen that in the period after first second there is more discrepancy between two signals but these are very small vibrations which are below 1 mm and therefore it is even more difficult to describe these dynamical oscillations in a numerical model simulation such as Plaxis 3D.

3.5 Blessington Piles - Concluding Remarks on Verification Process

The Blessington Case was a perfect match for the verification process of the Plaxis 3D HS Small Strain soil mode. The verification was done on three different levels and the comparison between numerical solutions and response was compared to: experimentally obtained pile natural frequency (for both P1 and P2), the experimentally obtained soil damping ratio (P2 only) and lastly the experimental (converted) displacement response (P2 only).

Firstly, the pile natural frequency was compared, where the Plaxis 3D simulations resulted in an excellent response. The numerically obtained frequency was under 4% difference compared to the experimental one in both pile cases. Additionally, the numerical frequency was also compared to the other theoretical approaches from where it has been proven that Plaxis yielded a more accurate prediction of first natural frequency, especially in the case of Pile 1. Moreover, the Plaxis 3D seems to be an efficient numerical solution for estimation of structural natural frequency which is vibrating at small-strain levels.

Second step involved the soil damping estimation which is directly related to structural response (e.g. displacement, acceleration, etc.). In this case, for the estimation of damping in Plaxis 3D the displacement curves were selected to be used for since they provided the most stable solution while on the other hand acceleration had a lot of noise which could not be filtered out to the desired level of accuracy. Only Pile 2 was used for damping assessment, since the response of Pile 1 did not yield enough amplitude peaks which are eventually used in the estimation of logarithmic decrement. The Pile 1 had a slenderer L/D ratio and it was surrounded more soil medium which has led to very quick absorption of energy from structure to soil, therefore less amplitude peaks were available. This can be considered a natural response since the vibrations that were recorded at pile control points were

mostly below 1 mm range and this is difficult to replicate the same response by the numerical model. In the case of Pile 2, the soil damping was estimated well within the experimentally obtained range.

The last step involved a complicated conversion in which the experimental acceleration was converted to displacement response. The converted displacement was compared to numerically obtained solution from Plaxis in which a sufficient match was achieved. Once again, most of the displacement response for P2 were well below 1 mm range and to be more precise most of them were around 0.5 mm.

All of those three mentioned verification steps were crucial to confirm that the Plaxis HSS model is capable of describing the structural behaviour while the structure is being exposed to some kind of dynamic load prior to the free vibration phase. Also, by doing this verification, the Blessington Sand soil parameters from (Tolooiyan & Gavin, 2011) were found to be in a good agreement with the results from this study. Plaxis has shown some promising capabilities for dynamic simulations and also the importance of G_0 parameter has been confirmed, where the improper estimation of this parameter led to less accurate results. Finally, it can be said that the model was verified successfully and that all of these verification processes gave a decent level of confidence to keep using the HSS soil model further in this research.

Chapter 4 - Case II: Monopile Design and Soil Damping Assessment

After the HSS soil model has been successfully verified, the research proceeds to the second case where the true size monopile is designed in order to estimate damping contribution to the total structure damping. For this purpose, a realistic design for the typical offshore wind turbine was utilized along with its suitable environmental loading scenarios (SLS and ULS conditions) which were tailored specifically for this type of offshore wind turbine. Moreover, various loading scenarios were analysed and multiple conclusions were drawn from the research. The general workflow which was followed can be seen in the Figure 28.

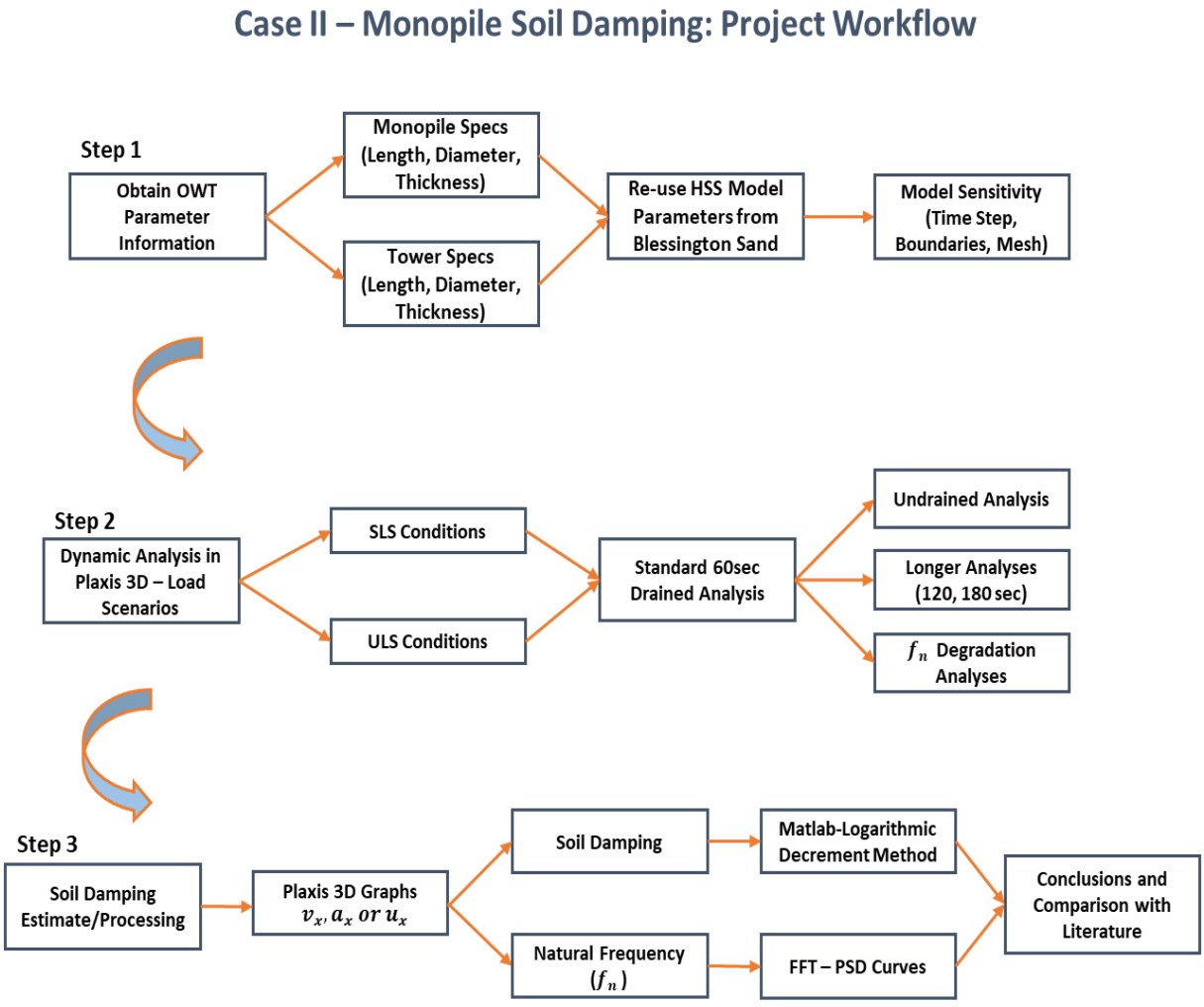

Figure 28: Case II - Project Workflow

4.1 Previous Studies and Methodologies for Soil Damping in Offshore Wind

As it was already mentioned in the introduction, soil damping is the least studied and most uncertain damping source when it comes to the OWT damping (Det Norske Veritas AS, 2014) and (Germanischer Lloyd, 2005). In the past few years, uncertainties about soil damping values have gained a lot of popularity among the research community and there are multiple studies which were done (mostly PhD thesis research projects) with an aim of estimating the damping of the OWT structure and the contribution of soil damping towards overall OWT damping.

Most of the conducted studies have undertaken the approach which includes some true experimental data measurements (or some small-scale modelling) and numerical simulation with advanced FEM software. Typical offshore measurements were done by means of so-called rotor stop test, where the OWT is shut down and the blades are pitched out (to almost 90°), or so to say the blades are in feathering position in order to reduce the drag and loads on the structure; those test examples can be seen in the literature (Versteijlen, 2011), (Shirzadeh, Devriendt, Bidakhvidi, & Guillaume, 2013), (Devriendt, Jordaens, De Sitter, & Guillaume, 2013) , (Damgaard, Ibsen, & Andersen, 2012) and (Carswell et al., 2015). Considering this situation, it can be assumed that the aerodynamic damping contribution is very low and almost negligible (Shirzadeh, Devriendt, Bidakhvidi, & Guillaume, 2013) and (Versteijlen, 2011) which makes this test suitable for estimation of soil damping, since it isolates the contribution of other damping sources. Some of the most relevant studies are described below in order to understand the various approaches along with their possibilities and limitations.

In his work (Versteijlen, 2011) conducted multiple rotor stop tests on the offshore wind turbines, including morning and afternoon measurements campaigns where the OWT was exposed to wind speeds of 10.96 m/s in the morning and 19.7 m/s for afternoon tests. Compared to the other studies, this study has covered respectable wind speed range but it does not include so to say “storm” conditions. On top of its experimental measurements, the study included so-called “constrained” beam model which was based on Euler-Bernoulli beam model. The term constrained was described by Versteijlen which means that the beam is not clamped or pinned at one of its ends. For the results, the study utilized the frequency domain approach (e.g. similar technique as half-bandwidth) and also a logarithmic decrement was used as a way of additional check. Versteijlen has concluded his study with estimation of soil damping which was much larger compared to other studies. This can be justified by the fact that in his measurements stronger wind loads were used and therefore more hysteretic energy is dissipating leading to more soil damping.

Moreover, (Shirzadeh, Devriendt, Bidakhvidi, & Guillaume, 2013) performed a combination of experimental and numerical study for estimation of damping during overspeed stop and ambient excitation tests. While the ambient measurements are economical they also provide limited information about soil damping which leads towards the main drawback regarding this study. Each of two performed tests were done at relatively low wind speeds (e.g. 6.5 m/s for overspeed stop and 4.5 m/s for ambient excitation test) which can be considered not enough for estimation of soil damping portion in total damping. The reason why the tests should be done at the higher wind speeds can be found in a fact that at lower applied load levels the soil is not completely mobilized and the soil behavior cannot be considered as non-linear (which is the case when stronger load histories are applied) which leads towards less damping in their measurements. On the other side for the estimation of soil damping the study utilized an exponential curve fit on the amplitude peaks.

Going further (Devriendt, Jordaens, De Sitter, & Guillaume, 2013) performed the same study as mentioned in the paragraph above. This study justifies reasons for performing rotor stop and ambient excitation tests. Their reasoning is related to the assumption that an aerodynamic portion of damping is considered excluded from total damping which happens during these two mentioned tests (e.g. mass damper turned off, low wind speeds and pitch angle almost 90°).

(Carswell et al., 2015) performed a numerical free vibration analysis in the software package “Adina” by gradually displacing the tower top (up to 0.1 m) then holding at the desired displacement level for

10 seconds in order to avoid any transient vibrations and then finally releasing the tower top in order to record free vibration measurements. The authors mentioned that is questionable what amount and type of load should be applied at the mudline and this is their reasoning for using prescribed displacements instead applying the load. In the mentioned study, the amount of soil damping calculated was in the lower range compared to the other literature findings. As a second part of their research, six different load time history analyses (each 1 hour long) were performed on top of the free vibration analysis. These loads were corresponding to extreme wave and wind load conditions (50-year environmental conditions). After utilizing the logarithmic decrement method, the results for the second part of research yielded larger amount of damping compared to the free vibration analysis. The study concluded that the soil damping could serve as potential factor in reducing fatigue damage, although the 50-year storm does not happen often.

In their study (Aasen, Page, Skau, & Nygaard, 2017) focused on different foundation modelling approaches in order to estimate their effect on fatigue and foundation lifetime. As part of this study they have also included a chapter which is dedicated to soil damping. One of their models or so-called "Model 4" is relevant for this master thesis since it accounts for the soil damping influence and it utilizes Plaxis 3D approach in combination with a HSS soil model. The drawback in their approach can be found in lack of available soil data; they have used soil correlations based on sand relative density which can lead to some errors when estimating soil parameters. For damping calculation, they have concluded the free vibration test which included displacing the tower top by 0.2 m. Although the main focus of the paper was fatigue estimation, the damping obtained in this study was in the lower range compared to other studies.

4.2 Monopile Design and Plaxis 3D Implementation

In order to perform further analyses, a true size model of the OWT had to be created in the Plaxis 3D environment. This study analysed a typical offshore monopile with a diameter size which can support wind turbines in a range from 2 to 5 MW (e.g. Siemens 3.6 MW). Typically, these sizes are used nowadays, although the industry is increasing the size of monopiles and the turbine power output (in MW) constantly. For the purpose of modelling, the guidelines were followed according to the paper (Prendergast, Reale, & Gavin, 2018) where a 6 m diameter monopile is implemented in the model with only a slight modification which is related to usage of an average diameter of the tower (4.25 m diameter) instead using a tapered diameter (gradual reduction in diameter while approaching the hub from the monopile direction). An assumption has been made that this will not affect the results of the simulations and this has been proven since the first natural bending frequency of the model (monopile and tower) yielded similar values compared to the model from the mentioned paper.

Going forward, in their study (Prendergast, Reale & Gavin, 2018) used a Critical Pile Length Criterion which resulted in a monopile embedment depth equal to 30 m. Above the mudline, the monopile extends up to 45 m where it supports a 70 m long steel tower. On the top of tower, there is a dead load (230 tons) which comes from the nacelle and rotor mass and in the Plaxis model, a specific "trick" had to be applied to represent the magnitude of rotor/nacelle load; a 25 cm thick steel plate was applied at the tower top, which has an extremely high material density (65,000 kg/m^3) in order to realistically represent the mass in dynamic calculations for the half size model. This has proven to be a correct choice, since initially the static surface load was applied and in dynamic analysis this has no

influence on the structural response since it neglects the inertia effect which is produced by the mass. Moreover, it has to be mentioned that this is a simplified model since the transition piece is not included because of its complexity which would be difficult to implement into software environment (complex connection and grout medium between monopile, transition piece and tower). Furthermore, the OWT model schematic used in this study can be seen in the following Figure 29 and its geometry and properties can be seen in the Table 6.

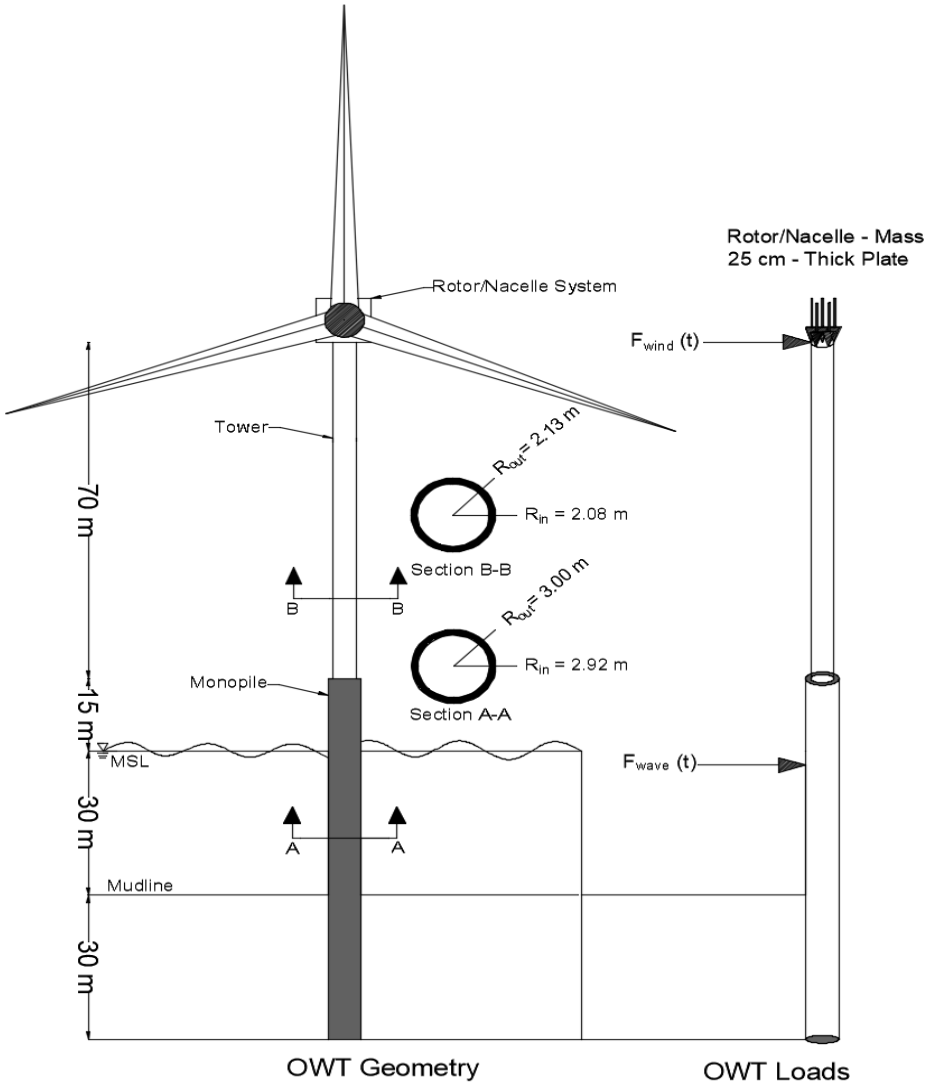

Figure 29: OWT Model Schematic and Load Positioning

Table 6: OWT Model Material Properties and Geometry Values. Source: (Prendergast, Reale & Gavin, 2018)

Tower/ Nacelle Properties	Value	Monopile Properties	Value
Tower Length [m]	70	Monopile Length [m]	75
Material	Steel	Embedded Length [m]	30
Density [kg m^{-3}]	7850	Material	Steel
Young's Modulus [GPa]	210	Density [kg m^{-3}]	7850
Tower Diameter [m]	4.25	Young's Modulus [GPa]	200
Tower Wall Thickness [mm]	45	Monopile Diameter	6
Nacelle / Rotor Mass [kg]	230,000	Monopile Wall Thickness [mm]	80
Tower Top Plate Thickness [mm]	100	Monopile Top Plate Thickness [mm]	250
		Top Plate – Steel Density [kg m^{-3}]	65,000

In order to ensure the model relevance, the tower /monopile size and thickness were tailored in order to satisfy design requirements (e.g. to be in the desired frequency range between 1P and 3P). Moreover, in the paper (Arany L. , Bhattacharya, Macdonald, & Hogan, 2016) there are design procedures which cover all the requirements such as Ultimate Limit State (ULS), Serviceability Limit State (SLS), Fatigue Limit State (FLS) and Target Natural Frequency (TNF). This research will cover most of the design checks (except FLS) in order to estimate soil damping contribution.

In the Plaxis 3D environment, the model is implemented as a half-space model (due to symmetry); this modelling assumption allows for a great reduction in computational time which is highly valuable due to time constraints for the thesis research. Again, the simulations are divided into three phases: initial stress generation (K_0) for the model field, second phase is a plastic one where the structural elements are installed along with interfaces, and lastly, the dynamic phase where the environmental loads are applied to the OWT model structure via dynamic multiplier input. The soil which is incorporated in the model follows the same example which was used and described in the Case I (Chapter 3 - Case I Blessington Piles and Plaxis Model Verification). Therefore, the Blessington Sand is used as the reference soil model along with the HS Small Strain constitutive soil model parameters. The reasoning behind reusing the Blessington Sand can be found in the fact that its soil parameters were available and they are considered reliable because the soil parameters are calibrated through other research projects and also verified in the Case I.

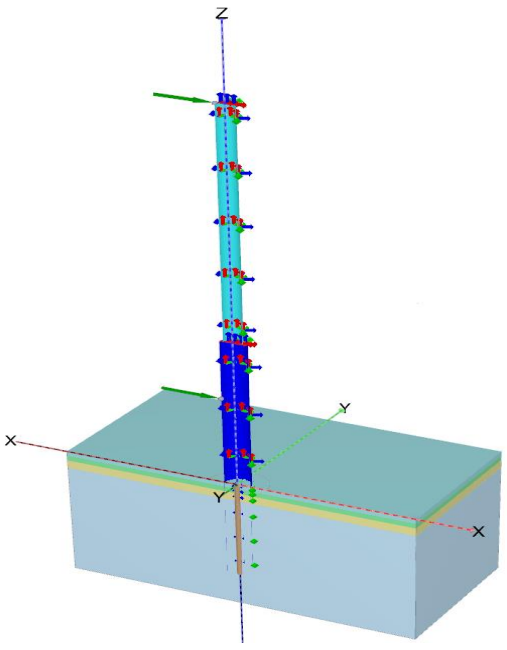

Figure 30: Plaxis 3D Monopile/Tower Model

The soil model was divided into four different zones which represent four different values for the small strain stiffness (G_0). A division of these zones can be seen in the Figure 18 (previous chapter). Assumption was made regarding small-strain stiffness for the last (deepest) soil layer and it was implemented that this 4th layer has the same small-strain stiffness value for the whole length of layer (-5.50 m to -40 m) which

was obtained from the Shear Wave velocity (V_s) profile. The reason for this can be found in fact that the V_s profile was available only for the first 8 meters of the soil profile and the following assumption was made because it is expected that small-strain stiffness will not affect the response of the monopile at deeper depths (4^{th} layer small-strain stiffness already has a much higher value compared to the first three layers). A typical model which is implemented in the Plaxis 3D can be seen in the Figure 30.

In terms of drainage type, the Plaxis 3D analyses were treated as drained and therefore the water level is omitted from the model. The reasoning behind this is justified by the fact that HS Small Strain model does not allow for pore water pressure accumulation and therefore this could lead to wrong estimation of soil damping. Only the limited set of simulations was done for the case of the ULS loading, since in this case it is assumed that excess pore water pressure will develop. The exclusion of water level in the model leads to isolation of the damping sources in the analyses, although it is up to further discussion what could be the influence of pore water pressure which accumulates in every load/unload cycle. Moreover, since there is no water, it is assumed that only structural and soil damping exist in this case.

The interface strength (R_{inter}) which simulates a zone between steel structure (embedded monopile) and the soil (sand) has a reduced value of R_{inter}=0.7. Usually, this value is between 0.6 and 0.7 which ensures a realistic friction between two mediums; therefore, the friction of this zone is reduced and adopted in the Plaxis model (Elwakil & Azzam, 2016). Moreover, along the length of the monopile portion which is embedded into the soil (30 m) both the positive and negative interfaces are assigned to simulate the zone between the monopile and soil realistically.

The tower and monopile elements are modelled in the Plaxis 3D as plate elements which are assigned with steel material properties mentioned in the Table 6. The thickness of the top plates was increased to represent rotor/nacelle mass and also in order to avoid failure of the structure due to sudden wind load application. Finally, the wave and wind loads are assigned as dynamic point loads (via dynamic multiplier table input option) and they are placed on the left side of the structure with height positions located at 27 meters and 115 meters above the mudline, respectively. The loads are direct input of the user, so they are changed according to the desired load scenario. On the other hand, the top load (230 tons or 115 tons for the half-model) at the hub level which is equal to the mass of the rotor/nacelle is placed within the 25 cm thick steel plate.

A sensitivity study took place in order to achieve optimal calculation time and also to have reasonable but still accurate results in the available time-frame of the thesis research. For this purpose, a sensitivity study was employed to evaluate the effects of the time stepping (Δt), boundary sizing (width and length) and also mesh coarseness. If these factors are not considered and analysed in a proper way, then there is a great chance of getting results which are out of order. For the sensitivity study, the chosen evaluation testing included loading the top of the structure (hub) with a load equal to 4,500 kN. The simulation included a 2 seconds ramp (zero load application) to avoid the FEM model failure, following this, the mentioned hub load was applied for 3 seconds and finally, after the load is suddenly released in order to allow the structure to simulate the free vibration phase. The simulations took place to see how the different sensitivity factors influence the response and to see what combination is suitable enough to reach the convergence in output results. Almost all considered time steps, mesh sizes and boundary sizes options satisfied the requirements for the potential final analyses, which were undertaken after the optimal parameters were decided. The results of the

sensitivity analysis are presented in the Appendix A – Sensitivity Study and here in the Table 7 the standard model is shown with the chosen sensitivity parameters for the final simulations.

Table 7: Chosen Sensitivity Parameters for the Standard Plaxis 3D Model

Standard Sensitivity Parameters - Final Simulation	
Parameter	**Value**
Medium Mesh Elements	15,862 [-]
Medium Mesh Nodes	24,607 [-]
Time Step (Δt)	0.05 [s]
Width	80 [m]
Length	40 [m]
Depth	40 [m]

Although the chosen parameters do not necessarily represent the most economic combination (in terms of computational time) they are chosen in order not to have accuracy issues later in the process when the longer time simulation take place (especially in the case of the ULS loading conditions where non-linearity is included). In the Figure 31, the standard medium mesh and geometry dimensions which are used in the final simulation can be seen.

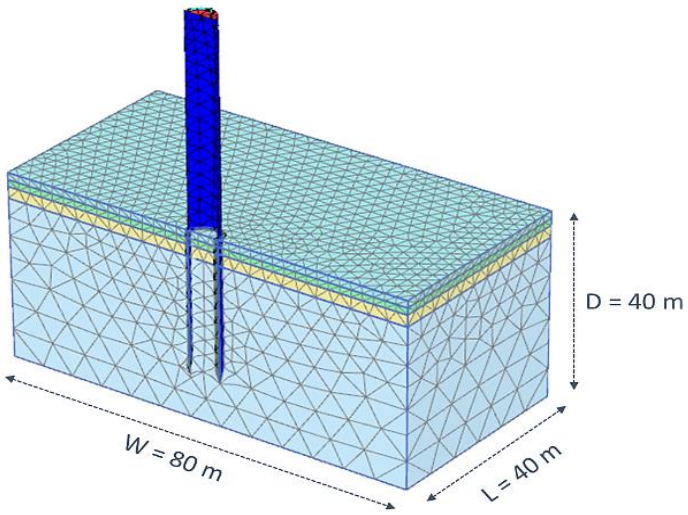

Figure 31: Standard Medium Mesh and Dimensions Utilized in the Final Plaxis 3D Analyses

4.3 Loading Scheme Derivation

Different loading scenarios are implemented in the Plaxis 3D simulations and they account for the SLS and ULS environmental loading conditions. The SLS scenario has been chosen since it is considered as a representative example of the OWT under normal operation (production of electricity), also the structure is designed to operate under the SLS conditions for the most of its life cycle. On the other hand, the ULS conditions will be analysed as well, since this loading environment tends to push soil behaviour towards non-linearity and also due to higher loading rates more damping is expected as a consequence of more energy being dissipated to the soil medium. Another loading test was considered in this study which consists of loading the OWT structure at the hub level with some predefined loading and this was utilized for the sensitivity analysis. There could be many different loading combinations for this case, including loading rate (e.g. load the hub in 5 second increment and then release the load). The hub load release was a common approach in some previous studies such

as (Aasen, Page, Skau, & Nygaard, 2017) and (Carswell, 2015) but in this study it was only utilized as the part of sensitivity study which served to find the most time efficient solution for the final simulation. The mentioned approach does not expose soil and its accompanied structure to a realistic time-loading history, therefore it is not a very suitable approach to estimate soil damping values since the loading does not reflect the situation which happens when the real environmental (wave and wind) loads are applied.

The SLS and ULS loading scenarios and load equations derivations are adopted from the previous studies study (Prendergast, Reale, & Gavin, 2018) and (Corciulo, Zanoli, & Pisanò, 2017). In the mentioned studies, they follow the theory regarding application of the appropriate wave (F_{wave}) and wind (F_{wind}) load derivation. The loading scheme follows a simplified approach towards loading scenarios for both wave and wind. F_{wave} and F_{wind} are considered as force thrusts and according to the above-mentioned studies, the following assumptions about force thrusts are made:

- Depend on OWT geometry and wind speed (velocity)
- Depend on the application of empirical factors (related to aero and hydro-dynamics)
- Force thrusts are co-directional (applied in the same direction)

The following equations explain how the force thrust values are derived on a step by step basis. Starting from the Eq. 24 which calculates wind force thrust based on the A_r (swept area of the rotor – m^2), ρ_{air} = 1.2kg m^{-3}, V_{wind} (wind speed – m s^{-1}), C_T=0.688 (empirical wind coefficient).

$$F_{wind}(t) = \frac{1}{2} A_R C_t \rho_{air} V_{wind}^2 \qquad Eq.(24)$$

In (Pierson & Moskowitz, 1964) a so-called Pierson-Moskowitz wave spectrum is adopted in order to evaluate wave energy (S) which is related to each frequency (f) (see Eq. 25), where α=0.0081 and β=0.74 are the empirical constants, g=9.81 m s^{-2}, $V_{wind}^{19.5m}$ is the wind speed at 19.5 m above the MSL, which serves as the reference height. Also, the equilibrium sea state with a steady wind flow field is assumed.

$$S(f) = \frac{\alpha g^2}{(2\,\pi\, f)^5} \exp\left[-\beta \left(\frac{g}{2\,\pi\, V_{wind}^{19.5m}}\right)^4\right] \qquad Eq.(25)$$

Following on this, the wave frequency can be calculated (f_s – at maximum spectrum amplitude) and also wave height (H_s) can be obtained, see Eq. 26 and Eq. 27.

$$f_s^4 = \frac{4\beta}{5}\left(\frac{g}{2\,\pi\, V_{wind}^{19.5m}}\right)^4 \qquad Eq.(26)$$

$$H_s = 2\sqrt{\frac{\alpha}{\beta}} \cdot \frac{(V_{wind}^{19.5m})^2}{g} \qquad Eq.(27)$$

By using the Morison Equation (Morison, Johnson, & Schaaf, 1950) it is possible to transform the wave frequency (f_s) and wave height (H_s) to a hydrodynamic thrust or so-called F_{wave} and this conversion is obtained by means of introducing the drag and inertial force (see Eq. 28 and Eq. 29), where the drag and inertia coefficients are C_d=0.65 and C_m=1.6, D is the monopile diameter (m), ρ_w = seawater density (1025 kg m^{-3}) and k is the wave number which relates to the wave length (λ_w). The parameter k is

obtained with explicit approximation since the parameter depends on the wave frequency ($\omega = 2\pi f_s$), and T = 2π/ω as it is shown in the Eq. 30.

$$F_{Wave}^{Drag} = \rho_w\, g\, \frac{C_d\, D}{8}\, H_s^2 \left(\frac{1}{2} + \frac{kH}{\sinh 2\, kH}\right) \qquad Eq.(28)$$

$$F_{Wave}^{Inertia} = \rho_w g\, \frac{C_m \pi\, D^2}{8}\, H_s \tanh kH \qquad Eq.(29)$$

$$k = \frac{\omega^2}{g\left[tanh\left\{\left\{\frac{2\pi\sqrt{\frac{H}{g}}}{T}\right\}^{\frac{3}{2}}\right\}\right]^{\frac{2}{3}}} \qquad Eq.(30)$$

Finally, since the wave drag and inertia components are out of phase, the mudline wave force can be calculated by the Eq. 31 which concludes the derivation of wave and wind loading derivation.

$$F_{wave}\,(t) = \sqrt{\left(F_{wave}^{Inertia}\right)^2 + \left(F_{wave}^{Drag}\right)^2} \qquad Eq.(31)$$

4.3.1 SLS Loading Conditions

The Serviceability Limit State (SLS) conditions are adopted from study (Prendergast, Reale, & Gavin, 2018) and this loading regime is suitable for the modelled wind turbine which has a 3.6 MW output power capacity. According to this approach, the SLS loading is calculated using abovementioned derived equations. For this purpose, the chosen wind speed is equal to 12 m s^{-1} and this represents a typical wind speed during wind turbine power production. The following Table 8 shows the derived forces F_{wind} and F_{wave}.

Table 8: Derived Wind and Wave Loads – SLS Conditions

SLS Wind and Wave Loads			
V_{wind} (m s^{-1}]	$V_{wind}^{19.5\,m}$ (m s^{-1}]	F_{wind} [kN]	F_{wind} - Plaxis [kN]
12	10.05	670	335
f_s [Hz]	H_s [m]	F_{wave} [kN]	F_{wave} - Plaxis [kN]
0.136	2.16	480	240

For the Plaxis 3D analyses the calculated loads had to be divided by factor of two since they are initially calculated for the full monopile geometry and in the Plaxis 3D only one half of the monopile is modelled, which means in reality only half of the derived load is applied to modelled structure. The loading regime can be visualized in the following Figure 32 which represents a typical simulation involving the SLS loading environment. The wave force is implemented in a simplified manner by means of sine function with frequency f_s equal to 0.136 Hz which results in a return period of 7.35 seconds. Moreover, the assumption has been made with F_{wind}, where it is assumed that wind acts as a constant force and for this purpose the wind force is applied with slight variations (up to 10%) around its mean value in order to represent a realistic wind environment.

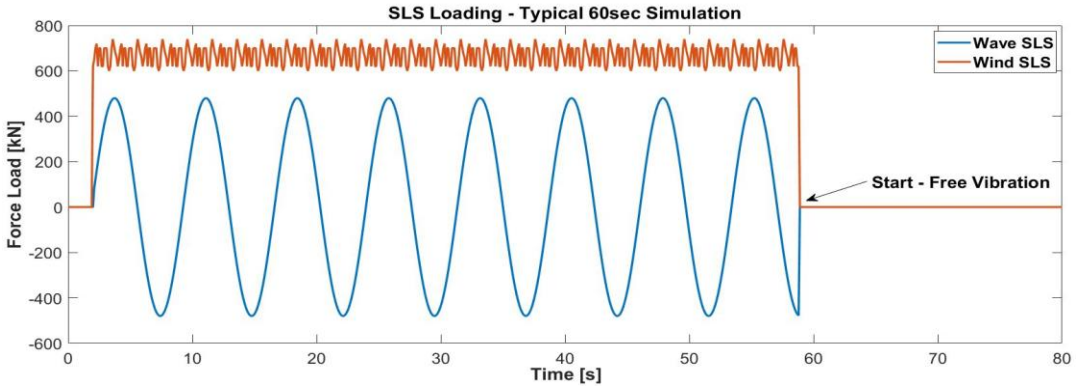

Figure 32: SLS Loading Conditions (Wind and Wave) – for Full OWT Geometry

4.3.2 ULS Loading Condition

The Ultimate Limit State (ULS) loading conditions were tailored to represent the storm conditions in which the soil non-linear behavior occurs and the excess pore water pressures are developing at a higher rate. While applying the ULS wind and wave loads it is assumed that the amount of soil damping will increase due to more hysteretic energy in the system. Higher displacement values will occur and they are expected to be in the maximum range of 10% of monopile diameter (up to 60 cm). For the purpose of the ULS loading the reference wind speed is chosen to be 25 m/s. The following Table 9 shows the derived values where it can be seen that the loading frequency of wave loading is equal to half the frequency when compared to the SLS loading, while the derived wind and wave loads are about three times larger than the ones in the SLS loading. The Figure 33 shows the typical wave-wind loading history for the ULS loading case.

Table 9: Derived Wind and Wave Loads – ULS Conditions

ULS Wind and Wave Loads			
V_{wind} (m s-1]	$V_{wind}^{19.5\ m}$ (m s^{-1}]	F_{wind} [kN]	F_{wind} -Plaxis [kN]
25	20.95	2915	1458
f_s [Hz]	H_s [m]	F_{wave} [kN]	F_{wave} - Plaxis [kN]
0.065	9.36	1430	715

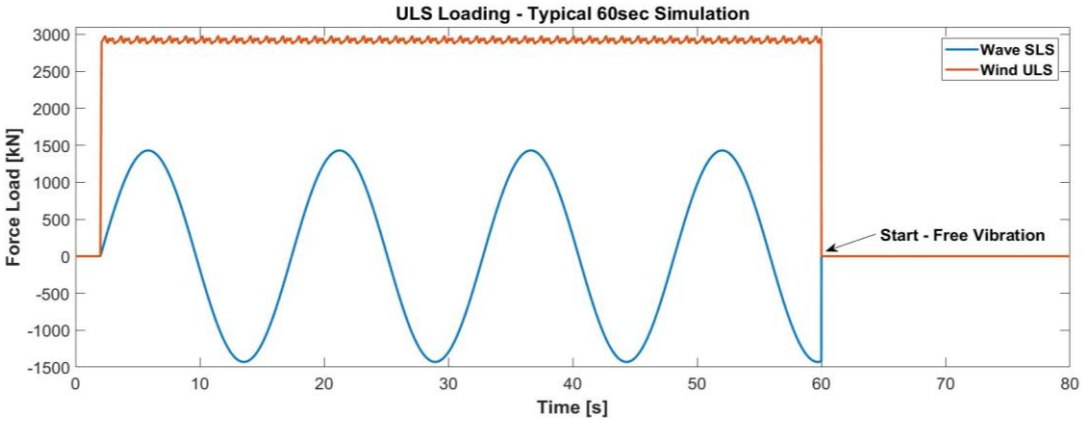

Figure 33: ULS Loading Conditions (Wind and Wave) – for Full OWT Geometry

4.4 Monopile Positioning for Free Vibration

An interesting dynamic structural response can be observed when the monopile's free vibration stage starts. This response depends on the structure (monopile and tower) location at the point where the external loads F_{wind} and F_{wave} are cut down or to say in other words when the loads are equal to zero. Initially, all the analyses were done with the start of free vibration while the wave load is approaching zero force value, and at this point the velocity of the wave is at its peak (since it starts climbing up afterwards – slowing down). At the same time, since the wave is governing the dynamic behaviour of the monopile, the location of the structure would be just a few centimetres to the positive side (to the right) and therefore this location is not suitable for the estimation of the soil damping since the monopile behaviour does not include peak amplitude values (does not reach its full displacement potential) and also there is a lot of vibration in the response (e.g. structure tends to swing to the right but is also vibrating while reaching its maximum displacement value). Because of this, low values of soil damping were estimated, and also with application of higher wave and wind loads the damping did not change, which is against the assumption that the damping increases with loading rate.

Therefore, a brief but beneficial study on the structure positioning has been employed in order to estimate true values of soil damping. So far, in the literature there was no mention about structure location at the point where the free vibration phase starts. For the purpose of this study three locations cases were considered in order to compare the structural response and to estimate realistic soil damping values. From the Table 10 it can be seen which the selected cases are.

Table 10: Monopile Positioning Study Cases

Monopile Positioning Analysis			
Case	*Position*	F_{wind}	F_{wave}
1	Middle	Max (positive)	Zero
2	Right	Max (positive)	Max (positive)
3	Left	Max (positive)	Max (negative)
Force Direction = "positive" – right / "negative" – left			

In the Figure 34, the structure locations are explained graphically along with the F_{wave} sine function which depicts the selected locations depending on the wave load cut-off location. The figure is not scaled, and it serves just as the graphical aid in order to understand the positioning process. When observing the Position 1, it can be concluded that this position results in a response which is not suitable for the soil damping analysis; the wave load is approaching zero value but its velocity is at maximum, so once the loads are cut down the structure produces a lot of vibration and the amplitudes in free vibration are much lower (since the wave did not reach end of its cycle). While starting the free vibration, from the Position 1, the location of the structure is just a little bit to the right (and the structure has the tendency to go towards right once the loads are cut down). In this way the response is much different when compared to other two cases.

On the other hand, while the structure located at the Position 2, both wave and wind are at its maximum force value and the location of the structure is at its maximum value to the right. From this location the free vibration amplitudes are reaching high values which are comparable to the Position 3. Lastly, the Position 3 has a combination of the maximum (negative) value for wave force and maximum (positive) value for the wind force, which results in placing the monopile to the left.

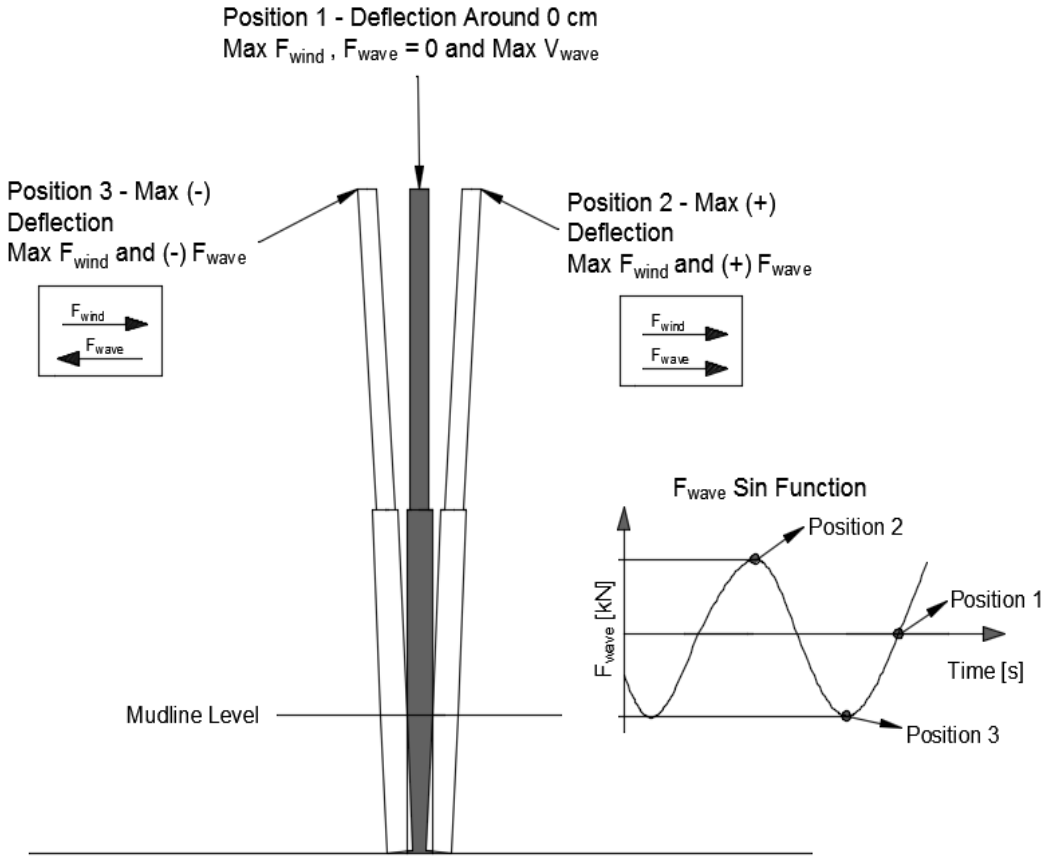

Figure 34: Monopile Position Analysis Description

4.5 Plaxis 3D Simulation Results and Soil Damping Assessment

After concluding multiple simulations in the Plaxis 3D, the obtained results can be presented, discussed and compared to other values obtained in the other research projects. The results are presented in different levels which are mainly focused on the obtained soil damping values for different loading scenarios. Moreover, the effect of monopile positioning on structural response is presented along with additional topics such as degradation of natural frequency due to load increase, and also the soil behaviour in different control (stress) points is presented. Before the results are presented, some assumptions regarding modelling conditions and soil damping estimation are revealed. Firstly, the material damping from steel sections (tower and monopile) is assumed to be 0.19% of critical damping. This approach is followed by the Eurocode (EN 1991, 2005) and it is implemented in few other studies such as (Swagata & Sumanta, 2014) and (Damgaard M. , Ibsen, Andersen, & Andersen, 2013). This means that the value of 0.19% is subtracted from the total critical damping and the final result represents the value of the soil damping contribution. Other assumption is implemented by exclusion of water table in the model in order to isolate soil damping contribution and also to avoid getting wrong estimates of the soil damping due to incapability of the HS Small Strain soil model to accumulate pore water pressures during loading/unloading cycles. This approach (drained analysis – dry sand) was also implemented in some experimental testing of monopiles which included free vibration analysis as well (Hanssen, Nordal, & Eiksund, 2016). It has to be mentioned that limited amount of simulations was undertaken with undrained approach to see what the influence of the PWP development in the ULS conditions is.

4.5.1 Soil Damping Results in SLS Loading Conditions

For the purpose of soil damping estimation two different output responses were considered and those are acceleration and displacement curves. Acceleration did not yield the desired results, since there was a high and low frequency noise in the signal and filtering the signal did not provide expected monopile response. For this occasion, the estimation of soil damping had to be done on displacement data curves, although an acceleration data is mostly used in the mentioned literature studies. In the case of this study, the analysed predefined node was positioned at the top of the monopile with coordinates being in the middle of the monopile (at the back side). Moreover, the analysed node can be seen in the following Figure 35 which shows the top view of the analysed monopile.

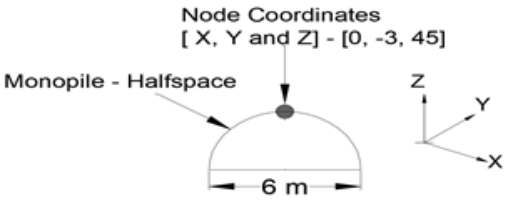

Figure 35: Analysed Monopile Node Location - Top View

Typical simulation was exposed to about 60 seconds loading, followed by the 30 seconds of free vibration. Three final simulations were undertaken in order to see what the response of the structure is. The outcome of simulations is based on the theory presented in the subchapter 4.4, where the monopile positioning concept is explained. Indeed, a different position of monopile influences the response of the structure in a free vibration phase. The outcome of the simulations can be seen in the following Figure 36. From the mentioned figure it can be concluded that Position 1 has the lowest potential in terms of displacement amplitude which is reaching its maximum peak and thus displacing the monopile at maximum value of about 4 cm. On the other hand, the Position 2 which is a combination of both wave and wind acting in the same direction resulted in a maximum displacement of the monopile (about 12 cm peak amplitude). Finally, the Position 3 which is a combination of maximum (negative) wave load and maximum wind (positive) load reached the values which are in between the other two positions with a maximum peak amplitude being around - 8 cm. Positions 1 and 3 have a portion of high-frequency noise (2nd mode) which had to be filtered out for damping. This proves that the position of the structure prior the start of the free vibration plays an important role in a monopile response and hence in estimating its damping value which will be shown afterwards.

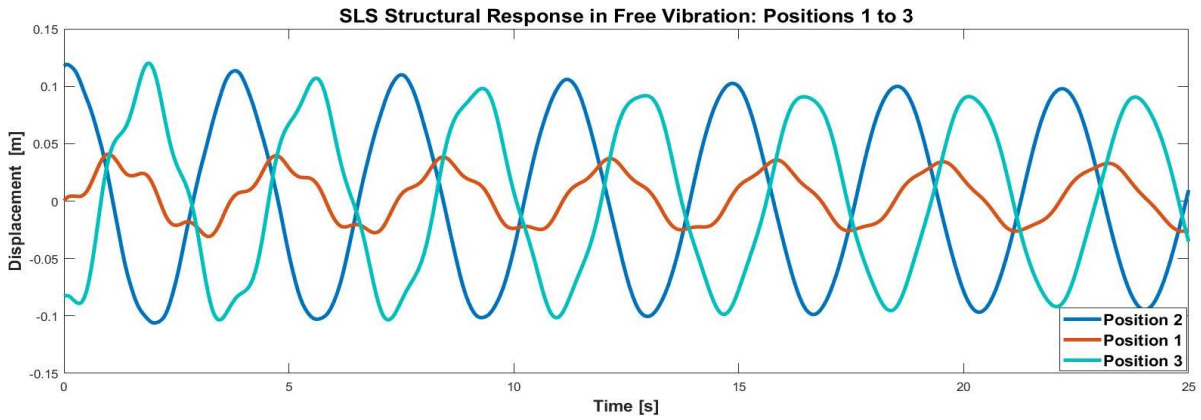

Figure 36: Structural Response for Different Positions (SLS Loading) - Unfiltered

All of the three mentioned positions were analysed for the damping estimation. After employing the logarithmic decrement method, it was revealed that the monopile positioning has an important role on the damping potential since the obtained damping values are much different from one position to another. In the Figure 37 and Figure 38, the damping comparison is made depending on different positions. Firstly, the Positions 2 and 3 are compared since they have the highest potential and then the Position 2 is compared to Position 1. Positions 1 and 3 needed an additional LP filtering which is used to remove the presence of 2nd bending frequency; the filter was set at 0.50 Hz.

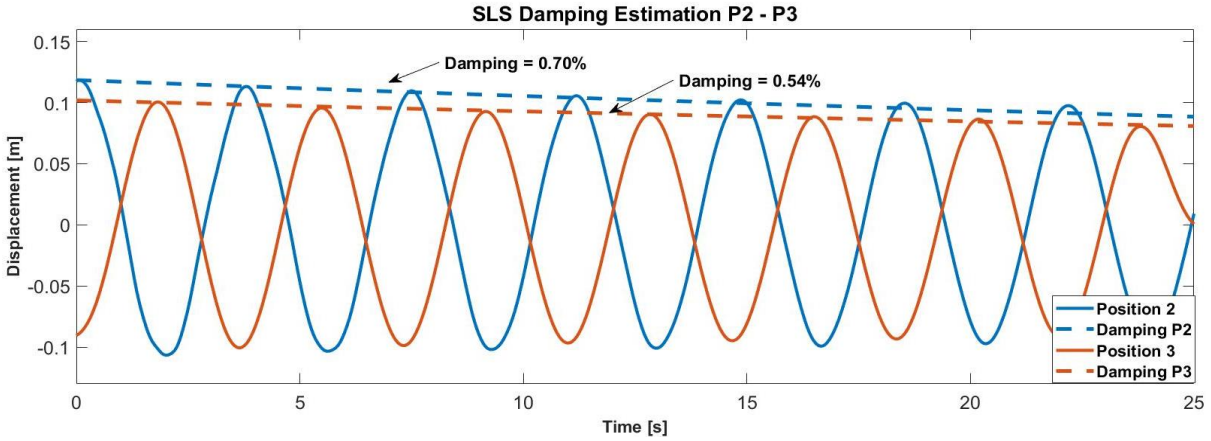

Figure 37: Damping Estimation and Comparison for Positions 2 and 3 (SLS Loading)

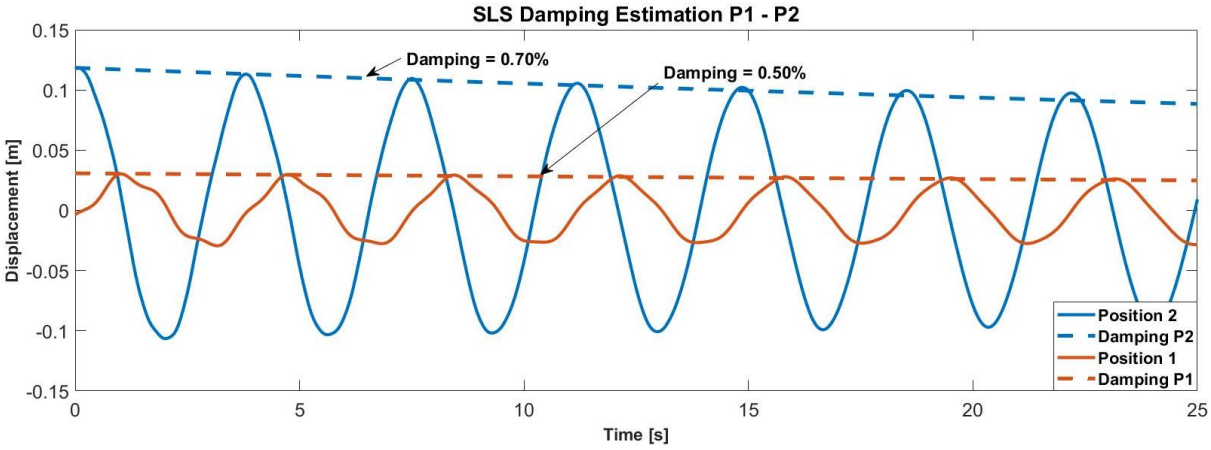

Figure 38: Damping Estimation and Comparison for Positions 1 and 2 (SLS Loading)

The obtained soil damping values are presented in the Table 11 where the value of 0.19% (structural damping) is subtracted from the total damping in order to arrive at the value which is solely assigned to the soil damping contribution.

Table 11: Soil Damping Estimation - Results for SLS Conditions

SLS Soil Damping Estimation			
Parameter	*Position 1*	*Position 2*	*Position 3*
Structural Damping – ζ_{struct}	0.19 %	0.19 %	0.19 %
Total System Damping – ζ_{total}	0.50 %	0.70 %	0.54 %
Soil Damping – ζ_{soil}	0.31 %	**0.51 %**	0.35 %

4.5.2 Soil Damping Results in ULS Loading Conditions

Again, the simulations were repeated for the ULS loading conditions and the soil damping was estimated. Prior proceeding to the estimation of damping, an interesting response can be observed for positions 1 and 3. The mentioned P1 and P3 had a portion of vibration (noise) which is assigned to the 2nd bending mode frequency. The response can be seen in the Figure 39 and the influence of the higher frequency mode had to be filtered out in order to get smoother amplitudes which are much more realistic case for damping estimation. Again, it is proven that amount of displacement highly depends on the monopile positioning theory where the combination of maximum wind and wave load (P2) yields the largest displacement values.

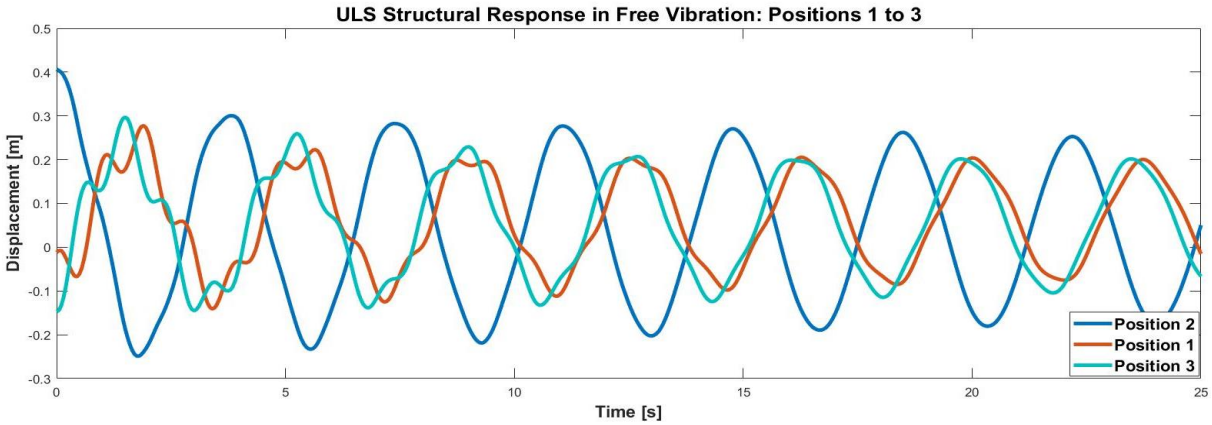

Figure 39: Structural Response for Different Positions (ULS Loading) - Unfiltered

A typical filtering application (see Figure 40) cuts down the influence of the 2nd bending mode, which eventually results in smoother amplitudes but also their displacement values are reduced due to filtering process taking place. Moreover, the LP filtering reduces amount of damping which otherwise, would be unrealistically high value.

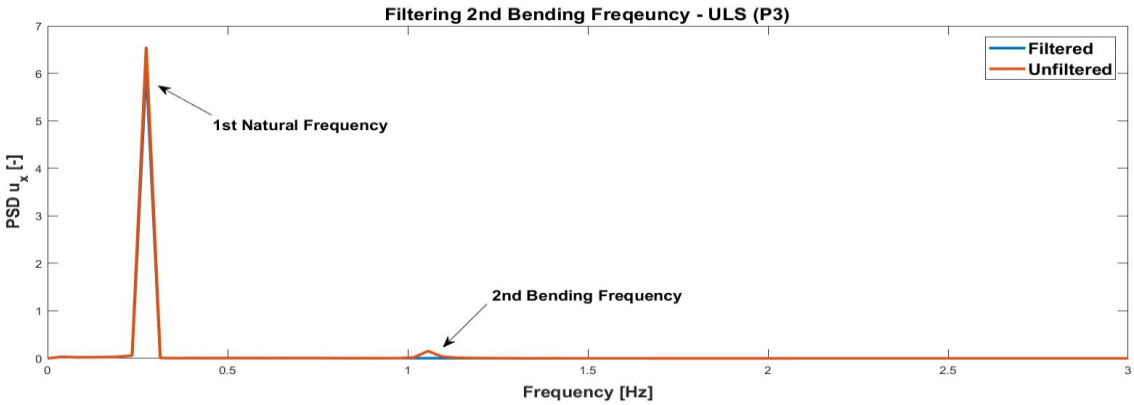

Figure 40: Application of LP Filter on 2nd Bending Frequency (Position 3)

Going further, the P2 and P3 (see Figure 41) are initially compared for estimation of total damping. Again, the P2 location produced a highest value of damping which was also the case in SLS conditions. The LP filter was applied on the P3 displacement signal which now has about 30% less damping compared to the unfiltered signal.

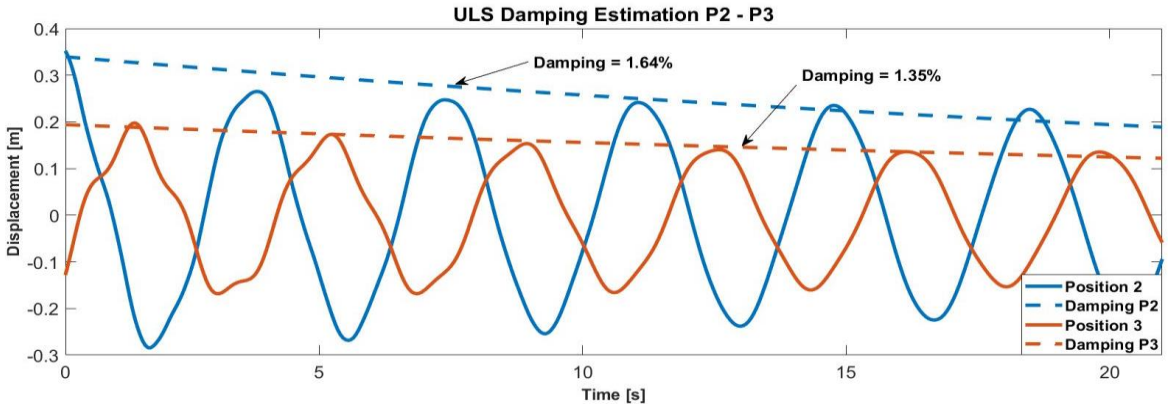

Figure 41: Damping Estimation and Comparison for Positions 2 and 3 (ULS Loading)

Lastly, the P1 and P2 (see Figure 42) are compared where the highest difference between obtained total damping values is recorded. All of the damping values are reported in the following Table 12. Depending on a specific position, the obtained soil damping values are about 3 times larger compared to the SLS case.

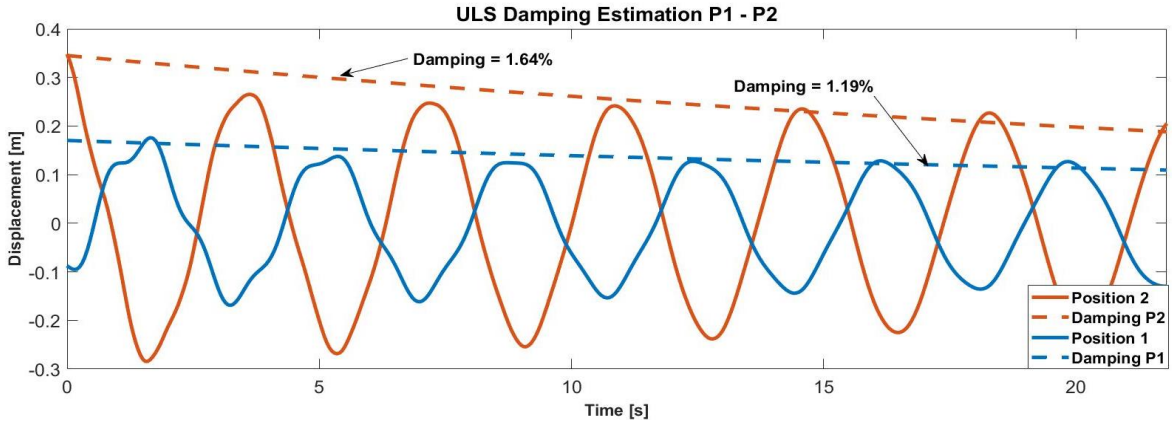

Figure 42: Damping Estimation and Comparison for Positions 1 and 2 (ULS Loading)

Table 12: Soil Damping Estimation - Results for ULS Conditions

ULS Soil Damping Estimation			
Parameter	*Position 1*	*Position 2*	*Position 3*
Structural Damping – ζ_{struct}	0.19 %	0.19 %	0.19 %
Total System Damping – ζ_{total}	1.19 %	1.64 %	1.35 %
Soil Damping – ζ_{soil}	1.00 %	**1.45 %**	1.16 %

4.5.3 Increase of Time-Loading History Effect

A limited set of simulations was undertaken in order to analyze the effect when the longer loading time history is employed on the OWT structure. For this purpose, the same loading scenarios were applied (SLS and ULS). The standard simulations were limited at applying the load histories for about 60 seconds while in this supplemental study, the simulations will have the loading which takes about 120 and 180 seconds, followed by 30 seconds of structural (load-free) free vibration. For this case, only the Position 2 (combination of maximum-positive wave and wind) will be considered due to time limitations and longer calculation time needed for each simulation. The aim of this study is to check

the sensitivity of damping values and natural frequency while the structure and accompanied soil medium are exposed in multiple load-unload cycles. From the Figure 43, an interesting observation can be made, a decay trend can be seen from the displacement amplitudes which are decreasing (while exposed to the same value of load) with an increase of loading time; this means that the soil stiffness does not degrade while it is exposed to the SLS loading conditions. The arrows in the Figure 43 show the stretch (length) of the initial displacement amplitude when the loads are cut-off.

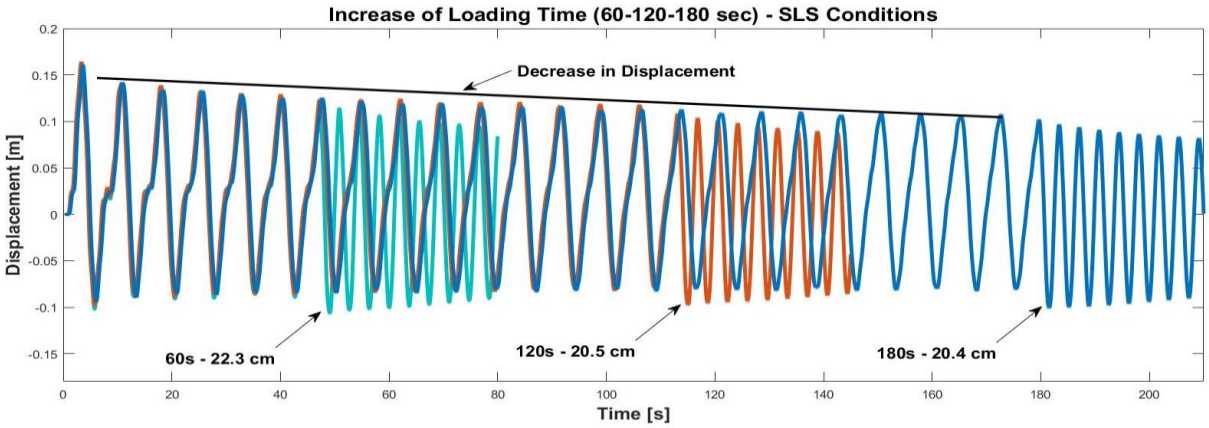

Figure 43: SLS - Effect of Loading Time Increase for 60-120-180sec Loading

When the damping estimation takes place (see Figure 44), it can be seen that damping value slightly decreases when the soil-structure is exposed to the longer loading histories (e.g. 120-180sec). This can be related to an increase of soil stiffness, which decreases the damping value while its stiffness is increasing; therefore, less energy is being absorbed by the sand for every following load cycle. Another trend which can be observed relates to damping, where after 120 seconds the damping value not decrease any further, which means that soil stiffness has reached its maximum value for these loading conditions. The value of damping obtained from the 120-180 seconds loading histories is around 0.62%, which means that the amount assigned to soil damping is equal to 0.43%.

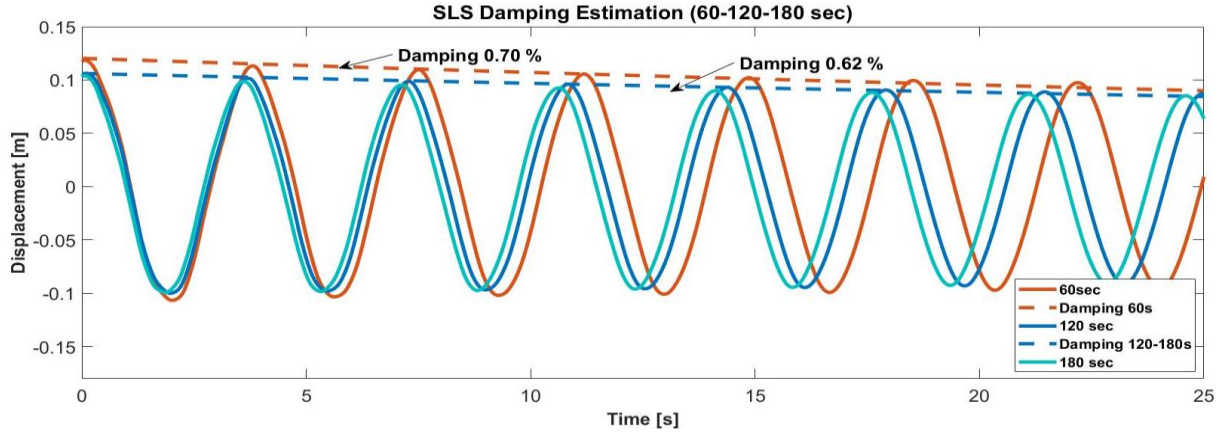

Figure 44: SLS Damping Estimation for 60-120-180sec Loading

Proceeding to the ULS case, a typical soil-structure interaction response can be observed which is following the same trend as it was in the SLS case. A similar drop (in percentage) between the initial displacement amplitudes is recorded, while for the ULS case there is no additional drop when the last (180 seconds) loading is considered. Looking at the loading part between 70 and 180 seconds it can be seen that the displacement amplitudes are reaching almost the same value for every cycle, which

is not the case in the first 70 seconds of loading; this implies that this dense Blessington sand (dilatancy angle - ψ=6.6°) tends to dilate under higher shear strain levels and therefore it reduces the displacement of the monopile. This also affects the initial length (stretch) of the free-vibration amplitude which are reaching the lower "potential" for both 120 and 180 seconds loading.

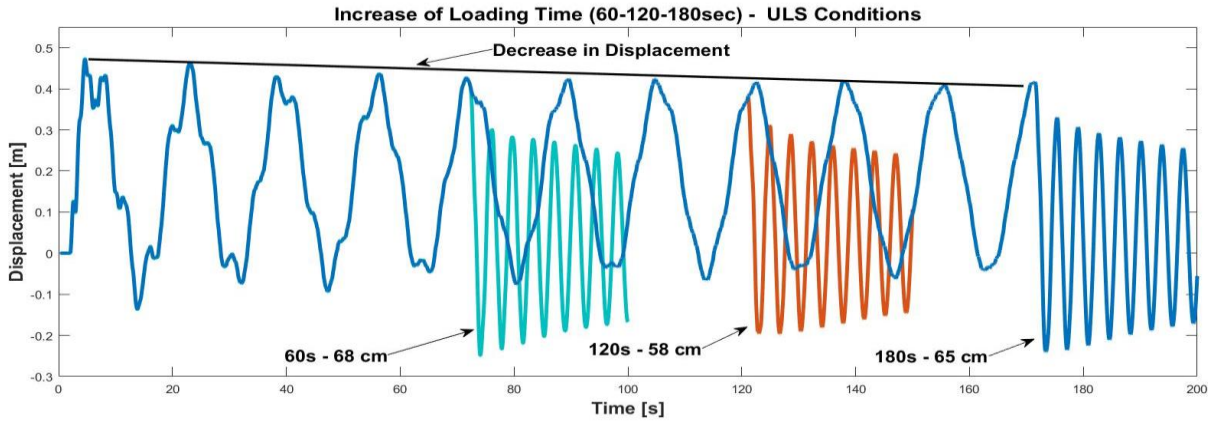

Figure 45: ULS - Effect of Loading Time Increase for 60-120-180sec Loading

In damping estimation, the value of damping is slightly affected by the increase of loading time and it is almost the same for 120-180 seconds loading case where the value of damping is found to be between 1.53 % and 1.56%, which means the amount attributed for soil damping is equal to 1.34% to 1.37%.

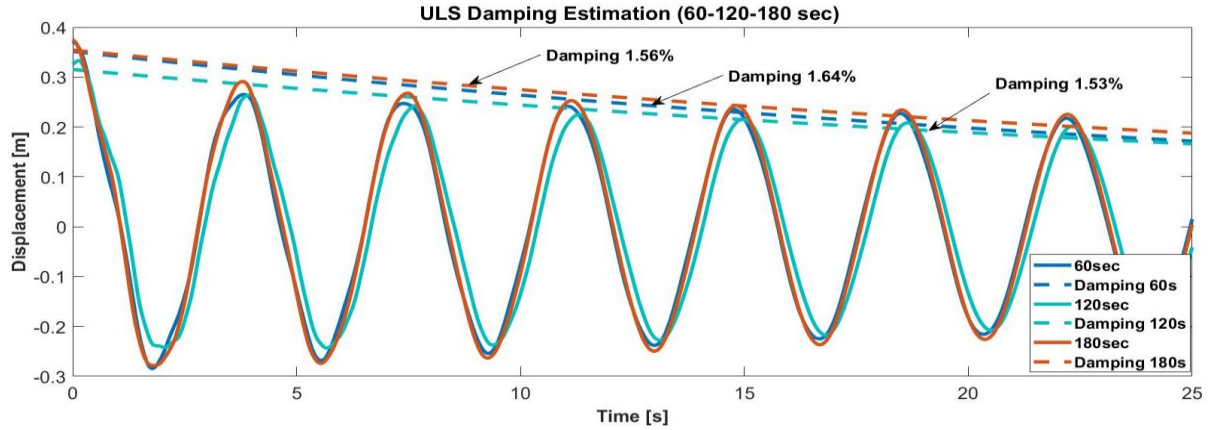

Figure 46: ULS Damping Estimation for 60-120-180sec Loading

4.5.4 Shear Stress-Strain - Soil Behaviour

Previously, only the structural response at monopile head was analyzed while in this subchapter a limited amount of simulations was undertaken in order to examine what is happening with the sand soil medium while it is exposed to the mentioned SLS and ULS loading histories. For this purpose, the Position 2 simulation was taken as a reference model, from which the shear stress-strain curves were obtained. The control points were strategically pre-defined by picking the stress points in Plaxis 3D and the locations of stress points are roughly close to the ones depicted in the Figure 47. This means that they are located at depth (Z-direction) of 3.5 m (SP 1 and SP 2) and at 14.5 m (SP 3 and SP4), while all the stress points are at the distance which is about 4.5 m from the pile (X-direction).

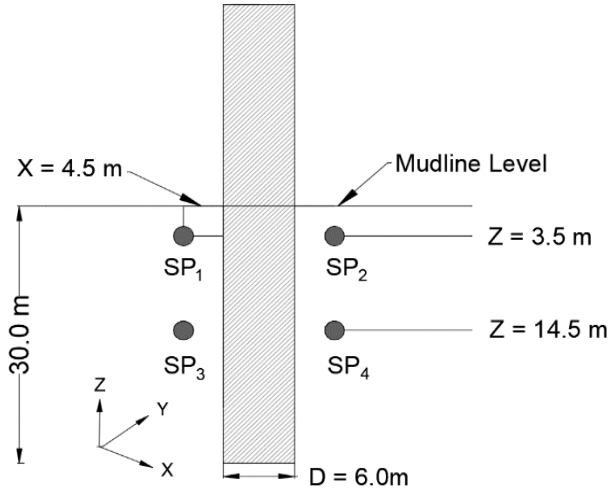

Figure 47: Positioning of the Stress Points in Plaxis 3D

Firstly, the SLS loading case is analysed for 210 seconds and this includes a typical loading history followed by the free vibration phase. To get an idea about the magnitude of accumulated strain levels, the Figure 48 shows the shear stress-strain response for all the analysed stress points in x-z direction.

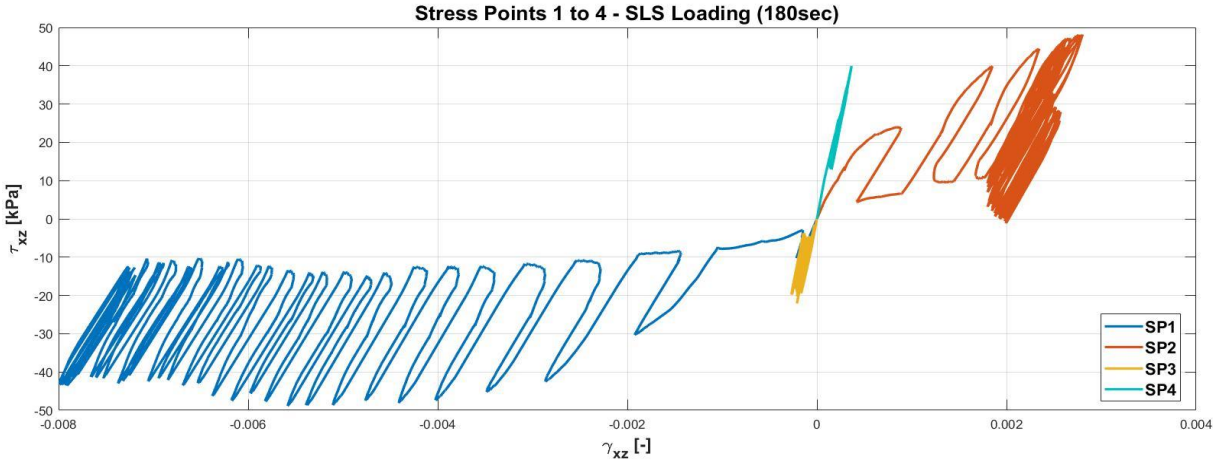

Figure 48: Stress-Strain Loops for all Stress Points - SLS Conditions

The following Figure 49 introduces a time color bar in the stress-strain graphs which allows the user to separate between the loading and free vibration phase (starts at 180 seconds). The time vector is placed on the right side and it is represented as a time colorbar which is progressing from 0 to 210 seconds. It can be noticed that the stress points which are closer to mudeline level (SP1 and 2) accumulate more strains since they are exposed to larger stress amplitudes. Generally, the soil stiffness does not change dramatically since the hysterisis cycles are alligned in a similar manner as the time progresses; this seems like a typical behaviour since the SLS conditions are considered. For SP1 and 2 the strains are further accumulated but in the free vibration phase (when there is no additional loading on the structure) some of the strains are recovered. For the SP 3 and 4 accumulation of strains occurs at much lower rate. Also, it can be said that the SP3 and 4 have less accumulated strains, since they are exposed to smaller stresses (deeper position and hence less affected), another reason can be found in the fact that this deeper sand deposit has a higher small-strain stiffness (G_0) value when compared to the top sand layers. The stress points on the right-hand side (2 and 4) are

accumulating positive while left-hand side (1 and 3) are accumulating negative strains, which is indeed in line with the direction of applied loading scenario.

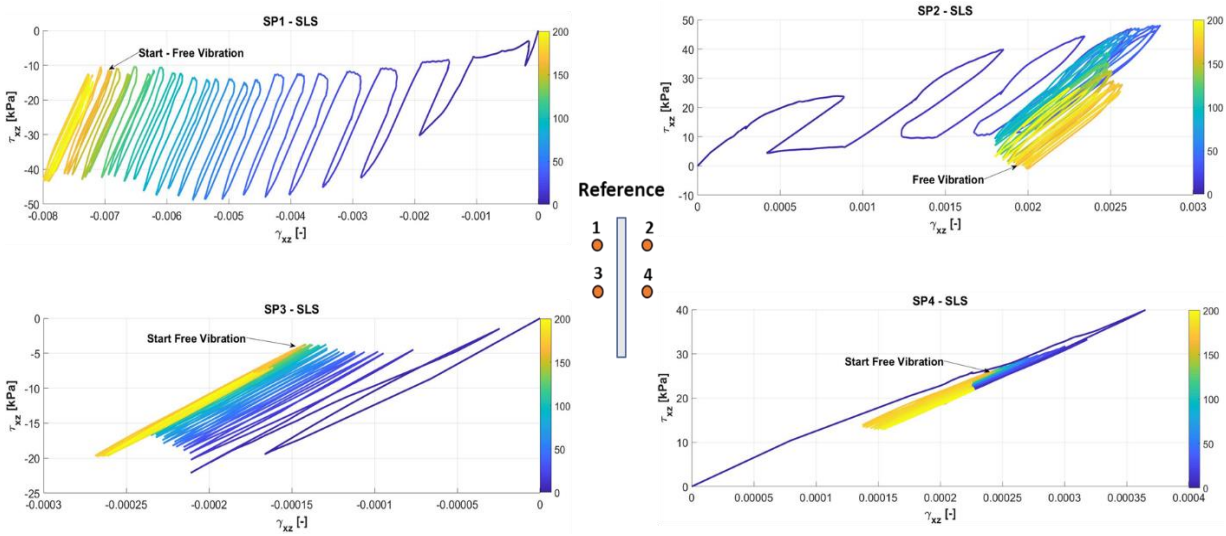

Figure 49: Stress-Strain Curves in Time for all Stress Points - SLS Conditions

For the second case (see Figure 50), the ULS loading is analysed for stress-strain response where a different behaviour is recorded. In the ULS conditions the top stress points (SP1 and 2) keep accumulating strains even after the load is removed, actually there is a huge accumulation when the free vibration occurs. The rate of accumulation is much higher when compared to the SLS conditions. Soil stiffness at bottom points (SP3 and 4) keeps its high value and this can be seen by very low accumulation of strains.

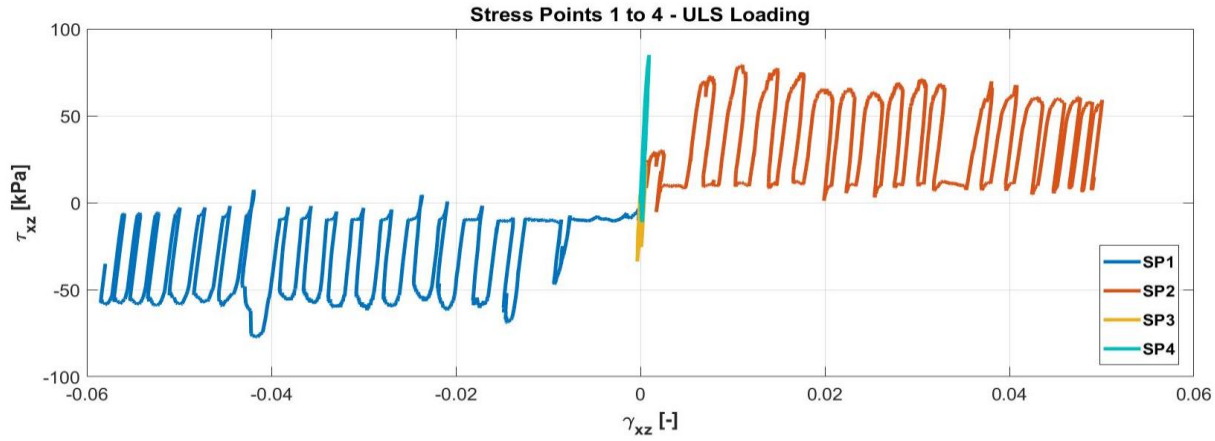

Figure 50: Stress-Strain Loops for all Stress Points - ULS Conditions

When analysing each stress point separately (see Figure 51), it can be seen that there is no recovery of strains for the SP1 and 2. In the case of the SP3 and 4, strains are partially recovered when the free vibration initiates, but then they are accumulating again. A great difference in maximum strain value is observed between bottom and top stress points (e.g. top – 5 to 6% and bottom – 0.1%). The top points are definitely reaching out of the small-strain range, while the bottom ones are right on the border between small-strains and large-strains (0.1% limit).

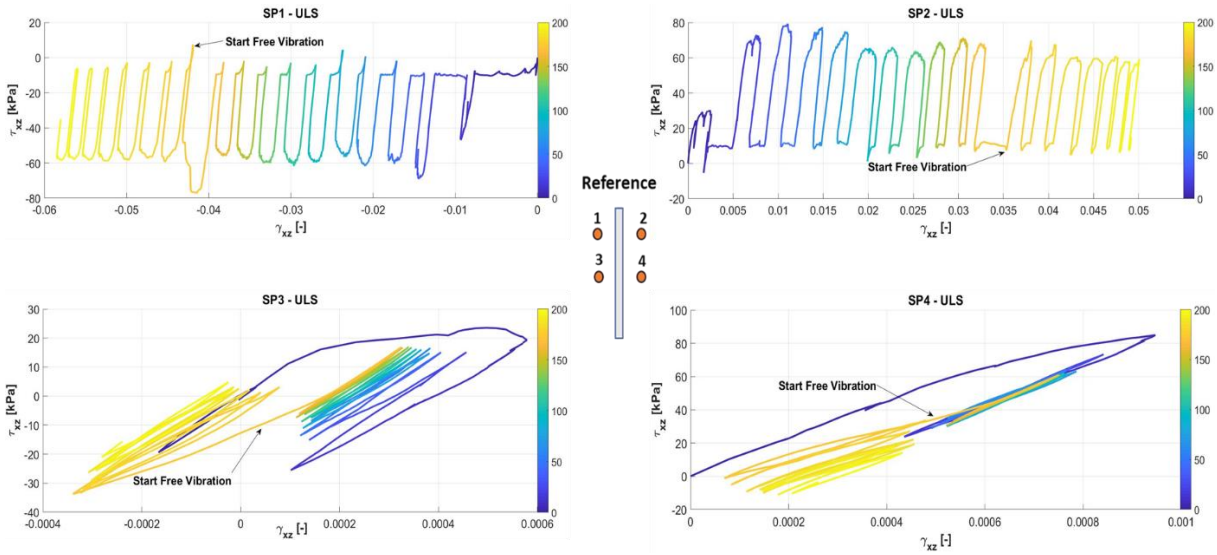

Figure 51: Stress-Strain Curves in Time for all Stress Points - ULS Conditions

4.5.5 Undrained Analysis

A limited amount of simulations was undertaken in order to test the soil-structure behavior in undrained conditions. For this case a hydraulic head was placed at 27 meters above the mudline level (just like it is depicted in the model description). The drainage conditions in Plaxis 3D are changed from "Drained" to "Undrained (A)". The mentioned undrained conditions utilize the effective stress analysis and therefore it works with the effective parameters. The main objective of these simulations is to check the influence of the undrained conditions with an emphasis on the ULS conditions since it is assumed that excessive pore water pressure generation affects the structural response and soil behavior.

Firstly, the amount of damping is analyzed to check the difference between drained and undrained approach and to verify the influence of the hydrodynamic damping values (ζ_{hydro}) which was reported in different studies from 0.07% to 0.23% (2.2 OWT Damping Sources). From the Figure 52 it can be seen that the amount of damping obtained is equal to 1.87% which confirms that the mentioned range for the ζ_{hydro} seems to be verified, since the difference between drained and undrained damping is equal to 0.23%. Moreover, this has to be further verified with more advanced soil models which are specifically designed for undrained behaviour conditions.

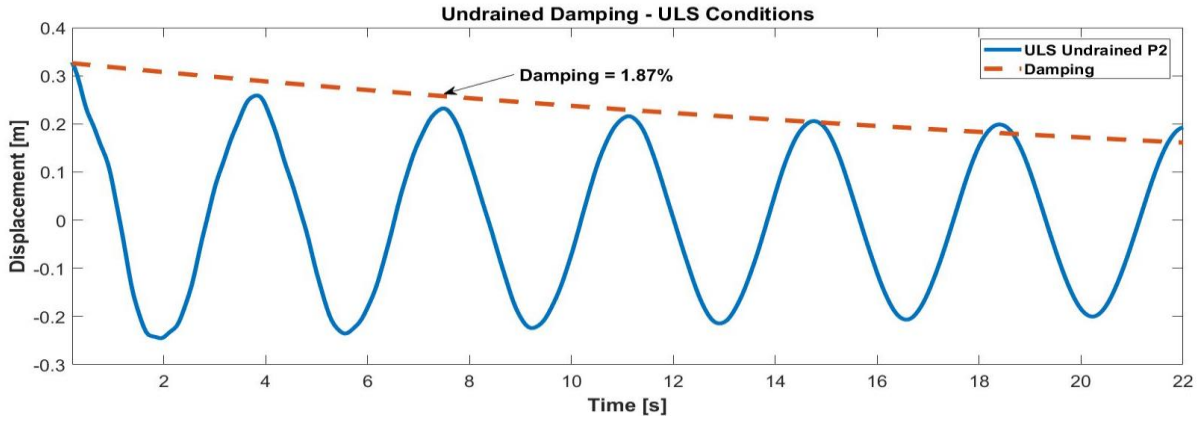

Figure 52: Undrained Damping Estimation for ULS Conditions

Going forward, the undrained analysis can be examined by looking at pore water pressure development through time. For this purpose, the "U-P" formulation is utilized (Zienkiewicz, Chan, Pastor, Schrefler, & Shiomi, 1999) where *u* represents the pore water pressure and the *p* is the mean stress. The ratio of u/p describes the soil behaviour in a manner where the ratio (u/p = 1) indicates a liquefaction limit; if pore pressure is larger than a mean stress (u > p) then a liquefaction phenomena occurs since the pore water pressure is increased and therefore the shear strength of soil is lost.

The SLS undrained conditions were analysed for 150 seconds (see Figure 53) where it can be seen that the top stress nodes (SP1 and 2) experience a slight increase in u/p (soil compression) and then there is small decay in pore water pressure which is connected to a dilative behaviour of top nodes due to shearing of soil and insufficient development of pore pressure while exposed to SLS loading conditions. Moreover, the behaviour of top nodes is a typical for dense sand (slight compression followed by dilation phase). The bottom stress nodes (SP3 and 4) can be considered not affected by the SLS conditions since there is almost no change in u/p ratio, hence no dilation (which happens due to high confinement stress and low development of pore pressure).

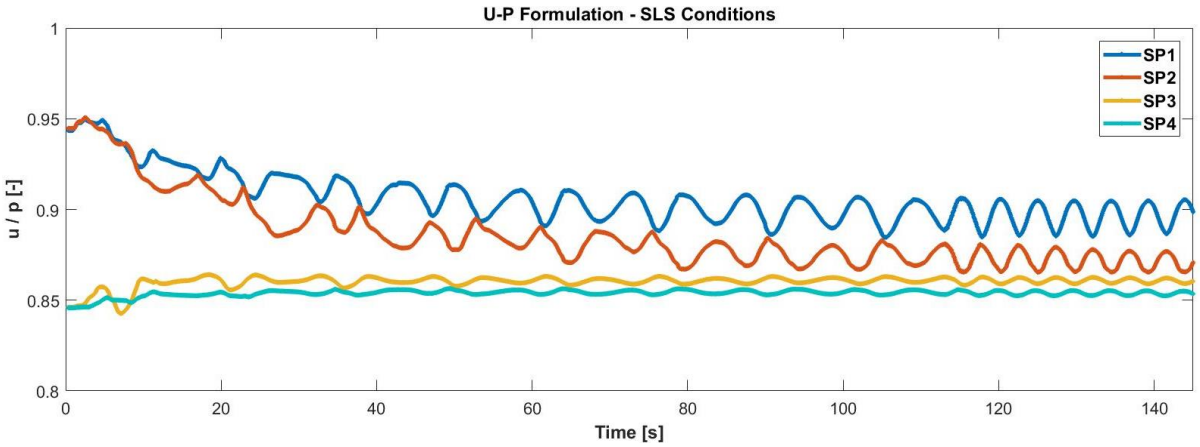

Figure 53: u/p Formulation for the SLS Loading Case

In the case of ULS loading conditions (see Figure 54), it is possible to see quite contrasting situation which is attributed to large changes in pore pressure and mean confining stress far-reaching even into the deeper soil layers (SP3 and 4). The right nodes (SP2 and 4) are considered to be on "passive" side (structure moves towards soil), and in the case of the deeper node (SP4), when the first load cycle is applied there is large increase in mean stress, therefore there is a drop in the u/p ratio. Complete opposite situation is happening on the "active" side which is the left lower node (SP3) which is experiencing a drop in the mean stress, therefore an increase in u/p ratio. Moreover, these rapid changes in mean stress can be related to a sudden movement of the monopile structure. After the initial load impact, the lower nodes seem to show a steady behaviour, although they are "less" stable compared to the top nodes (due to high u/p ratio). Top nodes (SP1 and 2) are experiencing a constant decrease in u/p ratio, while for the "passive" node (SP2) this happens on a larger rate due to larger increase of mean stress. Again, there is a dilative tendency of soil which can be seen for top nodes. An interesting observation can be seen in the fact that the amplitude stretch for the top nodes in free vibration phase are much longer compared to the bottom nodes, which again confirms the fact that lower nodes are less exposed to changes in pore pressure and mean stress.

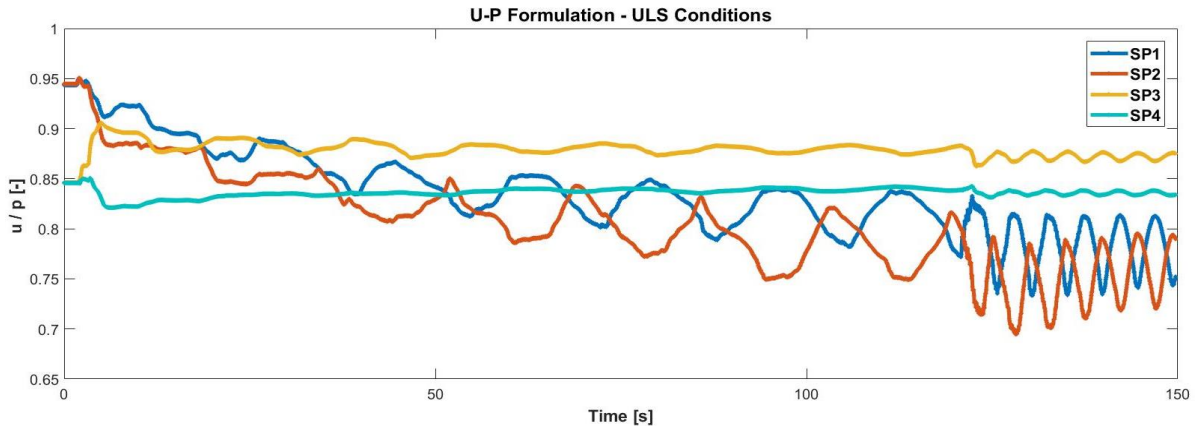

Figure 54: u/p Formulation for the ULS Loading Case

4.5.6 Natural Frequency Degradation

The last part of this thesis is dedicated to the brief analysis regarding a degradation of natural frequency. The natural frequency plays an important role in the design of OWT foundation structure and usually overconservative designs are implemented due to lack of accuracy in estimating the potential design value. Most of the OWT structures are meant to be placed in the design frequency range which is between 1P and 3P or more known as the "soft-stiff" range.

For this purpose, the natural frequency was estimated in four different cases with different wind speeds: 5, 12, 17 and 25 m/s respectively. The simulations were standard with drained approach utilized and the frequency spectra was obtained with the Plaxis output tool which allows for the extraction of the PSD curves. The natural frequency is obtained from the free-vibration part since there is no more loading influence on the OWT structure. The analyzed wind speeds along with natural frequencies can be seen in the Figure 55.

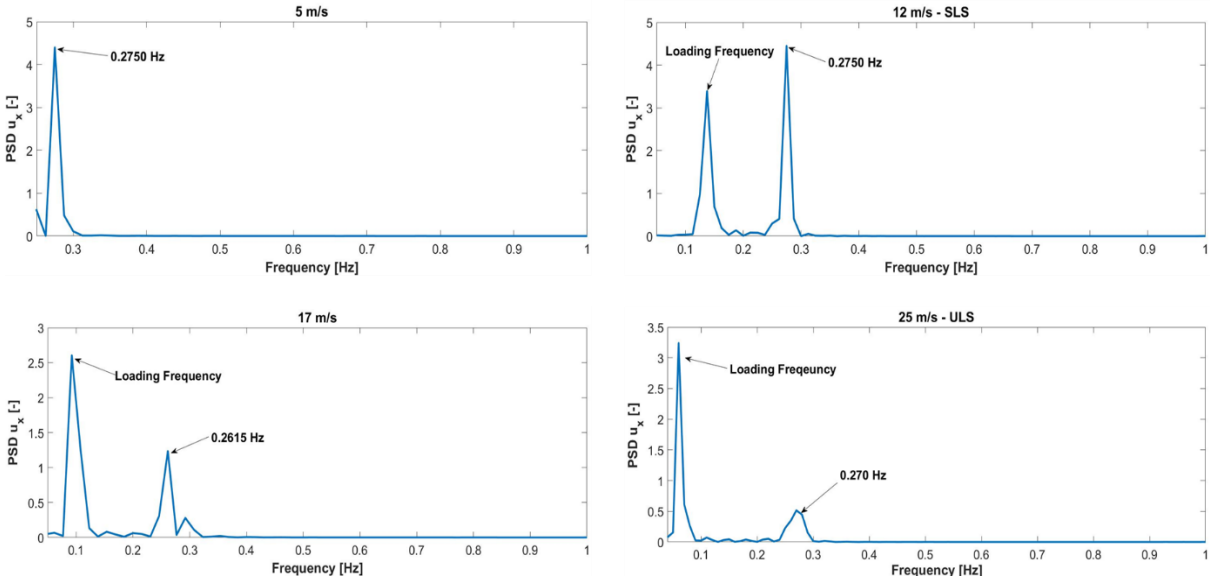

Figure 55: Natural Frequencies for Different Wind Speeds.

What it can be observed from the above Figure 55 is related to a drop in the OWT natural frequency, which is reaching a drop of almost 2% when comparing the SLS (operation) and ULS (storm) conditions. This is a significant value for the offshore wind circumstances since a very tight frequency-range design is utilized and this could have a significant impact on the lifecycle of the structure if the natural

frequency tends to go towards 1P and environmental forcing (wave) frequencies. This shift towards the lower frequencies tends to amplify the responses (resonance effect) in terms of larger amplitudes (e.g. stress, displacement) and therefore, it puts more accumulated fatigue damage on the structure which is in contrast reducing the lifetime of structure. On the other hand, this does not mean that the structural integrity of the OWT is in a danger-zone, which suggests that the structure is well designed.

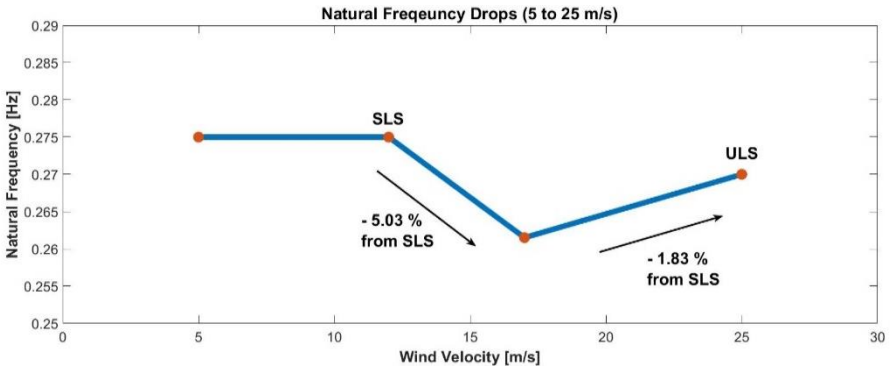

Figure 56: Percentage Drop in Natural Frequency for Different Wind Speeds

The drop in freqenucy could be related to a sudden load application which could produce a gapping effect in the mudline interface zone between the soil and monopile (see Figure 57). The soil around the monopile is disturbed due to short-term cyclic loading and the gapping may occur since the soil in the passive zone (behind the pile) experiences inelastic behaviour with permanent accumulation of strains (Carswell, et al., 2016), which is the case for the upper stress nodes in the shear stress-strain analysis.

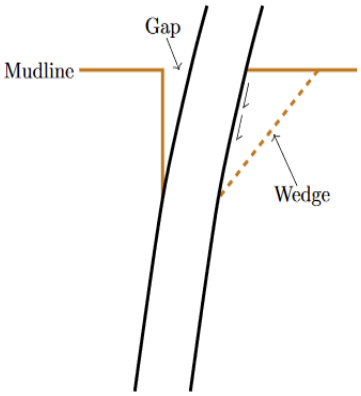

Figure 57: Soil Gapping. Source: (Beuckelaers, 2017)

The initial frequency-drop study was based on the short term wave and wind loading (60 seconds). Dilative behaviour is characteristical for dense sands, which can increase the soil stiffness and in return increase the natural frequency, for this purpose volumetric strains will be analyzed further in this subchapter. Regarding to dilative behaviour, the ULS conditions are analyzed for the three different loading scenarios (60-120-180 sec) and the drop is observed for the first two loading time frames, while for the 180 seconds loading the freqeuncy is increased back to its intial value (see Figure 58), which is attributed to the dense sand dilatative behaviour.

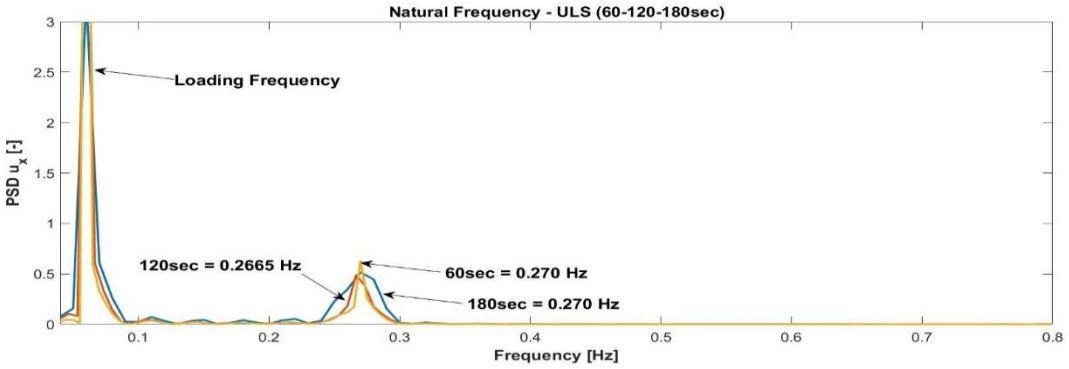

Figure 58: Frequency Estimation for the ULS Conditions (60-120-180sec)

In order to prove that the dense sand dilates, a volumetric strain is presented in the following Figure 59 for the top nodes (SP1 and SP2) where on the horizontal axis the axial strain (ε_1) is placed while on the vertical axis there is volumetric strain (ε_v). What can be observed that for the cases when the wind speed is equal to 12 and 17 m/s that there is predominantly compressive sand behaviour which is related to decrease in soil stiffness and therefore the natural frequency tends to drop, which is indeed the case for 17 m/s wind speed. When looking at the ULS case (based on the 25 m/s) there is a non-elastic (soil plasticity) strain accumulation. Moreover, from the Figure 59 it can be seen that for the ULS case there is a typical dilative sand behaviour which starts with initial compression, followed by the dilation phase. Dilation and volume expansion tend to stiffen the soil, therefore there is a slight increase in a natural frequency for the ULS case.

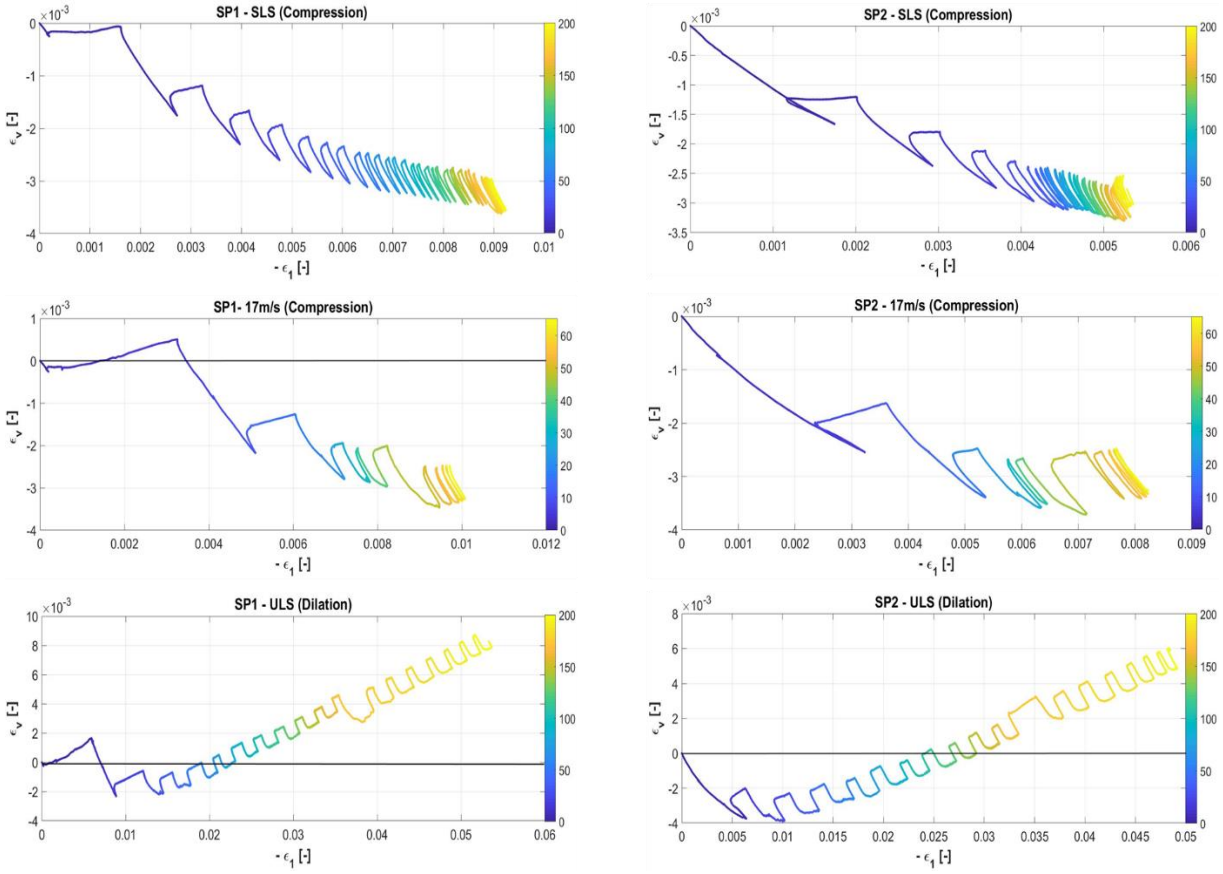

Figure 59: Analysis of Compression and Dilation for 12, 17 and 25 m/s. Below black line – compression, above – dilation

4.6 Comparison with Literature

The main aim of the thesis research was to estimate the soil damping contribution in the case of the offshore wind monopiles. For this purpose, the Plaxis 3D model was developed and simulated under different environmental loading conditions. In order to check the relevancy of the obtained results it is an imperative to make a comparison with the other research projects (mostly PhD projects). The following Table 13. was adopted from the similar study which gathered all the relevant information (Carswell et al., 2015) regarding other studies as well. The table was slightly modified in order to include more essential information such as: monopile L/D ratio and wind velocities to which the OWT structures were exposed.

Table 13: Various Studies on Offshore Monopile Damping. Information Adopted from: (Carswell et al., 2015)

	(Tarp-Johansen, et al., 2009)	(Versteijlen, 2011)	(Damgaard, Ibsen, & Andersen, 2012)	(Damgaard M. , Ibsen, Andersen, & Andersen, 2013)
Method	Experimental	Experimental	Experimental	Experimental
Analysis	3D Fem	Modified p-y	Hysteretic p-y	Hysteretic p-y
OWT	NREL 5 MW	Siemens 3.6 MW	-	Vestas 3 MW
Soil Profile	Generalized sandy or clayey North Sea	Med. dense Sand / Clay	Loose Sand to very stiff/hard clay	Medium dense Sand and soft Clay
Monopile (L/D)	4.26	4.68	5.38	-
Wind Velocity	-	11 to 19.7 m/s	3 to 13 m/s	-
ζ_{total}	0.75-0.99%	3.00%	0.77%	0.8-1.3%
ζ_{struct}	0.19%	1.50%	0.19%	-
ζ_{soil}	0.56-0.80%	1.50%	0.58%	0.8-1.3%
	(Shirzadeh, Devriendt, Bidakhvidi, & Guillaume, 2013)	(Carswell et al., 2015)		***This Study - 2018***
Method	Experimental	Numerical		***Numerical***
Analysis	HAWC2, Rayleigh	2D/3D FEM		***3D FEM - PLAXIS***
OWT	Vestas 3 MW/ NREL 5 MW	NREL 5MW		***2-5 MW Turbine / Siemens 3.6MW***
Soil Profile	Dense Sand with stiff Clay	Soft, stiff and hard Clay		***Dense Blessington Sand***
Monopile (L/D)	4.12	5.67		***5***
Wind Velocity	4.5 to 6.5 m/s	-		***12 to 25 m/s***
ζ_{total}	0.85%	1.17-1.28%		***SLS: 0.62-0.70% ULS: 1.53-1.64%***
ζ_{struct}	0.60%	1.00%		***0.19%***
ζ_{soil}	0.25%	0.17-0.28%		***SLS: 0.43-0.51% ULS: 1.34-1.45%***

From the above Table 13, it can be seen that obtained values are capturing a diverse range of soil damping values going from the 0.17% and all the way up to 1.5%. This thesis research along with its Plaxis 3D approach yielded a satisfactory set of values which is right in the mentioned range. The large scatter in obtained values could be due to many factors which are explained further herein. The other studies were done with different soil profiles, with combinations of clay, sand or both. Apart from the different soil profiles, there are various approaches to the problem which also leads to different estimates. A large range of environmental conditions was used, mostly the high wind speeds (e.g. 25 m/s) were not considered, therefore many of the studies did not include soil non-linearity while exposed to high stress-strain levels. Finally, different L/D ratio were utilized, although they are all in close range between 4.50 to 5. All of these mentioned factors could have led to a different estimation of the soil damping contribution to the total OWT damping.

Chapter 5: Research Conclusions

This chapter leads to the final stage of this thesis where based on the conducted research the main conclusions are drawn and discussed. Along with the conclusions, the recommendations will be presented for future potential projects. Finally, combined with recommendations, there were various research limitations which were faced during this 8-month long journey and they are further described in order to understand which parts can potentially be improved.

The thesis objective was stated in the first chapter and it is based on the main research question:

What is the contribution of soil damping on offshore monopile under different loading scenarios?

Following from the main question, the conclusions are presented here:

- After multiple simulations were undertaken with the Plaxis 3D, the results have shown that value of damping which is attributed to soil source can have a quite large scatter, which again highly depends on the applied magnitude of external wave and wind loads. From the results section it can be seen that the value of soil damping in free vibration (for first natural frequency) was found to be about 0.43% for the SLS conditions and all the way up to 1.45% which represents the ULS conditions. The values which were obtained are well within the range that was published so far in the other mentioned research studies which were mostly done at higher research level (e.g. PhD research projects). This was the first time that offshore soil damping was analysed specifically with Plaxis 3D and it yielded quite relevant results.

- To understand the source of the soil damping, it is necessary to shed some light on this mechanism and how its value increases. While applying different loading scenarios (SLS, ULS) it was clear that soil damping value increases with the loads being increased. Moreover, while the OWT structure is exposed to stronger loads it is also obvious that the displacement at monopile head increases, which eventually leads to larger displacement amplitudes and therefore this increases damping. Continuing from the structural side it also possible to look at soil behaviour where it can be also concluded that damping value increases when the strain levels in soil are larger. Naturally, if the strains are reaching larger values, then the soil stiffness is degraded and the soil which is less stiff has more damping potential because it can absorb more energy compared to the stiffer soil.

- Moreover, the utilized HSS soil model is based on the hysteretic damping (also most dominant source of soil damping when considering offshore conditions) and this value highly depends on the magnitude of load, which again proves that the model performs well according to the applied loading scenarios. During the simulations, it was observed that the damping value does not change while the frequency is changed, which again proves that hysteretic damping is frequency independent. For the frequency dependency, it would be beneficial to employ a viscous damping formulation by means of Rayleigh damping.

- Lastly, assigning a single value for soil damping is a misconception. A potential offshore foundation designer shall not be mistaken when deciding on the soil damping because its value is highly correlated to a certain combination of: monopile geometry specifications, soil profile and possible load scenario. Therefore, the values obtained in this study should be interpreted with the caution since this research was based on a certain combination made

of a dense sand profile combined with 6 meters diameter monopile (L/D was equal to 5). Moreover, from the study it is obvious that damping value is greatly influenced by the initial displacement amplitude (from free vibration) which is in return a product of environmental loads. On the other hand, the OWT will be mainly in a production regime during its lifecycle and the displacement amplitudes during production are undoubtedly on a smaller scale when compared to conditions which were used for free vibration herein and in other mentioned studies. From this statement it is obvious that soil damping is a complicated mechanism which is quite challenging to be obtained with a certain accuracy. To conclude the main focus of the thesis: soil damping potential is definitely there and eventually it should be implemented in the offshore design codes in order to make additional cost savings by means of extending the lifetime of structure and reducing the amount of steel.

Apart from the main research question, the additional complementary sub questions were also formulated in the Chapter 1 and they are directly answered within the thesis report with different choices regarding the chosen soil model in Plaxis, derivation of environmental loading scenarios and estimation technique for soil damping. Moreover, the reasoning and justification of these choices is already described in the appropriate chapters which account for each of the mentioned subjects. Therefore, here, just the main conclusions will be presented.

- The HSS constitutive soil model was chosen after the other potential models were evaluated. This model seemed to be the most appropriate one since it had soil parameters ready at disposal and there was a relevant case study (Blessington Piles) to which it could be compared and verified. On the other hand, the model accounts for hysteretic damping which is the main source of soil damping in the offshore conditions.

- The wave and wind loads were derived according to mentioned literature and this is considered a simplified approach. The loading scenario accounts for the appropriate wind speeds which are further implemented into wave and wind thrust forces. Also, the derivation takes into account the geometry of the OWT structure, derives the height of potential sea waves and it gives them certain time period (frequency). Although it is a simplified approach, it accounts for the most important factors and therefore this approach can be considered relevant.

- From this and other research studies it is clear that the logarithmic decrement method is quite convenient and yet simple and efficient method to estimate a decay in amplitudes (for only one frequency bending mode) which is directly used to estimate the damping. This study presents a straightforward and automated code which allows a potential user to choose the amplitude peaks and quickly analyse damping and natural frequency in free vibration phase.

- Touching on the numerical simulations, it was revealed that monopile positioning or the position of the structure at the start of free vibration phase plays an important role in determination of damping. Moreover, during literature study it was revealed that the monopile positioning was not considered in any of the previous studies. The value of damping was found to be fluctuating depending on the considered position and the difference in obtained damping values were significant in both SLS and ULS conditions. The Position 2, which is a combination of both wave and wind loads acting in the same direction has proven to be a position from which damping is reaching its highest potential; this is also related to

largest displacement level at this position since it is a combination of two maximum loads. On the other hand, the Position 1 yielded smallest damping values and this is related to the wave load which is reaching zero value and therefore displacement is not reaching its full potential. To conclude, from monopile positioning it was proven that the damping increase is associated with increase of displacement and applied load value.

- The application of LP and HP filtering has proven to be very crucial in obtaining a realistic displacement curve. The LP filtering was employed in multiple scenarios, especially for the Case I and some monopile positioning situations where the 2nd bending frequency was distorting the obtained signal and therefore without filtering it would lead to a false estimation of damping.

- From the Case I it was shown that Plaxis can also deal with small-strain range and it can estimate damping and natural frequency with high accuracy. The numerical Plaxis model was compared to experimental data from the Blessington Piles case and it performed much better than other theoretical approaches utilized in the research (Prendergast & Gavin, 2016). Moreover, it was found that soil parameters (Tolooiyan & Gavin, 2011) were in good agreement with obtained results which gave further confidence to keep the same parameters in the Case II. and that the G_0 small-strain stiffness is essential parameter for this type of testing.

- It was also shown that the natural frequency of the OWT structure generally follows the trend of degradation while the applied environmental loads are increasing. On the other hand, since the dense Blessington sand was analysed, it was concluded that when the OWT is exposed to the ULS loading the natural frequency is slightly increased which is a result of sand dilatative behaviour which is also supported by the obtaining the relevant volumetric strain graphs. The reduction of natural frequency did not jeopardize the structural integrity of the OWT but it places the structure closer towards 1P – frequency range which indeed can amplify the stresses and therefore boost the fatigue damage.

- The last thing to note is the undrained behaviour which was utilized as a part of additional study. It was proven that with inclusion of water level the damping increases and this difference was estimated to be within the range that was proposed in other studies (ζ_{hydro}) which gives another boost to the relevancy of the study. Interesting behaviour was recorded while analysing the stress nodes in undrained approach and it was shown how the change in mean stress and pore pressure (U-P) can have a significant influence on the response.

5.1 Recommendations and Limitations

The final words will be dedicated to a possible research improvements and recommendations which could be utilized potentially in the future projects. At the same time, while talking about recommendations, the main limitations will be mentioned in the same context as they are a major source from which the recommendations are formed. From the start, this research was bounded by few major factors and those are time for the execution of the project, the availability of software which in this case is Plaxis 3D and lastly lack of relevant information such as experimental offshore testing from the currently installed OWT's. The MSc thesis research usually takes about 7 to 8 months and this period covers an essential literature study along with the whole execution of the research.

The Plaxis 3D software is available only in the certain computer rooms at TU Delft campus and in many situations, the out-dated version was mostly available (e.g. 2016 version) which is not compatible with the current 2017 version. Moreover, the computers with installed Plaxis software were often used by the classes which are regularly held at the campus. In spite of all of these issues, the satisfactory amount of simulations was performed to reach a desired level of results.

Finally, it is possible to present some major recommendations which are the product of the learning process and conducted research on the soil damping in offshore monopiles.

- This research was based on a certain combination made of monopile, soil profile and appropriate loading scenario which is associated with the structure geometry. Building on this, it would be attractive to make similar models in Plaxis which include different pile geometries (e.g. L/D ratio). The soil profile was based on the dense Blessington sand which only differs its layers on the small-strain stiffness value and for this purpose it would be beneficial to obtain a relevant soil profile (e.g. typical North Sea profile), also it would be interesting to see how the model behaves when the structure is installed in the soil profile which is a combination of loose and medium-dense sand, or also a combination between sandy and clayey soil. It would be interesting to track the amount of damping while testing out sands with different relative densities (e.g. 60-80-100%). After mentioning some possible soil combinations, a heterogeneous soil profile would be appropriate thing to simulate with the Plaxis.

- The utilized HSS soil model accounts for hysteretic damping which is the main source of soil damping but it is not designed to perform in undrained drainage conditions, so its results are rather questionable. Since the offshore environment is surrounded by the sea water, it is recommended to analyse the same problem with more advanced soil models that have appropriate undrained formulation which yet might not be implemented in Plaxis. Appropriate undrained behaviour can give further insight, especially considering natural frequency and damping, where the development of pore water pressures could play a significant role. Also, it would be good to see the influence of permeability, which could have a major impact on the behaviour. Moreover, this could be crucial for clayey soil profiles in which the soil permeability is rather low compared to sand profiles, therefore a considerable pore water pressure development is expected.

- The loading scenario in this research used a simplified approach, which means that the wave and wind loads were derived by the potential wind speeds that were established as the SLS and ULS conditions. Although the mentioned loading scenario is derived according to the available literature guidelines, it would be recommended to obtain a realistic loading history from the relevant source. Also, in a real offshore situation it is possible that the wave and wind loads would come from various directions and in this study, it was assumed they are operating co-directionally or so to say in the same direction; therefore, it would be interesting to see how the structure behaves with different loading directions. Continuing on this, it would be also beneficial to develop a full 3D OWT model to investigate if there is a discrepancy between half model and full model. Finally, since the loading history is discussed, it is recommended to perform a longer analysis (e.g. 10 minutes of loading history) to see what is the influence on soil behaviour and damping.

- Final recommendations are based on the experimental testing which should be one of the major targets in the future research projects. The most valuable results should be obtained from the full-scale offshore measurements which keep track of the OWT response during operational (production) but also during parked, storm and shut-down conditions. There is a scarce of available information from the experimental measurements (e.g accelerometers placed on the hub level) and therefore this still insufficient to make a large-scale comparison between conducted research projects. In order to make a progress in this field of dynamic soil-structure interaction it is crucial to develop a database which would be beneficial for all potential offshore developers and designers. Lastly, a potential numerical FEM model such as the one developed in this study should be combined with small-scale experimental testing. These projects should be directed towards building a lab size model which would be installed in a certain soil profile and then tested with various loading scenarios. The development of small-scale model would allow for a decent verification of the numerical model.

Concluding this MSc thesis research, it was proven that there is still space for potential improvements in the offshore wind foundation design. Continuous research will eventually allow the offshore wind industry sector to be even more competitive with other energy sources. It is clear that there is a lot of opportunities to reduce the foundation cost, but still they need to be verified in order to be implemented in the current design codes and standards.

Bibliography

Aasen, S., Page, A., Skau, K., & Nygaard, T. (2017). Effect of foundation modelling on the fatigue lifetime of a monopile-based offshore wind turbine. *Wind Energy Science, 2*, 361-376.

Arany, L., Bhattacharya, S., Macdonald, H., & Hogan, S. (2016). Closed form solution of Eigen frequency of monopile supported offshore wind turbines in deeper waters in corporating stiffness of substructure and SSI. *Soil Dynamics and Earthquake Engineering, 83*, 18-32.

Arany, L., Bhattacharya, S., Macdonald, J., & Hogan, S. (2016). Design of monopiles for offshore wind turbines in 10 steps. *Soil Dynamics and Earthquake Engineering, 92*, 126-152.

Bayat, M., Andersen, L., & Ibsen, L. (2015). p-y-ẏ curves for dynamic analysis of offshore wind turbine monopile foundations. *Soil Dynamics and Earthquake Engineering, 90*, 38-51.

Benz, T. (2006). *Small-strain stiffness of soils and its numerical consequences.* Univesitat Stuttgart, Institut für Geotechnik.

Beuckelaers, W. (2017). *Numerical Modelling of Laterally Loaded Piles for Offshore Wind Turbines.* Oxford: University of Oxford.

Bhattacharya , S., Nikitas, N., Garnsey, J., Alexander, N., Cox, J., Lombardi, D., . . . Nash, D. (2013). Observed dynamic soil–structure interaction in scale testing of offshore wind turbine foundations. *Soil Dynamics and Earthquake Engineering, 54*, 47-60.

Bhattacharya, S. (2014). Challenges in Design of Foundations for Offshore Wind Turbines. *IET Engineering & Technology Reference*, 1-9.

Brinkgreve, R. (2018, February). Personal Communication on Suitable Soil Models.

Brinkgreve, R., Kappert, M., & Bonnier, P. (2007). Hysteretic damping in a small-strain stiffness model. *Numerical Models in Geomechanics*, 737-742.

Carswell et al. (2015). Foundation damping and the dynamics of offshore wind turbine monopiles. *Renewable Energy, 80*, 724-736.

Carswell, W. (2015). *Soil-Structure Modeling and Design Considerations for Offshore Wind Turbine Monopile Foundations.* Amherst, U.S.A: University of Massachusetts.

Carswell, W., Arwade, S., & DeGroot, D. (2016). Natural frequency degradation and permanent accumulated rotation for offshore wind turbine monopiles in clay. *Renewable Energy, 97*, 319-330.

Chen, C., & Duffour, P. (2018). Modelling damping sources in monopile-supported offshore wind turbines. *Wind Energy*, 1-20.

Chopra, A. (1995). *Dynamics of Structures* (Vol. 3). New Jersey, U.S.A: Prentice Hall.

Corciulo, S., Zanoli, O., & Pisanò, F. (2017). Transient response of offshore wind turbines on monopiles in sand: role of cyclic hydro–mechanical soil behaviour. *Computers and Geotechnics, 83*, 221-238.

Damgaard, M., Ibsen, L., & Andersen, J. (2012). Natural Frequency and Damping Estimation of an Offshore Wind Turbine Structure. *Proceedings of the Twenty-second International Offshore*

and Polar Engineering Conference (pp. 300-307). International Society of Offshore and Polar Engineers (ISOPE).

Damgaard, M., Ibsen, L., Andersen, L., & Andersen, J. (2013). Cross-wind modal properties of offshore wind turbines identified by full scale testing. *Journal of Wind Engineering and Industrial Aerodynamics, 116*, 94-108.

Damgaard, M., Ibsen, L., Andersen, L., & Andersen, J. (2013). Time-varying dynamic properties of of offshore wind turbines evaluated by modal testing. *Proceedings of the 18th international conference on soil mechanics and geotechnical engineering*, *116*, p. 234.

Det Norske Veritas AS. (2014). *Design of Offshore Wind Turbine Structures.* DNV.

Devriendt, C., Jordaens, P., De Sitter, G., & Guillaume, P. (2013). Damping estimation of an offshore wind turbine on a monopile foundation. *IET Renewable Power Generation, 7*(4), 401-412.

Doherty, P., & Gavin, K. (2011). Laterally loaded monopile design for offshore wind farms. *Proceedings of the Institution of Civil Engineers: Energy, 165*(EN1), 7-17.

Elwakil, A., & Azzam, W. (2016). Experimental and numerical study of piled raft system. *Alexandria Engineering Journal, 55*, 547-560.

EN 1991. (2005). *Eurocode 1: Actions on Structures - Part 1-4: General Actions - Wind Actions.* Brussels, Belgium: European Comittee for Standardization.

European Wind Energy Association. (2015). *Wind energy scenarios for 2030.* Brussels, Belgium: Wind Europe.

Germanischer Lloyd. (2005). *Overall Damping for Piled Offshore Support Structures, Guideline for the Certification of Offshore Wind Turbines.* GL Wind Energie

Han, S. (2010). Measuring displacement signal with an accelerometer. *Journal of Mechanical Science and Technology, 24(6)*, 1329-1335. doi:10.1007/s12206-010-0336-1

Hanssen, S., Nordal, S., & Eiksund, G. (2016). Impact vibration test of monopile foundation model in dry sand. *International Journal of Physical Modelling in Geotechnics, 16*(2), 65-82.

Hardin, B., & Drnevich, V. (1972). Shear modulus and damping in soils: Design equations and curves. *ASCE: Journal of the Soil Mechanics and Foundations*.

Hashash, Y., & Park, D. (2002). Viscous damping formulation and high frequency motion propagation in non-linear site response analysis. *Soil Dynamics and Earthquake Engineering, 22*, 611-624.

Kallehave, D., Byrne, B., LeBlanc Thilsted, C., & Mikkelsen, K. (2015). Optimization of monopiles for offshore wind turbines. *Phil. Trans. R. Soc, A373*.

Kupfer, C. (2018). *Investigation and Measurement of Oscillations of the H.E.S.S. Telescopes.* Master Thesis, Friedrich-Alexander-Universitat.

Lombardi, D., Bhattacharya, S., & Muir Wood, D. (2013). Dynamic soil–structure interaction of monopile supported wind turbines in cohesive soil. *Soil Dynamics and Earthquake Engineering, 49*, 165-180.

MathWorks, Inc. (2018). IIR Filter Design. Natick, MA, USA. Retrieved from http://nl.mathworks.com/help/signal/ug/iir-filter-design.html

Mercer , C. (2006). *Acceleration, Velocity and Displacement Spectra – Omega Arithmetic.* ProSig. Retrieved from http://prosig.com/wp-content/uploads/pdf/blogArticles/OmegaArithmetic.pdf

Morison, J., Johnson, W., & Schaaf, S. (1950). The Force Exertedby Surface Waves on Piles. *Petroleum Transactions, Aime, 189*, 149-54.

Navigant Consulting Inc. (2013). *Offshore Wind Market and Economic Analysis: Annual Market Assessment.* Burlington, MA, U.S.A.

Page, A., Skau, K., Jostad, H., & Eiksund, G. (2017). A new foundation model for integrated analyses of monopile-based offshore wind turbines. *Energy Procedia, 137*, 100-107.

Pierson, J., & Moskowitz, L. (1964). A Proposed Spectral Form for Fully Developed Wind Seas Based on the Similarity Theory of S. A. Kitaigorodskii. *Journal of Geophysical Research, 69*(24), 5181-90.

Plaxis BV. (2017). *Plaxis 3D Material Models Manual.* Delft, the Netherlands.

Plaxis BV. (2017). *Plaxis 3D Reference Manual.* Delft, the Netherlands.

Prendergast, L., & Gavin, K. (2016). A comparison of initial stiffness formulations for small-strain soil–pile dynamic Winkler modelling. *Soil Dynamics and Earthquake Engineering, 81*, 27-41.

Prendergast, L., Reale, C., & Gavin, K. (2018). Probabilistic examination of the change in eigenfrequencies of an offshore wind turbine under progressive scour incorporating soil spatial variability. *Marine Structures, 57*, 87-104.

Sheil, B., & McCabe, B. (2016). Biaxial Loading of Offshore Monopiles: Numerical Modeling. *International Journal of Geomechanics, 17*(2).

Shirzadeh, R., Devriendt, C., Bidakhvidi, M., & Guillaume, P. (2013). Experimental and computational damping estimation of an offshore wind turbine on a monopile foundation. *Journal of Wind Engineering and Industrial Aerodynamics, 120*, 96-106.

Stewart, G. (2012). *Load reduction of floating wind turbines using tuned mass.* Armherst, MA: Univerisity of Massachusetts.

Swagata, B., & Sumanta, H. (2014). Dynamic analysis of offshore wind turbine in clay considering soil–monopile–tower interaction. *Soil Dynamics and Earthquake Engineering, 63*, 19-35.

Tarp-Johansen, N., Andersen, L., Christensen, E., Morch, C., Frandsen, S., & Kallesoe, B. (2009). Comparing sources of damping of cross-wind motion. *The European Offshore WInd Conference & Exhibition.* The European Wind Energy Association.

Tolooiyan, A., & Gavin, K. (2011). Modelling the Cone Penetration Test in sand using Cavity Expansion and Arbitrary Lagrangian Eulerian Finite Element Methods. *Computers and Geotechnics, 38*, 482-90.

Versteijlen, W. (2011). *Estimation of the Vibration Decrement of an Offshore Wind Turbine Spport Structure Caused by its Intercation with Soil.* TU Delft.

Wind Europe. (2018). *Offshore Wind in Europe Key trends and statistics 2017.* Brussels, Belgium: Wind Europe.

Yang, J., Li, J., & Lin, G. (2006). A simple approach to integration of acceleration data for dynamic soil–structure interaction analysis. *Soil Dynamics and Earthquake Engineering, 26*, 725-734.

Zienkiewicz, O., Chan, A., Pastor, M., Schrefler, B., & Shiomi, T. (1999). *Computational Geomechanics with Special Reference to Earthquake Engineering.* Chichester, England: John Wiley and Sons Ltd.

Appendix A – Sensitivity Study

The sensitivity analysis was undertaken on three factors which were deemed crucial for the final analyses and those are mesh coarseness, boundary size and time step. All of the three mentioned factors were implemented in the Plaxis 3D simulations to see what their effect on the free vibration is and also to find the most suitable combination to be used further. The main aim was to find a combination which provides the lowest computational time and also provides a decent accuracy in terms of describing the monopile behaviour while it is oscillating. For this purpose, the load release test was designed to simulate the conditions which would be similar to free vibration in the tests which will be taken further (SLS and ULS analyses). The load release test was designed to load the structure at the hub level with a load of 4.5 MN which is loaded in 3 seconds time-frame and then the load is suddenly released. After the load release the structure is oscillating for 15 seconds and the differences between sensitivity combinations are captured. Finally, the sensitivity test was limited to only 15 seconds of free vibration due to time constraints. In the Figure A1, the loading procedure for the sensitivity test can be seen.

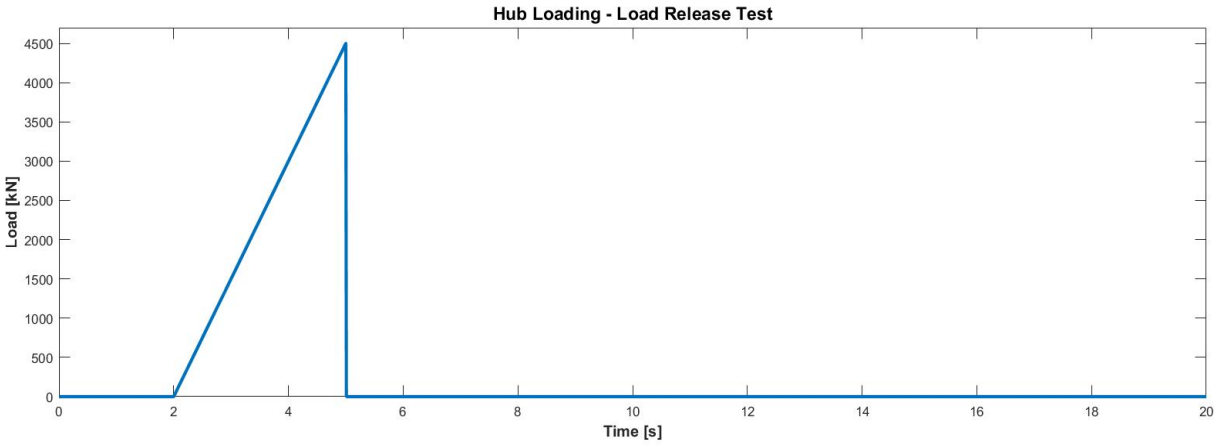

Figure A1: Hub Load Release Test

A.1 Mesh Sensitivity

As a first step in the sensitivity analysis the suitable mesh had to be chosen as a representative example mesh for the additional analyses (time step and boundary size). For this purpose, the time step was set up at dt=0.02 and the boundary size was at 80 meters for width and 40 meters for length of the model (depth is not changing and it is always set up at 40 meters). Four mesh cases were analysed and their information can be seen in the Table A1.

Table A1: Mesh Sensitivity Analysis Information

Mesh Sensitivity Analysis		
Mesh Type	**Elements**	**Analysis Time [min]**
Coarse	12420	59
Medium Standard	15862	89
Medium Improved	20812	145
Fine	26697	218

The result of the undertaken analyses can be seen in the Figure A2, from which can be concluded that all the tested mesh examples could be suitable candidates for the final analyses. Slight oscillation in

displacements is visible from the coarse mesh type and for this purpose the medium standard one is chosen as final mesh. It can be considered that the convergence is reached with usage of this mesh and the difference between this mesh and two finer ones is almost negligible while on the other side the computational time increases rapidly for other two mesh types, therefore this justifies the choice of the medium mesh. The increase of computational type with element increase can be seen in the Figure A3.

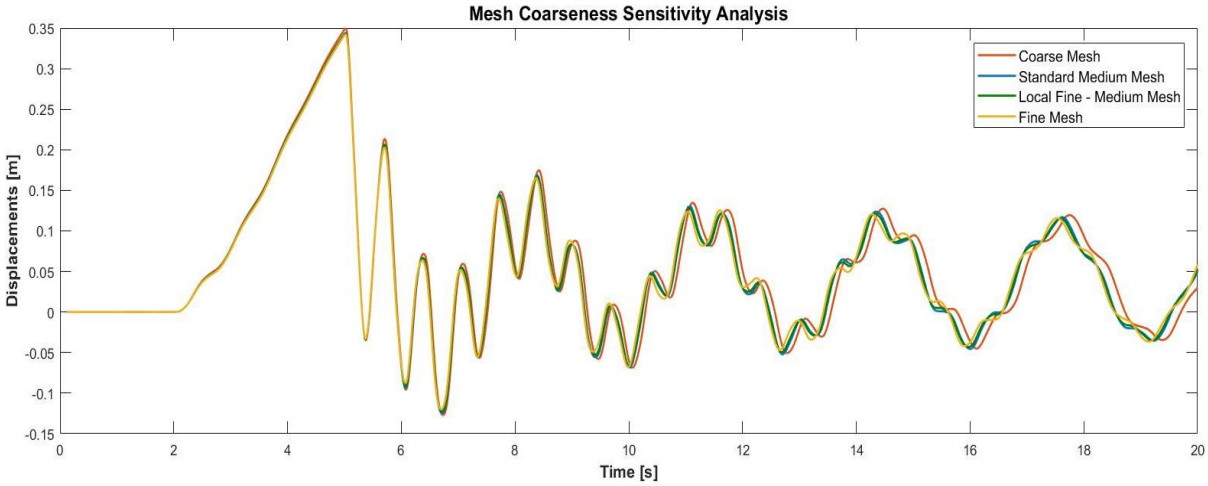

Figure A2: Mesh Sensitivity Analysis

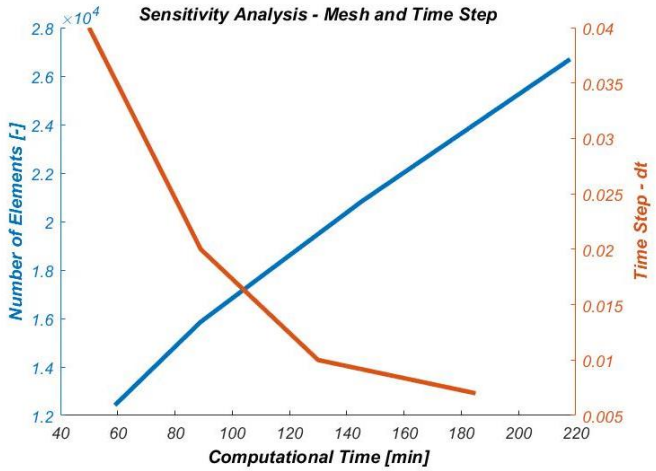

Figure A3: Mesh and Time Step Increase - Comparison with Time

A.2 Boundary Size Sensitivity

The second factor which was observed in the sensitivity analysis was the size of model boundaries. In this sense only, width (W) and length (L) were checked while the depth remained unchanged in every case (D = 40 m). The increase of the model boundaries also increases number of elements and nodes and therefore computational time is larger as well. The information on the different boundaries can be seen in the

Table *A2*.

Table A2: Boundary Sensitivity Analysis

Boundary Size Sensitivity Analysis	
Boundary Type (W x L)	**Analysis Time [min]**
50 x 25 [m]	47
60 x 30 [m]	65
80 x 40 [m]	89
100 x 50 [m]	145

There is a common rule of thumb for FEM simulations which advises to set up boundaries in static problem at distance five times the diameter (monopile) so this would result in distance of 30 meters to each side the model. For the dynamic analysis it is advisable to extend these limits even more; so, based on this information which served as starting point the boundaries were analysed from 25 to 50 meters to each side of the monopile. Although the model with largest boundaries is separated a little bit from the other ones, this difference is deemed insufficient to consider usage of this boundary because the computational time for this model is too long; therefore, this computational time burden had to be avoided due to limited time frame of the research.

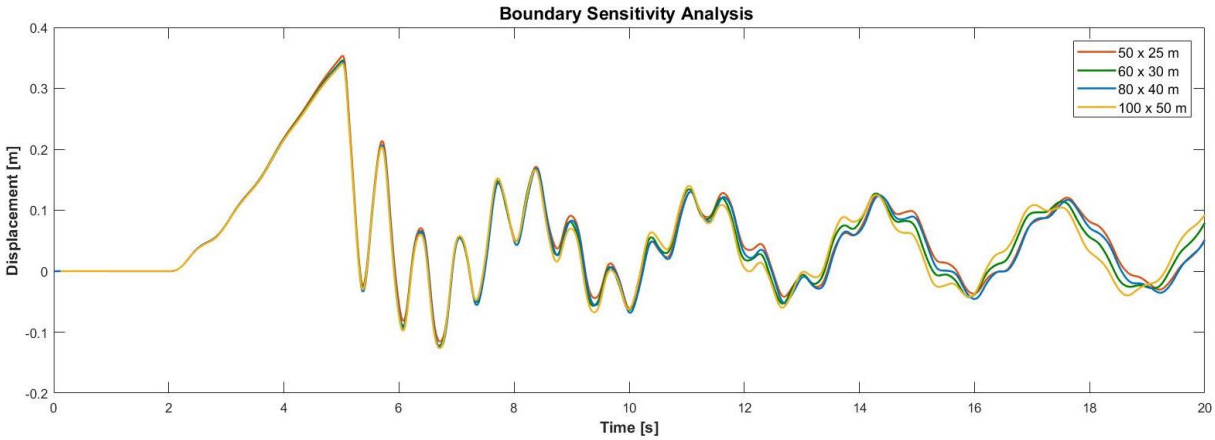

Figure A4: Boundary Sensitivity Analysis for Different Boundary Sizes

A.3 Time Step Sensitivity

Last sensitivity analysis was conducted on the time stepping effect which is basically the time between two data points (e.g. displacement data information at certain time) taken by the simulation. In Plaxis dynamic environment, the maximum number of steps is equal to 10,000 but this can be increased by involving sub-steps. The aim of this analysis was to see if there is effect on the output results if the time step is decreased (e.g. more data points available). The information about conducted cases can be seen in the

Table A3 and the increase of computation time with decreasing the time step can be seen in Figure A5.

Table A3: Time Step Analysis

Time Step - Sensitivity Analysis	
Time Step - dt	**Analysis Time [min]**
0.04	50
0.02	89
0.01	130
0.007	185

The analyzed time stepping cases can be seen in the Figure A5 and from the conducted sensitivity study it can be concluded that all of the time steps were sufficient to meet the accuracy criteria for the furhter analyses. The convergence in results is considered to be reached since the difference between results is neglibile. The chosen time step for further analyses is sligthly larger than those ones used here and it is equal to dt=0.05. With usage of this time step the most efficient analyses can be undertaken without having unfavourable effect on the accuracy criteria.

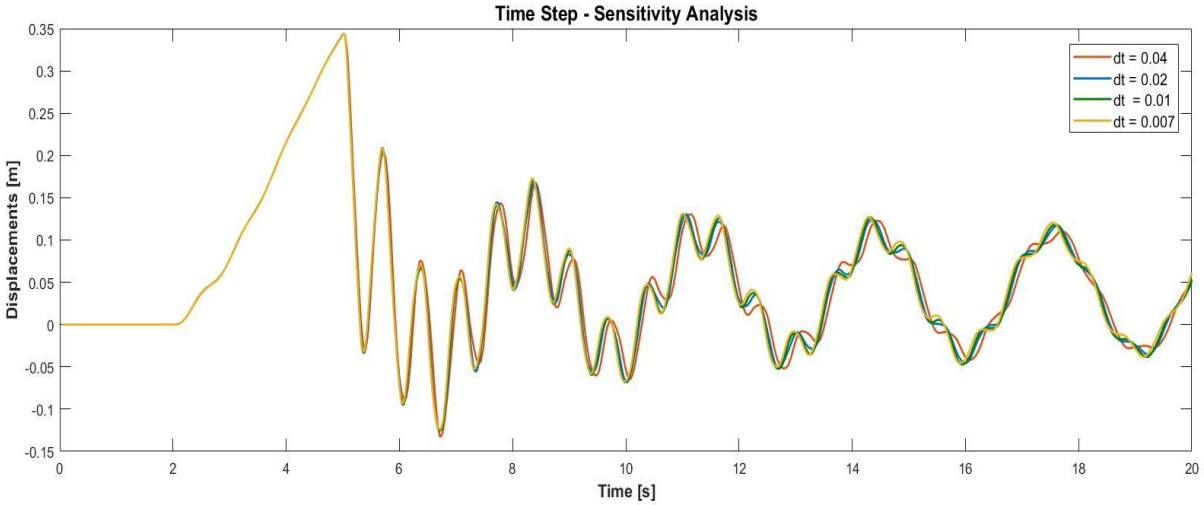

Figure A5: Time Step Analysis

Appendix B – Logarithmic Decrement Code

This appendix presents the example code which was used in this thesis for the estimation of damping in free vibration analysis. The code utilizes MATLAB option called “cursor-info”, which translates the information regarding the amplitude peaks into the workspace and therefore the information is utilized for the calculation of the mean logarithmic decrement value, which is a direct input for the damping equation. The code allows a user for a quick estimation of damping by just clicking the desired amplitude peaks and execution process is quite fast and yet simple to use.

```
%Example Code for Estimation of Damping on Free Vibration Data (e.g.
% displacement or acceleration signal)
%The code utilizes the Logarithmic Decrement Method

clear all;
close all;

Folderin='C:\Users\Luka\Desktop\Master Thesis\Monopile Design Files';
addpath(Folderin)
    % check existance
if ~exist ( Folderin, 'dir')
    disp ( [ ' output folder ' Folderin ' doesnot exist' ] );
    return;
end;
format short
file='ULS-180sec-displacement.txt'; %Example File

data =load(file);
 x = data(:,1); %Time vector
 y = data(:,2); %Displacement vector
 y_d=detrend(y,'constant'); %Displacement detrended

%-----------------------LP Filtering-IF-Necessary-----------------------%
Fs=20 %Sampling Frequency
cutoff=0.35; order=3; type='low';
[ filt_signal ] = my_filter( y_d, Fs, cutoff, order, type );
y_d=filt_signal;
%-----------------------------------------------------------------------%

figure(1);%Figure generated to pick the amplitude peaks
plot(x,y_d)
title('Time Displacement')
legend('Displacement','0')
set(gcf, 'Position', [50, 50, 1800, 900])
set(gca,'FontSize',15)
%---------------------Guide for Automated Calculation-------------------%
disp('Select data cursor in above icons of figure.')
disp('Pick amplitude neighbour picks from detrended data,')
disp('and export data to cursor-info, by right click, then press enter.')
pause
n=1;%time period between peaks

%-------------------------Cursor Info Set Up----------------------------%
lp=length(cursor_info);
```

```
for ind=1:lp
    yp=lp-ind+1;
py(ind,1)=cursor_info(yp).Position(1,2);
end

x0=cursor_info(2).Position(1,1); %First - Initial Peak
xn=cursor_info(1).Position(1,1);
a=cursor_info(2).DataIndex;
disp('Logarithmic Decrement')
for ind=1:(lp-1)
    y0=ind;
    y1=ind+1;
ldd(ind,1)=1/n*log(py(y0,1)/py(y1,1));
end
disp('Log Decrements')
ldd
disp('Mean Log Decrement')
ldd_mean=mean(ldd) %Calculation of mean Log value


disp('Frequency [Hz]')
omega=(((xn-x0)/n)^-1)*2*pi; %Frequency Calculation

f=omega/2/pi
disp('Damping')
xi=1/((1+(2*pi/ldd_mean)^2)^(0.5))%Damping Calculation
u=exp(-xi*omega*x);
A=y_d(a,1)/u(a,1); %Initial Amplitude
u=A*exp(-xi*omega*x); %Decay Logarithmic Curve

%-----------------------Plotting the Decay Curve-----------------------%
figure(2);
plot(x,y_d,x,u,x,-u)
title('Decay Curve')
set(gcf, 'Position', [50, 50, 1800, 900])
set(gca,'FontSize',15)
```